Habilitation à diriger des recherches

Astrid Lambrecht

UNIVERSITE PIERRE & MARIE CURIE
LA SCIENCE A PARIS

LABORATOIRE KASTLER BROSSEL

DOSSIER D'HABILITATION
À DIRIGER DES RECHERCHES

présentée par

Astrid LAMBRECHT

Soutenue le 26 Novembre 2002 devant le jury composé de

M. Claude BOCCARA (Président)

M. Martial DUCLOY (Rapporteur)

Mme Elisabeth GIACOBINO

M. Serge REYNAUD

M. Philippe TOURRENC (Rapporteur)

M. Jacques VIGUE (Rapporteur)

Table des matières

Première partie

Présentation générale

Curriculum vitæ

ASTRID LAMBRECHT
née le 20 Janvier 1967 à Mülheim an der Ruhr - Allemagne
Nationalité allemande
2 enfants, nés en 2000 et 2001

Coordonnées professionnelles

ADRESSE : Laboratoire Kastler Brossel
Université Pierre et Marie Curie, Case 74
4, place Jussieu, 75252 Paris Cedex 05
TÉLÉPHONE : +33 1 44 27 44 01
COURRIEL : lambrecht@spectro.jussieu.fr
INTERNET : http://www.spectro.jussieu.fr/Vacuum

Titres universitaires

1995 Thèse de doctorat de l'Université Paris VI
"Atomes froids et fluctuations quantiques"

1992 Thèse de Diplôme en physique de l'Université d'Essen (Allemagne)
"La réduction du bruit quantique par la superradiance à deux photons"
Equivalence du DEA "Physique Quantique", Université Paris VI

1986 Baccalauréat (Allemagne)

Parcours professionnel

2003 Organisatrice de la conférence internationale "Quantum Optics, Eurocon-ference on cavity QED and Quantum Fluctuations : From Fundamental Concepts to Nano-Technology", Grenade, prévue 09/2003

2002 Co-organisatrice de la journée thématique "Gravitation expérimentale sur Terre et dans l'Espace", Université Paris VI, 12/2002

2002 Co-organisatrice de la conférence "Gravitation and Experiment", Pise, 10/2002

2002 Co-organisatrice de la conférence internationale "Quantum Optics, Euro-conference on Quantum Atom Optics : From Quantum Science to technology", San Felio de Guixols, 09/2002

2000/.. Chargée de recherche 1ère classe au CNRS au Laboratoire Kastler Brossel

1998 et 99 Membre du jury d'oral de Physique, ENS Cachan, concours A1

1998 Séjour de 2 mois au Brésil dans les départements de physique de l'Université Fédérale de Rio de Janeiro, de l'Université de São Paulo et de l'Université Fédérale de Pernambuco (Recife)

1996/99 Chargée de recherche 2ème classe au CNRS au Laboratoire Kastler Brossel

1996 Membre du jury d'admission au Studienstiftung des Deutschen Volkes[1]

1995/96 Séjour postdoctoral au Max-Planck Institut für Quantenoptik dans le groupe de T.W. Hänsch, Garching (Allemagne) :
"Statistique quantique et aspects thermodynamiques dans un condensat de Bose-Einstein"

1992/95 Thèse de doctorat de l'Université Paris VI dans le groupe d'Elisabeth Giacobino au Laboratoire Kastler Brossel :
"Atomes froids et fluctuations quantiques"

1991/92 Thèse de Diplôme en Physique de l'Université d'Essen (Allemagne) dans le groupe de F. Haake :
"Réduction du bruit quantique par la superradiance à deux photons"

1990/91 Séjour prédoctoral au Blackett Laboratory, Imperial College, dans le groupe de P.M. Knight, Londres (UK) :
"Coopérativité et corrélations dans les états atomes-champ"

1989 Admise au concours de la Studienstiftung des Deutschen Volkes

Activités d'enseignement

1999 Travaux dirigés au DEA "Physique Quantique" de l'Université Paris VI (9h)

1998 Travaux dirigés au DEA "Physique Quantique" de l'Université Paris VI (10h)

1992 Travaux dirigés à l'Université d'Essen : Méthodes mathématiques en physique théorique pour des étudiants en DEUG ("Vordiplom") (209h)

1. en anglais : German Merit Foundation, http://www.studienstiftung.de

1992 Travaux pratiques à l'Université d'Essen : Electromagnétisme/optique/électronique pour des étudiants en DEUG (160h)

1991 Travaux pratiques à l'Université d'Essen : Mécanique/thermodynamique pour des étudiants en DEUG (208h)

1991 Travaux dirigés à l'Université d'Essen : Programme de rattrapage pendant les vacances d'été (juillet-octobre) (150h)

1990 Travaux pratiques à l'Université d'Essen : Physique pour les étudiants en médecine (130h)

1989 Travaux pratiques à l'Université d'Essen : Physique pour les étudiants en médecine (195h)

Encadrement

2002 Co-responsable de la thèse de 3ème cycle de Francesco Intravaia (Université Paris VI); début de thèse en septembre 2002

2002 Responsable du stage de DEA de Jean-Roch Vlimant (DEA de Physique Quantique)

2001 Co-responsable du stage de DEA de Brahim Lamine (DEA de Physique Théorique de Lyon)

2000 Responsable du stage de maîtrise de Tristan Meunier (Université Paris VII)

1999/2002 Co-responsable de la thèse de 3ème cycle de Cyriaque Genet (Université Paris VI); soutenance le 4 juillet 2002

1999 Responsable du stage de licence de Tristan Meunier (Université Paris VII)

Responsabilités collectives

2002/.. Membre nommée du Conseil du Laboratoire du Laboratoire Kastler Brossel

2002 Membre élue du Conseil de l'UFR 925 de l'Université Paris VI

2001 Coordinatrice de la collaboration franco-brésilienne CNRS-CNPq "Electrodynamique en cavité"

2000/01 Coordinatrice de la collaboration franco-brésilienne CAPES-COFECUB "Processus fondamentaux dans l'interaction entre rayonnement et matière"

2000/02 Organisatrice du séminaire hebdomadaire du Laboratoire Kastler Brossel

1998/2001 Membre de la Commission de Spécialistes, Université Paris VII, 30ème section

1998/2001 Membre élue du Conseil du Laboratoire du Laboratoire Kastler Brossel

Travaux scientifiques

Publications :

22 articles publiés dans des revues à comité de lecture; 2 articles soumis

4 contributions dans des ouvrages collectifs

16 articles dans des actes de conférence

4 articles de diffusion de l'information scientifique

Communications et séminaires présentés par moi-même :

9 communications invitées à des conférences

13 communications à des conférences

4 séminaires généraux (Colloquia)

11 séminaires

Publications dans des revues à comité de lecture

1. "Cooperativity and entanglement of atom-field states", I.K. Kudryavtsev, A. Lambrecht, H. Moya-Cessa, and P.L. Knight, *Journal of Modern Optics* **40**, 1605 (1993)

2. "Atomes froids en cavité: bistabilité optique et bruit quantique", L. Hilico, J.M. Courty, A. Lambrecht, C. Fabre, et E. Giacobino, *Revue Scientifique et Technique de la Défense* **25**, 139 (1993)

3. "Optical nonlinear dynamics with cold atoms in a cavity", A. Lambrecht, E. Giacobino, and J.M. Courty, *Optics Communications* **115**, 199 (1995)

4. "Cold atoms: a new medium for quantum optics", A. Lambrecht, J.M. Courty, S. Reynaud, and E. Giacobino, *Applied Physics* **B60**, 129 (1995)

5. "Atomic number fluctuations in a falling cold atom cloud", A. Lambrecht, E. Giacobino, and S. Reynaud, *Quantum and Semiclassical Optics* **8**, 457 (1996)

6. "Effect of transverse mode structure on squeezing with two-level atoms", A. Lambrecht, J.M. Courty, and S. Reynaud, *Journal de Physique II* **6**, 1133 (1996)

7. "Motion induced radiation from a vibrating cavity", A. Lambrecht, M.T. Jaekel, and S. Reynaud, *Phys. Rev. Lett.* **77**, 615 (1996)

8. "Transverse mode coupling in a Kerr medium", J.M. Courty and A. Lambrecht, *Phys. Rev.* **A 54**, 5243 (1996)

9. "Squeezing with cold atoms", A. Lambrecht, T. Coudreau, A. Steinberg, and E. Giacobino, *EuroPhys. Lett.* **36**, 93 (1996)

10. Comment on "Sonoluminescence as Quantum Vacuum Radiation" A. Lambrecht, M.T. Jaekel, and S. Reynaud, *Phys. Rev. Lett.* **78**, 2267 (1997)

11. "The Casimir force for passive mirrors", A. Lambrecht, M.T. Jaekel, and S. Reynaud, *Physics Letters* **A225**, 188 (1997)

12. "Thermodynamics of non-interacting bosons in low-dimensional potentials", G.L. Ingold and A. Lambrecht, *Eur. Phys. J.* **D 1**, 29 (1998)

13. "Frequency up-converted radiation from a cavity moving in vacuum", A. Lambrecht, M.T. Jaekel, and S. Reynaud, *Eur. Phys. J.* **D 3**, 95 (1998)

14. "Generating photon pulses with an oscillating cavity", A. Lambrecht, M.T. Jaekel, and S. Reynaud, *Europhys. Lett.* **43**, 147 (1998)

15. "Casimir force between metallic mirrors", A. Lambrecht and S. Reynaud, *Eur. Phys. J.* **D8**, 309 (2000)

16. Comment on "Demonstration of the Casimir force in the 0.6 to 6 μm Range", A. Lambrecht and S. Reynaud, *Phys. Rev. Lett.* **84**, 5672 (2000)

17. "Temperature dependence of the Casimir effect between metalic mirrors", C. Genet, A. Lambrecht, and S. Reynaud, *Phys. Rev.* **A 62**, 012110 (2000)

18. "Gravitational decoherence of planetary motions", S. Reynaud, P.A. Maia Neto, A. Lambrecht, and M.T. Jaekel, *Europhys. Lett.* **54**, 135 (2001)

19. "Quantum vacuum fluctuations", S. Reynaud, A. Lambrecht, C. Genet, and M.-T. Jaekel, *C.R. Acad. Sci. Paris* **2**, 1241 (2001)

20. "Correlation between temperature and plasma corrections to the Casimir force", C. Genet, A. Lambrecht, and S. Reynaud, *Int. J. Mod. Phys.* **A17**, 761 (2002)

21. "Decoherence and gravitational backgrounds", S. Reynaud, B. Lamine, A. Lambrecht, P. Maia Neto, and M.-T. Jaekel, *Int. J. Mod. Phys.* **A17**, 1003 (2002)

22. "Quantum vacuum, inertia and gravitation", M.T. Jaekel, A. Lambrecht, and S. Reynaud, *New Astronomy Reviews* (à paraître, 2002)

23. "The Casimir force and the quantum theory of lossy optical cavities", C. Genet, A. Lambrecht, and S. Reynaud, soumis (2002)

24. "Electromagnetic pulses from a cavity moving in vacuum : possible experiments", A. Lambrecht, soumis (2002)

25. "The Casimir force and the quantum theory of lossy optical cavities : Temperature effects", C. Genet, A. Lambrecht, and S. Reynaud, en cours de préparation (2002)

Contributions invitées à des ouvrages

26. "Relativité du mouvement dans le vide", M.T. Jaekel, A. Lambrecht, et S. Reynaud, contribution à l'ouvrage "Le vide", eds. E. Gunzig et S. Diner, 255 (Editions Complexe, 1998)

27. "Relativity of motion in vacuum", M.T. Jaekel, A. Lambrecht, and S. Reynaud, contribution à l'ouvrage "Vacuum", eds. E. Gunzig et S. Diner (Plenum, à paraître)

28. "Observing mechanical dissipation in quantum vacuum : an experimental challenge", A. Lambrecht, contribution à l'ouvrage "Laserphysics at the Limit", eds. H. Figger, D. Meschede, C. Zimmermann, 197 (Springer, 2001)

29. "Recent experiments on the Casimir effect : description and analysis", A. Lambrecht and S. Reynaud, contribution à l'ouvrage "L'énergie du vide", eds. B. Duplantier and V. Rivasseau, Séminaire de Poincaré (à paraître, 2002)

Publications dans des comptes-rendus

30. "Quantum optics with cold atoms", E. Giacobino, J.M. Courty, C. Fabre, L. Hilico, and A. Lambrecht, *Fundamentals of Quantum Optics* **III**, ed. F. Ehlotzky, 133 (Springer, 1993)

31. "Quantum optics with parametric and atomic media", E. Giacobino, J.M. Courty, C. Fabre, L. Hilico, and A. Lambrecht, *Laser Spectroscopy* **IX**, eds. L. Bloomfield, T. Gallagher, D. Larson, 349 (AIP, 1993)

32. "Nonlinear and quantum dynamics of an optical cavity containing cold atoms", E. Giacobino, J.M. Courty, and A. Lambrecht, *Quantum Optics* **VI**, eds. D.F. Walls, J.D. Harvey, 203 (Springer, 1994)

33. "Quantum noise eaters", C. Fabre, C. Richy, P. Kürz, A. Lambrecht, J.M. Courty, E. Giacobino, S. Reynaud, A. Heidmann, and M. Pinard, *Quantum Communication and Measurements*, eds. V.P. Belavkin, O. Hirota, R.L. Hudson, 455 (Plenum, 1995)

34. "Squeezing and QND with cold atoms", E. Giacobino, A. Lambrecht, J.M. Courty, P. Grangier, J.F. Roch, and J.P. Poizat, *Proceedings ICONO '95: Atomic and Quantum Optics: High Precision Measurements*, eds. Sergei N. Bagayev, Anatoly S. Chirkin, Proc. SPIE 2799, 112 (SPIE 1996)

35. "Squeezing the light with laser cooled atoms", E. Giacobino, A. Lambrecht, J.M. Courty, and T. Coudreau, *Microcavities and Photonic Bandgaps: Physics and Applications*, eds. J. Rarity, C. Weissbuch, Nato ASI 324, 467 (Kluwer, 1996)

36. "Squeezing with cold atoms", E. Giacobino, A. Lambrecht, and T. Coudreau, *Inter-*

national Quantum Electronics Conference, 113 (Optical Society of America, Washington D.C. 1996)

37. "Motion induced radiation from a vibrating cavity", A. Lambrecht, M.T. Jaekel, and S. Reynaud, *Dark Matter in Cosmology, Quantum Measurements and Experimental Gravitation*, eds. R. Ansari, Y. Giraud-Héraud, J. Trân Thanh Vân, 317 (Editions Frontières, 1996)

38. "Relativity of motion in vacuum", A. Lambrecht, *Frontier Tests of Quantum Electrodynamics and Physics of the Vacuum*, eds. E. Zavattini, D. Bakalov and C. Rizzo, 405 (Heron Press, 1998)

39. "Relativity of motion in vacuum", A. Lambrecht, *CD-ROM Around VIRGO*, eds. S. Reynaud and F. Fidecaro (CD-ROM INFN Pise, 1999)

40. "Relativity of motion in quantum vacuum", A. Lambrecht, *Gravitational Waves and Experimental Gravitation*, eds. J. Trân Thanh Vân (World Publishers, 2000)

41. "The Casimir force between metallic mirrors", A. Lambrecht, C. Genet, and S. Reynaud, *Proceedings of the Ninth Marcel Grossmann Meeting on General Relativity*, eds. V.G. Gurzadyan, R.T. Jantzen and R. Ruffini (World Scientific, Singapore, 2002)

42. "Relativity of motion in quantum vacuum", M.T. Jaekel, A. Lambrecht, and S. Reynaud, *Proceedings of the Ninth Marcel Grossmann Meeting on General Relativity*, eds. V.G. Gurzadyan, R.T. Jantzen and R. Ruffini (World Scientific, Singapore, 2002)

43. "Effet de la température sur la force de Casimir entre miroirs réels", C. Genet, A. Lambrecht, et S. Reynaud, *J. Physique IV* **12**, 143 (2002)

44. "Casimir forces", A. Lambrecht, C. Genet, and S. Reynaud, *Very High Energy Phenomena in the Universe*, ed. J. Trân Thanh Vân (Editions Frontières, à paraître)

45. "Fluctuations du vide quantique", S. Reynaud, A. Lambrecht, and M.T. Jaekel, *Conceptions de l'espace* , ed. M. Lachièze-Rey (à paraître)

Diffusion de l'information scientifique

46. "Identitätsverlust mit Folgen: vom Quantengas zur Bose-Einstein-Kondensation", A. Lambrecht und G. Ingold, *Physik in unserer Zeit* **5/96**, 200 (1996) (titre en français: "Les conséquences d'une perte d'identité: du gaz quantique vers la condensation de Bose-Einstein")

47. "Secouer le vide pour créer de la lumière", A. Lambrecht, *La Recherche* **295**, 40 (1997)

48. "Interferenzen zwischen zwei Bose-Kondensaten", A. Lambrecht, *Physik in unserer*

Zeit **2/97**, 88 (1997) (titre en français: "Observation d'interférences entre deux condensats de Bose")

49. "The Casimir effect : a force from nothing", A. Lambrecht, *Physics World* **15**, 29 (Septembre, 2002)

Thèses

1. "Réduction du bruit quantique par la superradiance à deux photons", Thèse de Diplôme (Université d'Essen, 1992)
2. "Atomes froids et fluctuations quantiques", Thèse de doctorat (Université Paris VI, 1995)

Communications invitées

1. "Motion induced radiation from a vibrating cavity", XXXIst Rencontres de Moriond, "Dark Matter in Cosmology, Quantum Measurements and Experimental Gravitation", Les Arcs, Janvier 1996

2. "Motion induced radiation from a vibrating cavity", Congrès "Quantum Vacuum", Instituto Nationale di Fisica Nucleare et Universita di Padova, Padoue, Avril 1996

3. "Fluctuations quantiques et mouvement", Congrès "Le bruit quantique", Peyresq, Juillet 1997

4. "Relativity of motion in quantum vacuum", Congrès de la Société Max-Planck, Ringberg, Bavière, Avril 1998

5. "Relativity of motion in quantum vacuum", XXXIVth Rencontres de Moriond "Gravitational waves and experimental gravity", Les Arcs, Janvier 1999

6. "Measurements of the Casimir force", Congrès "Gravitation and Experiment", Grasse, Octobre 2000

7. "Quantum radiation from moving surfaces and the Casimir effect", EURESCO Conference: Quantum Optics XI, Mallorca, Octobre 2000

8. "Casimir forces", XXXVIth Rencontres de Moriond "Very High Energy Phenomena in the Universe", Les Arcs, Janvier 2001

9. "Electromagnetic pulses from a cavity moving in vacuum", Congrès "Electromagnetism", Peyresq, Septembre 2002

Communications

1. "Optical nonlinear dynamics in cold atoms", Workshop on Quantum and Transverse Effects in Nonlinear Optical Systems, Come 1993 (affiche)

2. “Quantum optics with laser cooled atoms”, 4th European Quantum Electronics Conference EQEC ’93, Florence 1993 (affiche)

3. “Quantum optics with laser cooled atoms”, Colloque sur les Lasers et l’Optique Quantique COLOQ ’93, Limoges 1993 (affiche)

4. “Squeezing with cold atoms”, European Research Conference on Quantum Optics, Davos 1994 (affiche)

5. “Squeezing with cold atoms”, 5th European Quantum Electronics Conference EQEC ’94, Amsterdam 1994 (contribution ’post-deadline’ sélectionnée pour une présentation orale)

6. “Squeezing with cold atoms”, VIIth Conference on Coherence and Quantum Optics, Rochester 1995 (affiche)

7. “Squeezing with cold atoms”, Congrès de la Deutsche Physikalische Gesellschaft, Iéna 1996 (contribution orale)

8. “Motion induced radiation from a vibrating cavity”, Congrès de la Deutsche Physikalische Gesellschaft, Iéna 1996 (contribution orale)

9. “Radiation from a cavity moving in vacuum”, Workshop on Gravitation and Experiment, Les Houches 1997 (affiche)

10. “Relativity of motion in vacuum”, Workshop on Frontier Tests of Quantum Electrodynamics and Physics of the Vacuum, Sandansky, Bulgarie 1998 (contribution orale)

11. “Relativity of motion in vacuum”, European Quantum Electronics Conference EQEC ’98, Glasgow 1998 (contribution orale)

12. “Relativity of motion in vacuum”, Around Virgo, Tirrenia 1998 (affiche)

13. “The Casimir force between metallic mirrors”, The Ninth Marcel Grossmann Meeting, Rome 2000 (contribution orale)

Séminaires généraux

1. “Nobelpreis 1997: Ultrakalte Atome” (titre en français: “Le Prix Nobel 1997: Les atomes ultrafroids”), Colloquium de physique de l’Université d’Augsbourg, Augsbourg, Décembre 1997

2. “Relativity of motion in vacuum”, Colloquium de physique de l’Université Fédérale de Rio de Janeiro, Rio de Janeiro, Novembre 1998

3. “Relativity of motion in vacuum”, Colloquium de physique de l’Université Fédérale de Pernambuco, Recife, Décembre 1998

4. “Relativité du mouvement dans le vide quantique”, Séminaire de la Chaire de Physique Atomique et Moléculaire, Collège de France, Paris, Novembre 1999

Séminaires

1. “Squeezing and nonlinear dynamics with cold atoms”, Université de Constance, Constance, Septembre 1994

2. “Squeezing with cold atoms”, National Institute of Standards and Technology, Gaithersburg, Juin 1995

3. “Le rayonnement d’une cavité en mouvement dans le vide”, Université de Genève, Genève, Mai 1997

4. “Le rayonnement d’une cavité en mouvement dans le vide”, Laboratoire Kastler Brossel, Paris, Mai 1997

5. “Relativity of motion in vacuum”, Université de São Paulo, São Paulo, Décembre 1998

6. “The Casimir force between dielectric mirrors”, Université Fédérale de Rio de Janeiro, Rio de Janeiro, Décembre 1998

7. “Relativité du mouvement dans le vide quantique”, Département d’Astrophysique Relativiste et de Cosmolgie (D.A.R.C.), Meudon, Mars 1998

8. “Relativité du mouvement dans le vide quantique”, Groupe de Physique des Solides (G.P.S.), Université Pierre et Marie Curie, Paris, Octobre 1998

9. “Relativité du mouvement dans le vide quantique”, Institut de Physique Nucléaire de Lyon (I.P.N.L.), IN2P3 Lyon, Octobre 1998

10. “Casimir force between metallic mirrors”, Institut Nonlinéaire de Nice, INLN, Nice, Octobre 1999

11. “The Casimir effect in theory and experiments”, Institut de l’Optique Quantique, Université de Hanovre, Hanovre, Mai 2001

Présentation générale des travaux

Avant mon recrutement au CNRS j'ai effectué des travaux de recherche à l'Imperial College à Londres, à l'Université d'Essen, au Laboratoire Kastler Brossel à Paris et au Max-Planck-Institut pour l'Optique Quantique à Munich. Depuis octobre 1996 je travaille au Laboratoire Kastler Brossel de l'Ecole Normale Supérieure et de l'Université Paris VI dans l'équipe de Serge Reynaud. J'y consacre l'essentiel de mon activité à la définition d'expériences permettant de mettre en évidence les effets mécaniques des fluctuations du vide. Je décris ci-dessous d'une façon concise l'ensemble de mes travaux. La description plus détaillée ainsi que les conclusions et perspectives se trouvent dans la seconde partie de ce mémoire.

Ma première expérience de recherche a correspondu à un séjour d'un an en 1990/91 à Londres dans le Blackett Laboratory d'Imperial College où j'ai travaillé avec le professeur Peter Knight. Ce séjour, qui s'est intercalé dans mon cursus universitaire, a été encouragé et financé par la "Studienstiftung des Deutschen Volkes[1]".

Pendant ce séjour j'ai étudié la génération d'états de type "chat de Schrödinger" par l'interaction entre un ou plusieurs atomes et un champ électromagnétique dans une cavité. L'interaction entre les atomes et le champ crée en effet des corrélations qui résultent en un état intriqué pour lequel une séparation de l'état atomique et de l'état du champ n'est plus possible. Un état "chat de Schrödinger" a depuis été observé expérimentalement avec un nombre de photons et d'atomes très faible[2]. La réalisation d'un "chat de Schrödinger" macroscopique reste un enjeu expérimental intéressant.

Je me suis particulièrement intéressée à un phénomène typique dans ce genre d'interaction, où l'on décrit l'atome comme un atome à deux niveaux, à savoir le collapse et la réapparition temporels des corrélations atomes-champs. L'état intriqué n'est donc pas stable dans le temps et dépend des conditions initiales. Si plusieurs atomes interagissent avec le champ, les états atomiques se corrèlent entre eux par l'intermédiare du champ.

1. German Merit Foundation
2. X. Maître, E. Hagley, J. Dreyer, A. Maali, C. Wunderlich, M. Brune, J.M. Raimond, and S. Haroche, *J. Mod. Opt.* ***44****, 2023 (1997)*

De façon générale, ceci nuit à la génération d'un état "chat de Schrödinger". Son existence reste possible seulement dans certains cas particuliers concernant le couplage ou les conditions initiales[3].

A mon retour, j'ai effectué ma thèse de Diplôme (équivalent du DEA) à l'Université d'Essen avec le professeur Fritz Haake pendant l'année 1991/92. Mon sujet de thèse était la superradiance à deux photons. J'ai considéré un ensemble d'atomes en interaction avec un champ électromagnétique dans une cavité. Le phénomène de superradiance[4] peut se produire seulement si la taille du nuage atomique est beaucoup plus petite que la longueur d'onde du champ. Après l'excitation de l'ensemble des atomes par une impulsion π, les atomes agissent alors comme un seul atome en émettant une impulsion cohérente, dit superradiante. Cet effet a éte observé expérimentalement[5,6].

J'ai essentiellement travaillé sur deux questions. La première question était de savoir si ce processus pourrait être utile pour réduire les fluctuations quantiques du champ. En effet, dans la mesure où l'interaction entre les atomes et le champ est quadratique dans le champ, une réduction du bruit quantique paraissait possible. J'ai étudié en détail l'influence du temps de relaxation de la cavité. La réduction du bruit s'est avérée d'autant plus grande que la cavité a un facteur de qualité élévé avec une réduction du bruit maximale de l'ordre de 65% pour une cavité parfaite. Même pour une cavité de très mauvaise qualité, il subsiste une réduction du bruit de l'ordre de 13%.

Je me suis ensuite demandé dans quelle mesure un tel système pourrait être correctement décrit par une méthode semi-classique de relaxation[7], où l'on remplace les opérateurs par des nombres complexes et où l'incertitude de l'état initial est modélisée par un ensemble de trajectoires[8]. La comparaison entre les résultats du calcul semi-classique et le calcul quantique complet a montré que la méthode semi-classique donne une description correcte des observables physiques, à savoir l'intensité des impulsions et les propriétés statistiques du champ à quelques pourcents près pendant plusieurs cycles d'évolution temporelle. Ceci est non seulement le cas dans le régime "quasi-classique" avec un grand nombre d'atomes et de photons mais aussi dans un régime non classique où quelques atomes interagissent avec quelques photons. Quand le champ se trouve initialement dans l'état du vide électromagnétique, la méthode semi-classique perd sa validité dès l'émission de la première impulsion superradiante.

3. I.K. Kudryavtsev, A. Lambrecht, H. Moya-Cessa, and P.L. Knight, *J. Mod. Opt.* **40**, 1605 (1993)
4. R.H. Dicke, *Phys. Rev.* **93**, 99 (1954)
5. F. Gounand, M. Hugon, P.R. Fournier, and J. Berlande, *J. Phys.* **B 12**, 547 (1979)
6. M. Gross and S. Haroche, *Phys. Rep.* **93**, 308 (1982) et leurs références
7. R.W. Zwanzig, *Physica* **33**, 119 (1964)
8. R. Bonifacio, P. Schwendimann, and F. Haake, *Phys. Rev.* **A 4**, 302 (1971)

A Londres et à Essen, mes sujets de recherche concernaient des études théoriques dans le domaine de l'Optique Quantique. Après ces travaux théoriques, j'ai décidé de profiter de la période de la thèse pour acquérir de surcroît une formation en recherche expérimentale. J'ai choisi le Laboratoire Kastler Brossel de l'Ecole Normale Supérieure et de l'Université Pierre et Marie Curie où j'ai effectué ma thèse de doctorat avec Elisabeth Giacobino de 1992 à 1995. Le sujet de ma thèse correspondait parfaitement à mon souhait de mener en parallèle une recherche expérimentale et théorique. Lorsque j'ai commencé mon travail de thèse, le piégeage des atomes permettait depuis peu d'obtenir dans une petite cellule un nuage dense d'atomes refroidis. Celui-ci constituait à l'époque un nouveau milieu non-linéaire, prometteur pour l'Optique Quantique. Mon travail a consisté à étudier un nuage d'atomes froids sur le plan expérimental et théorique, à caractériser ses propriétés vis à vis de l'Optique Quantique et à l'utiliser pour réduire les fluctuations quantiques d'un faisceau laser.

En plaçant un nuage d'atomes de césium dans une cavité optique qui exalte l'interaction entre les atomes et le faisceau, on obtient un phénomène de bistabilité optique par effet Kerr qui est à la base de la réduction du bruit. C'est au voisinage des points tournants de la bistabilité que la réduction du bruit quantique est maximale. Il est apparu que les faisceaux pièges introduisaient de l'excès de bruit dû à l'émission spontanée et masquaient ainsi la réduction du bruit quantique. En coupant le piège pendant la mesure afin de supprimer cette perturbation, j'ai pu mettre en évidence une réduction du bruit de l'ordre de 40% en quadrature du champ[9]. Cependant, pour arriver à ce résultat, il a fallu comprendre l'origine des instabilités dynamiques, qui sont apparues dans le système lors de la coupure des faisceaux pièges. Le comportement instable résultait en effet d'une compétition entre l'effet Kerr et le pompage optique entre les sous-niveaux Zeeman de la transition atomique. Ces deux processus balayaient la cavité en sens opposé autour des points de bistabilité provoquant ainsi des oscillations violentes de l'intensité lumineuse[10].

De plus, cette réduction du bruit quantique a été obtenue dans une situation inhabituelle. En effet, la coupure du piège conduisait à l'explosion et à la chute libre du nuage atomique au cours du temps. La variation du nombre d'atomes dans le faisceau laser était suffisante pour balayer la résonance de la cavité. J'ai montré qu'il était possible de calculer le spectre de bruit caractérisant les fluctuations du nombre d'atomes si la section du faisceau laser est beaucoup plus petite que la taille du piège. Dans ce cas, le nombre d'atomes peut être considéré comme une variable quasistationnaire et les fluctuations du champ électromagnétique peuvent également être caractérisées par un spectre de bruit. Ainsi j'ai

9. A. Lambrecht, J.M. Courty, S. Reynaud, and E. Giacobino, *Appl. Phys.* **B 60**, 129 (1995)
10. A. Lambrecht, E. Giacobino, and J.M. Courty, *Optics Comm.* **115**, 199 (1995)

pu donner des estimations de l'influence des fluctuations atomiques sur la réduction du bruit dans différentes conditions expérimentales. Leur influence sur les fluctuations du faisceau sonde restait négligeable dans les conditions de notre expérience, mais elle pouvait être appréciable dans d'autres situations où un jet atomique est utilisé à la place du nuage d'atomes froids[11].

J'ai également poursuivi l'amélioration du traitement théorique des fluctuations quantiques en analysant en détail l'effet de la structure transverse du faisceau sonde sur la réduction du bruit. La comparaison avec l'ancien modèle, qui décrivait ce faisceau par une onde plane, a permis d'évaluer les conditions de validité des prédictions de ce dernier. En effet, le modèle "onde plane" ne donne pas le bon résultat en cas d'une forte réduction du bruit sauf si le milieu non-linéaire est non-absorbant[12]. Un autre effet de la structure transverse du faisceau est l'autofocalisation ou l'autodéfocalisation. Ceci conduit à un couplage et à un transfert de l'excès de bruit des modes d'ordre supérieur au mode fondamental. J'ai pu montrer que cet effet pouvait complètement détruire la réduction du bruit obtenue dans le mode fondamental si la cavité est dégénérée[13] ce qui n'était pas le cas dans notre expérience.

Une synthèse de ces développements théoriques qui tient compte à la fois de la structure transverse du faisceau sonde et de la variation du nombre d'atomes au cours du temps a permis de reproduire les spectres de bruit expérimentaux avec un accord très satisfaisant[14].

Après ma thèse, entre septembre 1995 et septembre 1996, j'ai effectué un stage postdoctoral à l'Institut Max-Planck pour l'Optique Quantique à Munich dans le groupe du professeur Theodor Hänsch. Là encore, mon travail de recherche a comporté des aspects théoriques et expérimentaux.

J'ai participé activement au développement d'une expérience sur la condensation de Bose-Einstein avec le Lithium, en particulier à la conception d'un piège magnétique à gradient fort. Cet outil devait permettre de piéger les atomes de Lithium avec une densité suffisante afin de pouvoir envisager l'étape suivante de la condensation. Bien que la condensation de Bose-Einstein ait été déjà observée auparavant avec cet atome[15], l'expérience restait très intéressante car le Lithium possède une longueur de diffusion négative qui aurait théoriquement dû l'empêcher de former un condensat. Nous savons aujourd'hui que ces condensats ont simplement une stabilité et une durée de vie inférieures aux autres.

11. A. Lambrecht, E. Giacobino, and S. Reynaud, *Quant. Sem. Opt.* **8**, 457 (1996)
12. A. Lambrecht, J.M. Courty, and S. Reynaud, *J. Physique* **II 6**, 1133 (1996)
13. J.M. Courty and A. Lambrecht, *Phys. Rev.* **A 54**, 5243 (1996)
14. A. Lambrecht, T. Coudreau, A.M. Steinberg, and E. Giacobino, *Europhys. Lett.* **36**, 93 (1996)
15. C.C. Bradley, C.A. Sackett, J.J. Tollett, and R.G. Hulet, *Phys. Rev. Lett.* **75**, 1687 (1995)

Parallèlement j'ai également étudié la condensation de Bose-Einstein au niveau théorique en collaboration avec Gert-Ludwig Ingold de l'Université d'Augsburg. En particulier, nous avons tenté de lever la confusion qui existe entre un processus de condensation de Bose et le développement d'une population macroscopique dans l'état fondamental du système considéré[16]. La condensation implique une apparition de signatures dans des grandeurs thermodynamiques et en même temps une population macroscopique dans l'état fondamental. Par contre, il existe aussi des situations où la population de l'état fondamental devient macroscopique sans qu'il y ait un phénomène de condensation[17]. Une telle distinction est importante vis à vis des propriétés de cohérence de l'ensemble d'atomes. Tandis que la condensation de Bose est toujours accompagnée d'un état atomique "cohérent", ceci n'est pas forcément le cas si l'augmentation de la population de l'état fondamental n'est pas accompagnée des signatures thermodynamiques nécessaires.

Depuis octobre 1996 je suis chargée de recherche au CNRS. Je travaille dans l'équipe de Serge Reynaud au Laboratoire Kastler Brossel sur les effets mécaniques des fluctuations du vide. Celles-ci correspondent aux fluctuations irréductibles de champ qui persistent dans une enceinte vidée de toute matière et à température nulle. En mécanique quantique, un mode du champ électromagnétique est décrit comme un oscillateur harmonique; les fluctuations du vide correspondent à l'état fondamental de cet oscillateur et ont donc une énergie de $\hbar\omega/2$ si ω est la fréquence du mode considéré.

Toute surface réfléchissante placée dans l'espace vide subit la pression de radiation des fluctuations du vide. Dans le cas de deux miroirs immobiles formant une cavité, ce phénomène est bien connu comme l'effet Casimir[18] qui se traduit par l'apparition d'une force attractive entre ces deux miroirs. Je présenterai cet effet plus loin. Les fluctuations du vide produisent également un effet mécanique lié au mouvement d'un diffuseur dans le vide. Par exemple, un miroir qui oscille dans le vide émet des paires de photons qui sont créées par un processus paramétrique dans le couplage entre la pression de radiation des modes du vide et le mouvement mécanique. Ce rayonnement motionnel met en évidence l'influence réciproque entre les fluctuations du vide et le mouvement mécanique. Par conservation de l'énergie, l'émission de photons est directement liée à la force de réaction de rayonnement qui freine le mouvement des miroirs[19].

Il s'agit là d'une force dissipative analogue à la force de friction subie par un objet dans un bain thermique en raison du mouvement brownien des particules. Dans ce cas, le

16. W. Ketterle and N.J. van Druten, *Phys. Rev.* **A 54**, 656 (1996)
17. G. Ingold and A. Lambrecht, *Eur. Phys. J.* **D 1**, 29 (1998)
18. H.B.G. Casimir, *Proc. Kon. Ned. Akad. Wetenshap* **51**, 793 (1948)
19. S.A. Fulling and P.C.W. Davies, *Proc. R. Soc. London* **A 348**, 393 (1976)

mouvement de l'objet brise l'équilibre entre les pressions des deux cotés de l'objet et une force de friction apparait pour une vitesse non nulle. Pour un miroir dans le vide, l'équilibre entre les pressions de radiation du vide des deux cotés du miroir est préservé pour un mouvement à vitesse ou à accélération uniforme. Par contre, l'équilibre est perturbé si le miroir suit un mouvement à accélération non-uniforme et une force dissipative apparaît alors.

Il serait très intéressant de mettre en évidence expérimentalement ces effets dissipatifs des fluctuations du vide[20,21]. Cependant, ils n'ont encore jamais été observés. En effet, les signatures mécaniques de ces effets sont proportionnelles à $\hbar$ et sont donc difficiles à détecter. Par contraste, le nombre des photons émis, qui est donné par l'énergie rayonnée divisée par l'énergie d'un seul photon, ne dépend plus de $\hbar$. Du point de vue d'une réalisation expérimentale, cet argument favorise clairement la détection du rayonnement, d'autant plus qu'il existe des techniques très sensibles de détection de photons. Le rayonnement motionnel émis par un seul miroir oscillant dans le vide reste cependant trop petit pour une observation expérimentale avec les moyens techniques disponibles aujourd'hui.

Afin d'améliorer les ordres de grandeur, j'ai alors étudié une cavité à la place d'un miroir unique. La plupart des calculs effectués dans le passé ne traitaient que le cas irréaliste d'une cavité construite avec des miroirs parfaits. Pour ma part, j'ai effectué des calculs permettant d'évaluer de manière quantitative l'influence de la finesse de la cavité. Par rapport au cas d'un miroir oscillant dans le vide, il existe pour la cavité des fréquences mécaniques résonnantes pour lesquelles le rayonnement est amplifié par le facteur de finesse. La présence de la cavité change aussi le spectre du rayonnement qui contient maintenant des pics de résonance optique. La cavité rayonne non seulement lorsque sa longueur mécanique est modulée, mais aussi lorsqu'elle oscille de façon à ce que sa longueur reste constante[22]. Ce résultat paraît paradoxal du point de vue de la mécanique, car la cavité se déplace alors dans le vide sans référence autre que le vide lui-même. Cette situation est la même que pour un miroir unique, mais on bénéficie ici de l'effet d'exaltation résonnante.

J'ai ensuite développé un traitement qui prend en compte de façon non-perturbative les multiples aller-retours du champ à l'intérieur de la cavité[23]. Ceci m'a permis d'étudier

20. M.T. Jaekel, A. Lambrecht, and S. Reynaud, in "Vacuum", eds. E. Gunzig and S. Diner (Plenum, à paraître)
21. S. Reynaud, A. Lambrecht, C. Genet, and M.T. Jaekel, *C.R. Acad. Sci. Paris* **2 IV**, 1287 (2001)
22. A. Lambrecht, M.T. Jaekel, and S. Reynaud, *Phys. Rev. Lett.* **77**, 615 (1996)
23. A. Lambrecht, M.T. Jaekel, and S. Reynaud, *Eur. Phys. J.* **D 3**, 95 (1998)

en détail les signatures du rayonnement motionnel. Pour une cavité de très haute finesse, le rayonnement est émis dans des impulsions de densité d'énergie très élevée et dans des fenêtres temporelles étroites et régulièrement espacées. De plus, une multiplication de fréquence a lieu par le couplage opto-mécanique entre fluctuations du vide et mouvement mécanique. Des photons peuvent être émis par la cavité à des fréquences plus élevées que la fréquence d'excitation mécanique des miroirs. Par contre, aucun photon n'est émis à des fréquences multiples de la fréquence d'oscillation mécanique. Grâce à ces caractéristiques, l'observation du rayonnement motionnel pourrait devenir un objectif réalisable avec une cavité de très grande finesse.

Afin d'étudier tous les aspects d'une réalisation expérimentale, j'ai également étudié l'influence de la température. A température non nulle, les fluctuations du vide s'accompagnent de fluctuations thermiques qui subissent les mêmes processus de diffusion par la cavité en mouvement. Le traitement non-perturbatif m'a permis d'évaluer précisément le rayonnement motionnel dû aux fluctuations thermiques[24]. Celui-ci présente des ordres de grandeur plus favorables que le rayonnement dû aux fluctuations du vide tout en ayant les mêmes signatures de formation d'impulsions et de multiplication de fréquence. Une expérience préliminaire pourrait alors être faite dans un champ thermique, mais en perdant bien sûr le lien direct avec les effets dissipatifs du vide.

Parallèlement je me suis aussi intéressée à la force de Casimir statique. Comme je l'ai déjà mentionné, cette force attractive s'exerce entre deux miroirs au repos dans le vide. Elle a une propriété d'universalité remarquable : dans le cas de miroirs parfaitement réfléchissants, elle ne dépend que de la géométrie du système, à savoir de la surface et la séparation des miroirs, ainsi que de deux constantes fondamentales, la vitesse de la lumière et la constante de Planck. La force de Casimir est de ce fait une prédiction importante de la théorie quantique des champs.

Nous avons développé une nouvelle méthode de calcul de la force de Casimir basée sur la théorie des réseaux optiques[25]. La diffusion du champ électromagnétique est décrite par des coefficients de réflexion qui obéissent à des propriétés physiques de causalité, de stabilité et de transparence à haute fréquence. Ces propriétés qui sont naturellement respectées par tout miroir réel, permettent une formulation de la force de Casimir sans aucune divergence. Ceci contraste avec des méthodes habituellement utilisées en théorie des champs quantiques pour lesquelles une régularisation de l'expression de la force de Casimir est inévitable.

La force de Casimir a été observée dans plusieurs expériences "historiques" dans les

24. A. Lambrecht, M.T. Jaekel, and S. Reynaud, *Europhys. Lett.* **43**, 147 (1998)
25. C. Genet, A. Lambrecht, and S. Reynaud, en cours de rédaction

années cinquante et soixante. Bien que la précision de ces expériences ne soit pas très bonne, elles ont permis d'identifier l'effet. En 1997, une nouvelle ère de mesure de la force de Casimir a commencé avec toute une série d'expériences aux Etats-Unis[26, 27, 28, 29], en Suède[30] et en Italie[31]. Ces expériences affichent une précision qui va jusqu'au niveau du pourcent, ce qui permet de tester la théorie quantique des champs de façon détaillée, sous la condition que les prédictions théoriques soient également évaluées avec la même précision. Une autre motivation pour des expériences de haute précision vient de la recherche d'éventuelles nouvelles forces faibles predites par des théories d'unification. Ces petites forces se manifesteraient entre deux objets à des distances entre le nanomètre et le millimètre[32, 33, 34, 35, 36]. Or, pour deux objets neutres, la force de Casimir est la force prédominante dans ce régime de distance. Comme elle est en particulier beaucoup plus grande que les hypothétiques nouvelles forces, celles-ci se manifesteraient comme une déviation entre la force de Casimir mesurée et la prédiction théorique. Une troisième motivation pour étudier précisément la force de Casimir vient du fait qu'elle joue un rôle très important dans le fonctionnement et le contrôle de systèmes microélectromécaniques (MEMS)[37]. Ces nouveaux systèmes servent comme senseurs et actuateurs microscopiques et promettent des progrès technologiques considérables en nano- et micromécanique.

Pour toutes ces raisons, il est crucial de mesurer et de calculer la force de Casimir avec précision. Dans un calcul précis, il faut tenir compte de la situation expérimentale réelle, par rapport à la situation idéalisée considérée par Casimir avec deux miroirs parfaitement plans et réfléchissants, à température nulle. Les miroirs utilisés dans les expériences récentes sont métalliques et leurs coefficients de réflexion dépendent donc de la fréquence. J'ai étudié l'effet de la conductivité des miroirs sur la force de Casimir en détail pour les métaux utilisés dans les expériences, à savoir l'aluminium, le cuivre et l'or. A des distances d'environ 100 nm, la force de Casimir entre miroirs métalliques s'avère être plus petite d'un facteur 2 que la force entre deux miroirs parfaits. Une comparaison précise entre

26. S.K. Lamoreaux, *Phys. Rev. Lett.* **78**, 5 (1997)
27. U. Mohideen and A. Roy, *Phys. Rev. Lett.* **81**, 4549 (1998)
28. A. Roy, C. Lin, and U. Mohideen, *Phys. Rev.* **D 60**, 111101 (1999)
29. B.W. Harris, F. Chen, and U. Mohideen, *Phys. Rev.* **A 62**, 052109 (2000)
30. Th. Ederth, *Phys. Rev.* **A 62**, 062104 (2000)
31. G. Bressi, G. Carugno, R. Onofrio, and G. Ruoso, *Phys. Rev. Lett.* **88**, 041804 (2002)
32. E. Fischbach and C. Talmadge, *The Search for Non-Newtonian Gravity* (AIP Press, 1998)
33. G. Carugno, Z. Fontana, R. Onofrio, and C. Rizzo, *Phys. Rev.* **D 55**, 6591 (1997)
34. J.C. Long, H.W. Chan, and J.C. Price, *Nucl. Phys.* **B 539**, 23 (1999)
35. M. Bordag, B. Geyer, G.L. Klimchitskaya, and V.M. Mostepanenko, *Phys. Rev.* **D 60**, 055004 (1999)
36. E. Fischbach and D. E. Krause, *Phys. Rev. Lett.* **82**, 4753 (1999)
37. H.B. Chan, V.A. Aksyuk, R.N. Kleiman, D.J. Bishop, and F. Capasso, *Science* 291, 1941 (2001)

théorie et expérience serait impossible sans tenir compte de cet effet.

De plus, les expériences récentes sont effectuées à température ambiante et il faut tenir compte des corrections thermiques. Tandis que l'effet de conductivité des métaux est important aux distances petites par rapport au micromètre, l'effet thermique devient non négligeable aux distances plus grandes que le micromètre. C'est pourquoi les deux effets sont habituellement traités indépendemment l'un de l'autre. Avec Cyriaque Genet, qui a effectué sa thèse sous ma co-responsabilité de septembre 1999 à juillet 2002, nous avons calculé la force de Casimir en tenant compte en même temps des deux corrections ce qui conduit à des calculs relativement importants. Nous avons montré que l'approximation qui consiste à calculer les deux effets séparément n'est pas suffisante, quand on vise une précision de l'ordre du pourcent. Pour la même situation, nous avons aussi donné une estimation de la force de Casimir qui est facile à calculer mais néanmoins beaucoup plus précise que l'approximation utilisée auparavant [38, 39].

En collaboration avec P.A. Maia Neto de l'Université de Rio de Janeiro, et avec Brahim Lamine qui a effectué un stage de DEA sous ma co-responsabilité en printemps 2001, j'ai récemment commencé à étudier un nouveau sujet de recherche, toujours centré autour de l'étude des fluctuations du champ. Il s'agit de la diffusion des ondes gravitationnelles, donc des fluctuations du champ de gravité, et la décohérence induite par celles-ci. Nous avons en particulier étudié l'influence des ondes gravitationnelles sur le mouvement planétaire, par exemple la Lune autour de la Terre. Bien que l'effet des ondes gravitationnelles soit négligeable en ce qui concerne la dissipation du mouvement, la diffusion des ondes gravitationnelles galactiques par les planètes est le mécanisme dominant responsable de la décohérence dans leur mouvement [40, 41].

38. C. Genet, A. Lambrecht, and S. Reynaud, *Phys. Rev.* **A 62**, 012110 (2000)
39. C.Genet, A. Lambrecht, and S. Reynaud, *Int. J. Mod. Phys.* **A 17**, 761 (2002)
40. S. Reynaud, P. Maia Neto, A. Lambrecht, and M.T. Jaekel, *Europhys. Lett.* **54**, 135 (2001)
41. S. Reynaud, B. Lamine, A. Lambrecht, P. Maia Neto, and M.-T. Jaekel, *Int. J. Mod. Phys.* **A 17**, 1003 (2002)

Deuxième partie

Présentation détaillée des travaux

Coopérativité et corrélations dans les états atomes-champ

Pendant mon séjour à Londres de 1990 à 1991, j'ai travaillé au Blackett Laboratory dans le groupe du professeur Peter Knight sur la théorie des états intriqués *("entangled states")* et la préparation d'une superposition de deux états cohérents. Une telle superposition, appelée état "chat de Schrödinger", constitue une manifestation de la mécanique quantique dans le monde macroscopique. Depuis, un tel état a été crée et observé expérimentalement avec un nombre d'atomes et de photons très faible[1]. La mise en évidence expérimentale d'un "chat de Schrödinger" macroscopique reste un objectif particulièrement intéressant.

Dans ce contexte, je me suis intéressée à l'interaction d'atomes à deux niveaux avec un champ électromagnétique. Une telle interaction conduit à corréler les deux systèmes puisque le vecteur d'état du système composé ne peut plus être décrit comme le produit d'un état atomique par un état du champ[2]. La corrélation apparaît au cours de l'évolution temporelle du système mais elle peut également disparaître. Le degré de corrélation des deux systèmes donne des informations sur l'état quantique du champ. Dans le cas particulier où un seul atome interagit avec le champ, nous avons montré que l'évolution temporelle engendre un chat de Schrödinger dont l'état dépend de façon cruciale des conditions initiales mais aussi de l'existence d'autres états atomiques. Pour étudier d'autres possibilités de préparation expérimentale, j'ai aussi considéré le cas où le champ interagit simultanément avec plusieurs atomes. Les états des atomes se corrèlent entre eux via l'interaction avec le champ dans la cavité. Nous nous sommes en particulier servi des états collectifs de Dicke pour décrire ces effets coopératifs. Nous avons montré que la présence de plusieurs atomes diminue en général la pureté de l'état du champ mais qu'il existe cependant des cas particuliers pour lesquels la génération d'un chat de Schrödinger reste

1. X. Maître, E. Hagley, J. Dreyer, A. Maali, C. Wunderlich, M. Brune, J.M. Raimond, and S. Haroche, *J. Mod. Opt.* **44**, 2023 (1997)
2. H. Everett, *Rev. Mod. Phys.* **29**, 454 (1957)

possible.

Réduction du bruit quantique par la superradiance à deux photons

De 1991 à 1992 j'ai effectué ma thèse de Diplôme (équivalent au DEA) à l'Université d'Essen dans le groupe du professeur Fritz Haake. Ce travail de thèse a été consacré à une étude théorique de la génération d'états comprimés par la superradiance à deux photons. Je me suis en particulier efforcée d'évaluer la validité de la méthode semi-classique pour décrire les phénomènes d'interaction atomes-champ dans un régime quantique.

Le système étudié est un ensemble d'atomes dans une cavité micro-onde ouverte, la taille de l'échantillon étant supposée plus petite que la longueur d'onde du champ. Cette condition est par exemple satisfaite pour un ensemble d'atomes froids. Le phénomène de superradiance a été observé expérimentalement dans de tels systèmes[1, 2].

J'ai supposé que les atomes et le champ étaient couplés par une interaction à deux photons. Ce couplage change les fluctuations du champ car l'interaction dépend de l'intensité du champ. Les atomes sont initialement préparés dans l'état excité et leur évolution est décrite par le vecteur de Bloch. Si le nombre d'atomes est assez élevé, les atomes ont un comportement collectif et émettent ensemble un rayonnement superradiant[3]. L'intensité de cette superradiance n'augmente pas de façon linéaire, comme pour la fluorescence habituelle, mais de façon quadratique avec le nombre d'atomes dans l'échantillon. L'impulsion émise par les atomes est beaucoup plus intense et étroite qu'une impulsion de fluorescence ordinaire. Nous avons montré que le système produit de la lumière non-classique avec une réduction de bruit en quadrature du champ depuis 13% pour une cavité de basse finesse jusqu'à 65% dans le cas où les pertes dues aux miroirs de la cavité deviennent négligeables.

J'ai aussi étudié l'évolution d'un tel système par une méthode semi-classique de relaxation[4] où on remplace les opérateurs par des nombres complexes. La dynamique des va-

1. F. Gounand, M. Hugon, P.R. Fournier, and J. Berlande, *J. Phys.* **B 12**, 547 (1979)
2. M. Gross and S. Haroche, *Phys. Rep.* **93**, 308 (1982) et leurs références
3. R.H. Dicke, *Phys. Rev.* **93**, 99 (1954)
4. R.W. Zwanzig, *Physica* **33**, 119 (1964)

riables classiques reproduit celle des opérateurs. Les fluctuations quantiques sont simulées par la prise en considération d'un ensemble de trajectoires. La méthode semi-classique non-linéaire s'est avérée être un outil puissant et efficace de simulation de l'évolution quantique du système. Elle donne des résultats corrects non seulement dans la limite macroscopique d'un grand nombre d'atomes et de photons dans la cavité, mais aussi pour des situations microscopiques où quelques atomes interagissent avec quelques photons. Le seul cas où la méthode semi-classique perd sa validité est celui où tous les atomes sont excités dans l'état initial en l'absence de champ. L'état évolue alors exclusivement à cause des fluctuations du vide, et les fluctuations initiales sont amplifiées d'une façon tellement importante au cours de l'évolution qu'elles ne sont plus négligeables par rapport aux valeurs moyennes.

Atomes froids et fluctuations quantiques

En 1992 j'ai commencé mon travail de thèse de doctorat au Laboratoire Kastler Brossel de l'Ecole Normale Supérieure et de l'Université Paris VI dans l'équipe d'Elisabeth Giacobino. A cette époque, le piégeage des atomes permettait depuis peu d'obtenir dans une petite cellule un nuage dense d'atomes quasiment immobiles. Cependant, les caractéristiques du nuage d'atomes froids utilisé pour des expériences d'optique quantique ou d'optique non-linéaire avaient été assez peu étudiées. Mon travail a consisté à développer cette étude sur le plan expérimental et théorique et à utiliser ce milieu non-linéaire pour réduire les fluctuations quantiques d'un faisceau laser, qui interagit avec le nuage atomique.

Les atomes sont placés au milieu d'une cavité optique pour renforcer l'interaction entre les atomes et le faisceau. Dans ce cas, le phénomène à la base de la réduction du bruit s'identifie à la bistabilité par effet Kerr optique connu depuis longtemps[1]. Un milieu Kerr idéal est un milieu purement dispersif, dont l'effet sur la lumière peut être complètement décrit par un coefficient $\chi^{(3)}$. Il n'y a pas de niveaux résonnants, et par conséquent il n'existe ni absorption ni émission spontanée. Quand la lumière traverse le milieu Kerr, le seul effet qu'elle subit consiste en un déphasage non-linéaire, qui dépend de l'intensité. L'interaction est amplifiée en plaçant le milieu Kerr dans une cavité. La possibilité de génération d'états comprimés du champ par ce phénomène a été évoquée pour la première fois en 1982[2,3]. Pour certaines valeurs des paramètres, le système composé a un comportement bistable et c'est au voisinage des points tournants de la bistabilité que la réduction du bruit quantique est maximale.

Par rapport à un milieu Kerr idéal, les atomes ont des résonances et constituent donc un milieu réel dissipatif. Le couplage avec la lumière correspond à une interaction de type $\chi^{(3)}$ qui présente l'avantage de pouvoir être exaltée par résonance avec une transition atomique. Elle présente aussi l'inconvénient que l'effet de réduction est dégradé par les fluctuations liées à l'émission spontanée. Une idée naturelle consiste alors à utiliser un

1. H.M. Gibbs, S.L. Mc Call, and T.N.C. Venkatesan, *Phys. Rev. Lett.* **36** (1976)
2. L.A. Lugiato and G. Strini, *Opt. Comm.* **41**, 67 (1982)
3. L.A. Lugiato and G. Strini, *Opt. Comm.* **41**, 374 (1982)

ensemble d'atomes froids comme milieu non-linéaire. Un piège magnéto-optique fournit dans une petite cellule un nuage dense d'atomes ayant une température telle que la largeur Doppler soit inférieure à la largeur naturelle de la transition. Les conditions sont alors excellentes pour une interaction avec un faisceau laser assez décalé en fréquence par rapport à la résonance atomique pour que l'absorption soit faible, tout en conservant un indice non-linéaire élevé. Ce milieu convient donc parfaitement aux besoins d'une expérience de réduction du bruit quantique via la bistabilité.

3.1 Dispositif expérimental et mesure du bruit quantique

Le nuage d'atomes de césium refroidis est préparé dans un piège magnéto-optique formé par un piège à césium en cellule, trois faisceaux laser rétro-réfléchis dans une configuration σ^+-σ^- et un champ magnétique quadrupolaire. Contrairement à la plupart des autres pièges, qui devaient refroidir les atomes à une température la plus basse possible, notre piège devait fournir un grand nombre d'atomes dans le faisceau sonde à une température inférieure à la température Doppler de telle sorte que la largeur Doppler soit plus petite que la largeur de la transition atomique.

Le nuage atomique est placé dans une cavité optique, comme indiqué sur la figure 3.1. La cavité est traversée par un faisceau sonde fourni par un laser Titane-Saphir asservi en fréquence. L'intensité moyenne est mesurée en transmission. Le faisceau sortant de la cavité est séparé du faisceau incident par un circulateur optique et superposé avec un oscillateur local. Les fluctuations du faisceau sonde sont ensuite mesurées à l'aide d'une détection homodyne. Le spectre de bruit est enregistré par un analyseur de spectre.

Il est apparu que les faisceaux pièges tendaient à introduire de l'excès de bruit dû à l'émission spontanée des atomes qui masquait toute réduction du bruit quantique. Nous avons alors décidé de couper le piège pendant la mesure afin de nous affranchir de toute perturbation liée aux faisceaux pièges. Cela a conduit à de nombreux problèmes. Tout d'abord, lors de la coupure du piège, nous avons observé l'apparition d'instabilités dans le champ moyen sortant de la cavité. Nous avons pu expliquer l'orgine de ces instabilités dues à une forte compétition entre deux processus non-linéaires, à savoir un processus rapide, la bistabilité due à l'effet Kerr, et un processus lent, le pompage optique entre les sous-niveaux Zeeman des atomes par le faisceau sonde. Les deux processus balayaient la cavité en sens opposé autour des points tournants de la bistabilité ce qui provoquait des

oscillations importantes de l'intensité[4]. La compréhension de l'origine des instabilités a permis de les supprimer, condition bien sûr indispensable à l'observation expérimentale d'une réduction du bruit quantique.

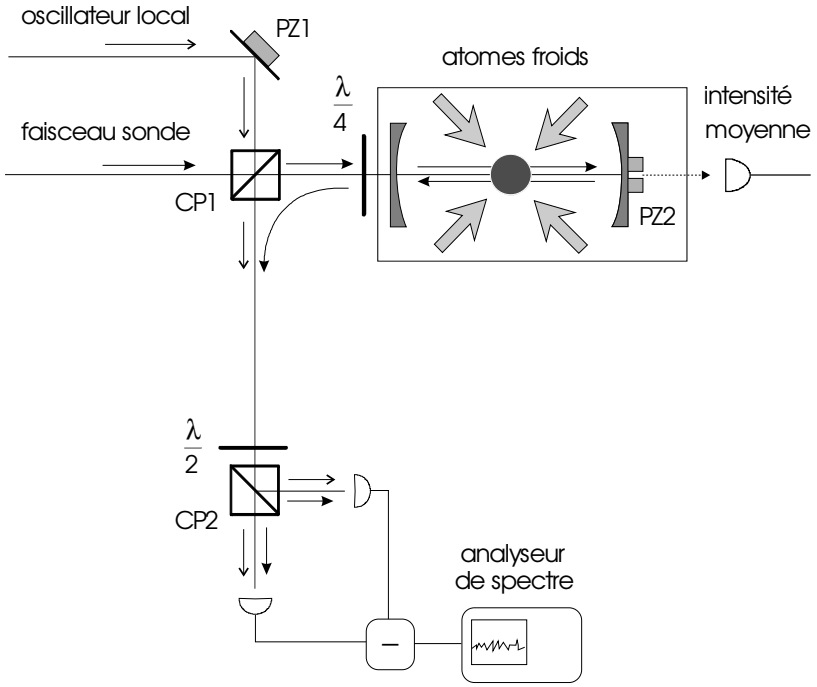

FIG. 3.1 – *Schéma d'expérience pour la réduction du bruit quantique à l'aide des atomes refroidis par laser.*

De plus, après la coupure du piège, les atomes quittent la zone d'interaction avec le faisceau sonde à cause de l'explosion du nuage et de l'influence de la gravité. On dispose seulement d'environ 20 ms pour effectuer les mesures de la courbe de bistabilité et du bruit quantique. Pendant ce temps, la fuite des atomes change l'indice de réfraction, ce qui conduit automatiquement à un balayage de la cavité sur la résonance. Pour les mesures du bruit, il n'est plus utile de moduler la longueur de la cavité.

En tenant compte de ces différents phénomènes, j'ai pu me placer dans les conditions optimales pour l'observation d'une réduction du bruit quantique. Le résultat montré sur la figure 3.2 correspond à des valeurs de 30 à 40% de réduction, supérieures à toutes les valeurs observées avec des milieux atomiques à l'époque. L'axe vertical correspond à la puissance du bruit en unités de bruit quantique standard et à l'intensité moyenne normalisée pour l'encadré. L'axe horizontal correspond au temps en milliseconde après le moment de la coupure du piège. Nous observons une réduction du bruit quantique de 40% au-dessous du bruit quantique standard sur la branche basse de la courbe de bistabilité

4. A. Lambrecht, E. Giacobino, and J.M. Courty, *Optics Comm.* **115**, 199 (1995)

au moment où la cavité commence à devenir résonnante avec le faisceau sonde[5]. Nous estimons l'erreur de la mesure à $\pm 10\%$ à cause du bruit sur le bruit. Les oscillations correspondent au balayage de la phase de l'oscillateur local.

Les deux courbes en tirets sont les prédictions du bruit quantique pour le bruit minimal et maximal dans le système. Elles enveloppent les oscillations et l'accord entre théorie et expérience est satisfaisant. Pour arriver à cet accord j'ai dû tenir compte d'un certain nombre d'effets dans l'expérience que je vais exposer dans la section suivante.

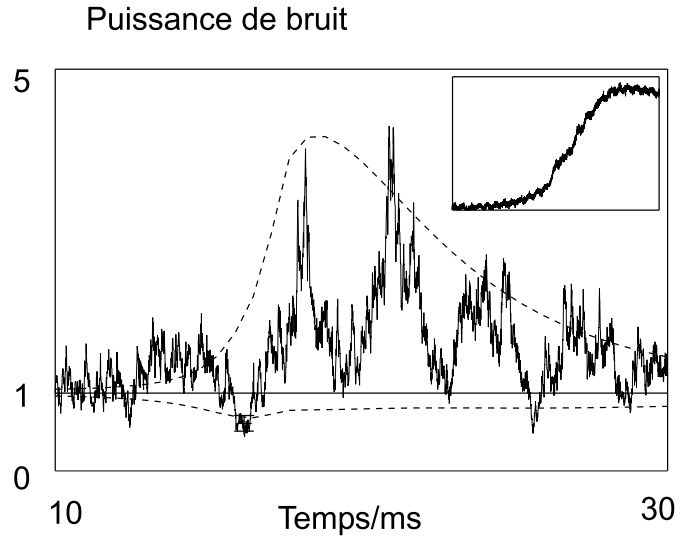

FIG. 3.2 – *Puissance de bruit et intensité moyenne correspondante (encadré) en fonction du temps après la coupure du piège. Avant que la cavité n'atteigne la résonance, on voit une réduction du bruit de l'ordre de* 40% *au-dessous du niveau du bruit quantique standard, indiqué par la ligne droite. La courbe en tirets est la prédiction théorique du bruit quantique pour le système.*

J'ai ensuite cherché à diminuer l'influence perturbatrice des faisceaux pièges en évitant une coupure complète du piège, grâce à une meilleure compréhension des effets perturbateurs. J'ai observé une réduction du bruit de 20% en présence du piège magnéto-optique, dans la limite où les faisceaux pièges saturent très peu la transition atomique[6].

3.2 Traitement théorique

Le milieu atomique est modélisé par un ensemble d'atomes à deux niveaux. Bien que l'atome à deux niveaux n'existe pas réellement dans la nature, il peut être réalisé

5. A. Lambrecht, J.M. Courty, S. Reynaud, and E. Giacobino, *Appl. Phys.* **B 60**, 129 (1995)
6. A. Lambrecht, T. Coudreau, A.M. Steinberg, and E. Giacobino, *Europhys. Lett.* **36**, 93 (1996)

approximativement dans une expérience. Nous avons calculé le bruit quantique par une méthode basée sur la théorie de la réponse linéaire[7]. Par rapport au traitement basé sur les équations différentielles stochastiques, il est plus intuitif[8] et en particulier, les étapes intermédiaires des calculs fournissent des interprétations beaucoup plus transparentes du comportement du système non-linéaire.

Lorsque le piège est coupé, le nuage d'atomes froids subit une explosion balistique liée à la température résiduelle dans le piège, ainsi qu'une chute libre sous l'influence de la pesanteur. La variation du nombre d'atomes dans le faisceau laser est tellement importante qu'elle permet de balayer la résonance de la cavité. L'étude de la réduction du bruit avec un signal qui dépend du temps constituait une situation inhabituelle. Pour décrire les fluctuations dans ces conditions, j'ai développé un traitement statistique pour modéliser à la fois le vol balistique et la chute des atomes après la coupure du piège. La variation du nombre d'atomes moyen en fonction du temps ainsi obtenue correspond de façon très satisfaisante aux mesures expérimentales de ce paramètre. De plus, ce traitement a montré que le nombre d'atomes dans le faisceau sonde était une variable quasi-stationnaire par rapport aux échelles de temps correspondant aux fréquences d'observation du bruit. Les fluctuations du faisceau sonde restent alors bien décrites par un spectre de bruit bien que le nombre moyen d'atomes varie au cours du temps. Le même raisonnement m'a aussi permis de calculer le spectre de fluctuations du nombre d'atomes. Leur influence sur les fluctuations du faisceau sonde restait négligeable dans les conditions de l'expérience, mais elle pouvait être appréciable dans d'autres situations où un jet atomique était utilisé à la place du nuage d'atomes froids[9].

Dans pratiquement tous les calculs de l'époque, l'effet du système bistable sur le bruit quantique d'un faisceau laser était décrit par une théorie qui traitait le faisceau sonde comme une onde plane. Ce modèle ne tenait pas compte de la variation de l'intensité moyenne du faisceau laser. Mais les atomes placés dans un faisceau gaussien voient des intensités lumineuses différentes et, par conséquent, ont des réponses aux fluctuations quantiques différentes. Dans le but d'améliorer le traitement du système bistable et en particulier de s'approcher des conditions expérimentales, j'ai étendu la méthode de calcul en traitant le faisceau sonde comme une onde gaussienne. D'une part, ceci a permis d'améliorer l'accord entre les prédictions théoriques et les résultats expérimentaux. En effet, la structure transverse du faisceau conduit à une dégradation de la réduction du bruit. D'autre part j'ai pu évaluer les conditions de validité des prédictions du modèle

7. S. Reynaud, C. Fabre, and E. Giacobino, *J. Opt. Soc. Am.* **B 4**, 1520 (1987)
8. B. Yurke, *Phys. Rev.* **A 29**, 408 (1984)
9. A. Lambrecht, E. Giacobino, and S. Reynaud, *Quant. Sem. Opt.* **8**, 457 (1996)

"onde plane". En particulier, ce dernier ne donne jamais des prédictions correctes dans un régime de forte réduction du bruit, sauf pour un milieu Kerr idéal [10].

Finalement j'ai étudié le couplage entre le mode fondamental et les modes d'ordres supérieurs de la cavité induit par des effets d'autofocalisation ou d'autodéfocalisation. En effet, un couplage entre modes peut transférer de l'excès de bruit d'un mode d'orde supérieur vers le mode fondamental et ainsi dégrader la réduction du bruit. Mon étude a montré que cet effet pouvait complètement détruire la réduction du bruit dans une cavité dégénérée [11]. Par contre, l'effet devient négligeable pour une cavité non-dégénérée, telle que nous l'avons utilisée dans l'expérience.

Une synthèse de ces développements théoriques qui tient compte à la fois de la structure transverse du faisceau sonde et de la variation du nombre d'atomes au cours du temps a permis de reproduire les spectres de bruit expérimentaux avec un accord satisfaisant. C'était la première fois qu'un tel accord était obtenu pour une expérience de réduction du bruit quantique utilisant des atomes comme milieu non-linéaire.

3.3 Publication jointe

Reproduction de l'article "Squeezing with cold atoms" A. Lambrecht, T. Coudreau, A.M. Steinberg, and E. Giacobino, *Europhys. Lett.* **36**, 93 (1996)

10. A. Lambrecht, J.M. Courty, and S. Reynaud, *J. Physique* **II 6**, 1133 (1996)
11. J.M. Courty and A. Lambrecht, *Phys. Rev.* **A 54**, 5243 (1996)

EUROPHYSICS LETTERS 10 October 1996

Europhys. Lett., **36** (2), pp. 93-98 (1996)

Squeezing with cold atoms

A. Lambrecht, T. Coudreau, A. M. Steinberg(*) and E. Giacobino

Laboratoire Kastler Brossel, UPMC, ENS et CNRS
Université Pierre et Marie Curie - case 74, F75252 Paris, France

(received 25 March 1996; accepted in final form 27 August 1996)

PACS. 32.80Pj – Optical cooling of atoms; trapping.
PACS. 42.50Lc – Quantum fluctuations, quantum noise, and quantum jumps.
PACS. 42.65Pc – Optical bistability, multistability, and switching.

Abstract. – Cold atoms from a magneto-optic trap have been used as a nonlinear ($\chi^{(3)}$) medium in a nearly resonant cavity. Squeezing in a probe beam passing through the cavity was demonstrated. The measured noise reduction is 40% for free atoms and 20% for weakly trapped atoms.

Soon after the first implementations of magneto-optic traps [1], [2], the strong nonlinear properties of laser-cooled atoms were recognized [3]-[5]. In particular, when cold atoms are driven by a slightly detuned probe laser beam inside an optical cavity, bistability is very easily observed at very low light powers [6]. This high nonlinear dispersion comes from the fact that, since the atoms are virtually motionless, the Doppler width is smaller than the natural linewidth and the probe frequency can be set close to atomic resonance. Such nonlinear behavior indicates that the system is capable of significantly modifying the quantum fluctuations of a probe beam, in particular leading to squeezing [7]. However, no experiment has been performed so far, where cold atoms have been used as a nonlinear medium. The use of atomic media in a squeezing experiment looked particularly promising in the absence of any Doppler broadening [8]-[10]. In this paper we report quantum noise reduction in a probe beam that has interacted with cold atoms in an optical cavity. Quadrature squeezing as large as 40% was measured at the output of the cavity. This value is the largest ever measured in an atomic medium. The squeezing was first observed in a free cloud, just after the trap had been turned off. It was also observed in a weakly bound trap with trapping beams turned down by a factor of 10 as compared to the original trap.

Up to now, all experiments of this type had been performed on atomic beams, where the transverse Doppler effect is small but often not completely negligible [11]-[13]. The best value of quantum noise reduction measured in that case is of the order of 20%. In contrast to atomic beams, cold atoms constitute a well-controlled medium, where theoretical models can in principle be fully tested against experimental results. To fit our experimental data, we have developed a theoretical model which fully takes into account the transverse structure of the probe beam [14] and which also considers the influence of additional noise sources like atomic-number fluctuations [15]. With this treatment we have obtained a correct prediction for the minimal and maximal noise power as a function of cavity detuning which fits the experimental result well.

(*) Present address: Department of Physics, University of Toronto, Toronto, ON M5S 1A7, Canada.

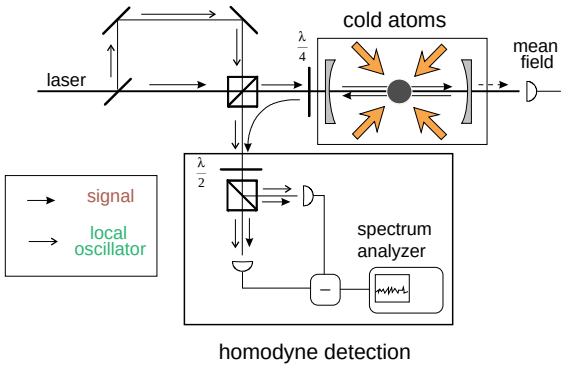

Fig. 1. – Experimental set-up designed to study the quantum fluctuations of a probe beam that has interacted with cold atoms in a nearly single-ended cavity.

The experimental set-up used to demonstrate squeezing with cold atoms has been described in detail elsewhere [16]. Here, we will only recall its main features. We investigate the phenomenon by sending a circularly polarized probe beam into a resonant optical cavity containing a cloud of cold cesium atoms prepared in a standard magneto-optic trap [1], [2]. With large and rather intense trapping beams, with the linewidth of the upper state on the low-frequency side of the $6S_{1/2}$, $F = 4$ to $6P_{3/2}$, $F = 5$ transition detuned 3 times, we obtain a cloud of 1 cm in diameter, with densities on the order of 10^9 atoms/cm^3. The temperature of the atoms is of the order of some mK. The number of trapped atoms interacting with the probe beam is measured with a method described below.

The cavity is a 25 cm long linear cavity, with a waist of 260 μm, built around the cell (fig. 1). The input mirror has a transmission coefficient of 10% and the end mirror is highly reflecting. The cavity is thus close to the "bad cavity" case, where the linewidth of the cavity (5 MHz) is larger than the radiative linewidth ($\gamma = 2.6$ MHz) *and which is expected to be the most favorable for squeezing.* The cavity is in the *horizontal* symmetry plane of the trap, making a 45° angle with the two trapping beams that propagate in this plane. The probe beam, generated by the same Ti : sapphire laser as the trapping beams, can be detuned by 0 to 130 MHz on either side of the $6S_{1/2}$, $F = 4$ to $6P_{3/2}$, $F = 5$ atomic transition. We measure the power of the probe beam transmitted through the cavity with a photodiode located behind the end mirror.

The field coming out of the cavity is separated from the incoming one by an optical circulator, made of a polarizing beamsplitter and a quarter-wave plate, and mixed with a local oscillator beam using the second input port of the same beamsplitter. Orthogonally polarized at the output of the beamsplitter, the signal and local oscillator beams are split into equal-intensity sum and difference fields by a half-wave plate and a second polarizing beam splitter. Both parts are detected by photodiodes with a quantum efficiency of 96%. The total homodyne efficiency is of the order of 90%. The ac parts of the photodiode currents are amplified and subtracted. The resulting signal is further amplified and sent to a spectrum analyzer and to a computer.

When the cavity length is scanned through resonance, bistability *due to the nonlinear dispersion of the cold atoms* is easily observed with incident powers as low as a few μW, as soon as the number N of interacting atoms is large enough. *The nonlinear phase shift of the cavity giving rise to bistability is proportional* to the cooperativity parameter C *also called bistability parameter*: $C = g^2N/\gamma T$ (where g is the atom-light coupling coefficient, γ the radiative linewidth of the transition and T the energy transmission coefficient of the mirror).

C is determined for each recording by measuring the ratio between the amplitudes of the bistability curve and of the resonance curve of the empty cavity.

The fluorescence emitted by the atoms excited by the trapping beams constitutes a source of excess noise for the experiment, which decreases the amount of quantum noise reduction attainable in principle. To avoid this effect, we turn off the trap during the noise measurements. With this method the available measurement time is limited to 20 to 30 ms, due to the expansion and the free fall of the atomic cloud. When the trap is turned off, the number of atoms interacting with the probe beam becomes time-dependent. The variation of the refractive index due to the escape of the atoms out of the probe beam provides a natural scan of the cavity across the resonance. In this way, the resonance peak is scanned in about 10 ms. However, under these conditions, the C value, being proportional to N, is no longer constant over the scan and it becomes necessary to adopt a specific model of its time dependence in order to interpret the noise spectra. A model for the variation of C with time can be obtained by calculating the variation of the linear phase shift caused by an expanding and falling ensemble of atoms in a Gaussian laser beam [15].

The atomic sample is supposed to have initially a Gaussian velocity and position distribution. Assuming, according to experimental conditions, that the Rayleigh length of the beam is much larger than the cloud size which itself is large compared to the beam waist, the variation of $C\,(t)$ is given by the product of a Lorentzian function representing the ballistic flight of the atoms with an exponential function accounting for the effect of gravity

$$C(t) = C(0)\frac{\tau_r^2}{\tau_r^2 + t^2} \exp\left[-\frac{t^4}{\tau_g^2(\tau_r^2 + t^2)}\right], \tag{1}$$

where $C(0)$ is the cooperativity value right after the trap is turned off; the time constant $\tau_r = \sigma_r/\sigma_v$ is the time for the atoms with temperature T_{at} and with mean velocity $\sigma_v = \sqrt{kT_{\mathrm{at}}/m}$ to fly through the cloud of radius σ_r and $\tau_g = 2\sqrt{2}\sigma_v/g$ is the time it takes for the falling atoms to accelerate to $2\sqrt{2}$ times their original thermal velocity.

To check this model, the cooperativity was experimentally studied as a function of time. Figure 2 shows the result of such a measurement. The experimental points are fitted by the theoretical expression given above for a cloud radius of 4 mm and a temperature of 5 mK, which corresponds to the characteristics of our trap. These parameters were subsequently used for calculations of the noise spectrum.

While the cavity is scanned across resonance by the escape of the atoms the field fluctuations of the output beam are monitored with the homodyne detection described above at a fixed analyzing frequency of 5 MHz. At the same time, the phase of the local oscillator is rapidly varied with a piezoelectric transducer in order to explore all noise quadratures of the probe beam. Since we have only 20–30 milliseconds to perform the measurement, the phase of the local oscillator must be scanned at frequencies of the order of kHz, which determines the analyzing bandwidth to be about 100 kHz. The bandwidth of the videofilter of the spectrum analyzer should be adjusted to avoid any distortion of the spectrum. As the filter of our spectrum analyzer (Tektronix 2753 P) did not have enough flexibility, we used numerical filters in the processing of the spectrum.

The spectrum shown in fig. 3 was obtained in such a manner. *The electronic noise was subtracted from the signal provided by the spectrum analyzer before the filtering process.* The averaged shot noise level (determined by blocking the cavity) is indicated by the straight line. It can be seen that the noise on the left-hand side of the figure, when the cavity is out of resonance, is at shot noise, whereas it goes below shot noise on the lower branch of the bistability curve. The observed squeezing is $(40 \pm 10)\%$. On the upper branch (right-hand part of the figure), large excess noise is observed in some quadratures. The powers of the

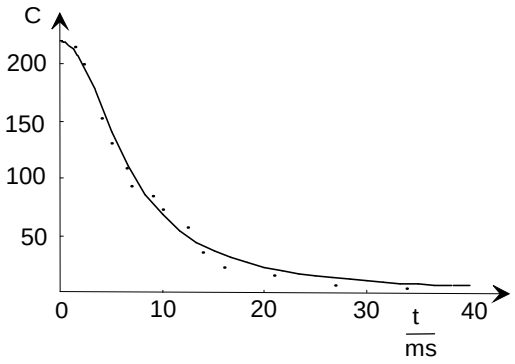

Fig. 2.

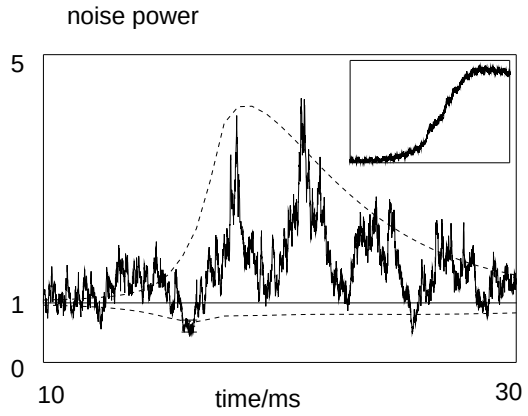

Fig. 3.

Fig. 2. – Time dependence of the cooperativity parameter C as the cloud of cold atoms is released at $t = 0$. The dots correspond to experiments as described in the text, the curves are derived from eq. (1).

Fig. 3. – Noise signal (ratio of the noise power to the shot noise power on a linear scale) taken with free atoms at a fixed observation frequency of 5 MHz as a function of time, while the cavity resonance is scanned by the departure of the atoms. Oscillations correspond to phase scan of the local oscillator. The broken lines are theoretical predictions for the minimal and maximal noise, the solid line indicates the shot noise level. Experimental parameters are atomic detuning: 52 MHz to the red, probe beam power: 25 μW. The error bar is due to the width of the noise trace. The insert shows the corresponding mean intensity (arbitrary units).

probe laser and local oscillator were 25 μW and 9 mW. *The large ratio of these powers ensures that the noise measured by the homodyne detection does not require any normalization, even if the probe beam reflected by the cavity does not have a constant intensity.* The detuning from atomic resonance was 52 MHz on the red side of the atomic resonance. The cooperativity parameter C was found to be 220 right after turning off the trap. The error bar for the squeezing measurement is due to the random fluctuations of the noise signal and is estimated to be ±10% at the minimum of fig. 3. The variation of the transmitted field reproduced in the insert of fig. 3 shows that the system is slightly below the bistability threshold. *The spectrum presented in fig. 3 shows the best squeezing value obtained in a series of experiments where several parameters such as the detuning of the probe field from the cavity and atomic resonances, the analyzing frequency and the atomic number were varied.*

In a second series of experiments, we have looked for quantum noise reduction in the presence of the trap. As mentioned above, the trapping beams with full power produce too much excess noise to allow observation of squeezing. However, we have been able to find a compromise by first trapping the atoms from the vapor with intense laser beams, and then turning down the trapping beams to about 1/10 of their original power. Under these conditions, the cooperativity parameter is on the order of 20. The noise spectrum shown in fig. 4 is recorded under similar conditions as above (detuning of 52 MHz and incident probe power of 16 μW) except that the cavity is scanned by means of a piezoelectric transducer while the number of atoms is constant during the measurement. The best value for squeezing obtained under such conditions is on the order of $(20 \pm 10)\%$.

Here, the quantum-noise reduction appears on the upper branch of the bistability curve. An interesting feature of the present result is that the steep edge on the left-hand side of

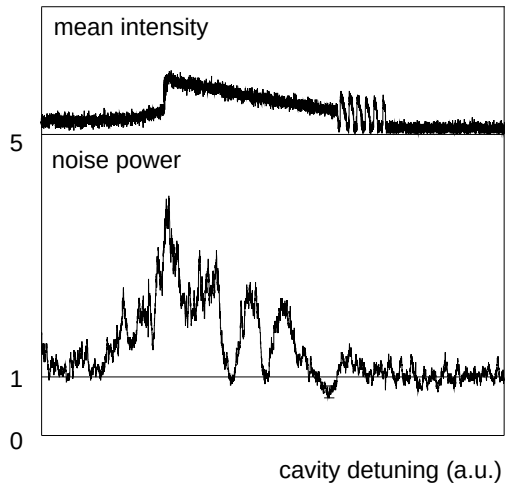

Fig. 4. – Noise signal (ratio of the noise power to the shot noise power on a linear scale) and mean intensity (arbitrary units) taken with weakly trapped atoms. The noise was measured at a fixed frequency of 5 MHz as a function of time, while the cavity length was swept with a piezoelectric transducer and the local oscillator phase was modulated rapidly. The solid line indicates the shot noise level. The error bar is determined as in fig. 3.

the bistability curve observed on the mean field (upper trace in fig. 4) is due to optical pumping, rather than to the saturation. Squeezing is reproducibly observed only in the range of parameters where the bistability curve originates from optical pumping. However, squeezing is still linked to the saturation of a two-level transition and the observed features can be interpreted as a consequence of the dynamical processes that take place in the cavity. As the cavity length is scanned, light from the probe beam enters the cavity and pumps the atoms towards the sublevels with the highest magnetic quantum number. At that stage, saturation of the atomic transition starts to take place, and this non-linearity is at the origin of squeezing in the output field. As was shown in [17], the instabilities that can be seen on the right-hand side of the curve (after the region where the squeezing occurs) come from a competition between optical pumping and the saturation of the atomic transition.

The experimental spectra for free atoms have been compared with the theoretical predictions given by the two-level atom model derived from ref. [14]. The measured experimental parameters are included in the model, which takes into account the Gaussian character of the beam. It is actually shown in ref. [14] that the plane-wave approximation is not valid in the range of experimentally obtainable saturation parameters where large squeezing appears. The minimal and maximal quantum noise were calculated in conditions reproducing those of the experiments, *i.e.* by including the variation in time of the cooperativity as represented in fig. 2 and the homodyne efficiency of 90%. The resulting spectra are shown by the broken lines in fig. 3. It can be seen that the agreement between theory and experiment is satisfactory.

As far as the squeezing in the presence of the trap is concerned, one can calculate the value of squeezing from the same two-level atom theory. The expected quantum noise reduction is then 20%, in good agreement with the observed value. Squeezing is here limited by the lower value of the cooperativity, which is only of the order of 20 in this experiment.

We have evaluated the potential effect of spurious noise sources in the experiments. In the experiment with free atoms, the excess noise due to the atomic-number fluctuations in the cold atom cloud in the process of expanding and of falling [15] was shown to have a spectrum

peaked at frequencies that are too low to affect the noise measurements at 5 MHz. Additional causes of excess noise are the repumping laser and the weak trapping beams in the second experiment. Their effects have been evaluated with a calculation based on the atomic-number fluctuations they produce. In the frequency range studied, we find their excess noise to be negligible for the rather low powers that are used for repumping and trapping beams.

This study shows that cold atoms provide a powerful medium for quantum optics. The measured squeezing is higher than any value observed in previous atomic experiments. *Even higher values are expected by increasing the ratio of the cavity linewidth to the atomic linewidth, i.e. by going more towards the bad-cavity limit.* One of the difficulties of our first set of experiments, in which the trapping beams had to be turned off during the noise measurements, is avoided in the second kind of experiments. It should be possible to go further by working with cold trapped atoms that do not interact at all with the trapping beams, for example, by using a "dark SPOT" set-up [18].

***

This work was supported in part by the EC contract ESPRIT BRA 6934 and the EC HMC contract CHRX-CT 930114.

REFERENCES

[1] Raab E., Prentiss M., Cable A., Chu S. and Pritchard D., *Phys. Rev. Lett.*, **59** (1987) 2631.
[2] Monroe C., Swann W., Robinson H. and Wieman C., *Phys. Rev. Lett.*, **65** (1990) 1571.
[3] Grison D., Lounis B., Salomon C., Courtois J. Y. and Grynberg G., *Europhys. Lett.*, **15** (1991) 149.
[4] Tabosa J., Chen G., Hu Z., Lee R. and Kimble H. J., *Phys. Rev. Lett.*, **66** (1991) 3254.
[5] Hilico L., Fabre C. and Giacobino E., *Europhys. Lett.*, **18** (1992) 685.
[6] Giacobino E., Courty J. M., Fabre C., Hilico L. and Lambrecht A., in *Fundamental of Quantum Optics III*, edited by F. Elhlotzky (Springer-Verlag) 1993.
[7] Giacobino E. and Fabre C. (Editors), *Quantum Noise Reduction in Optical Systems*, *Appl. Phys. B*, **55** (1992) 189.
[8] Castelli F., Lugiato L. A. and Vadacchino M., *Nuovo Cimento B*, **10** (1988) 183.
[9] Reid M. D., *Phys. Rev. A*, **37** (1988) 4792.
[10] Hilico L., Fabre C., Reynaud S. and Giacobino E., *Phys. Rev. A*, **46** (1992) 4397.
[11] Raizen M. G., Orozco L. A., Min Xiao, Boyd T. L. and Kimble H. J., *Phys. Rev. Lett.*, **59** (1987) 198.
[12] Hope D. M., Bachor H. A., Manson P. J., McLelland D. E. and Fisk P. T. H., *Phys. Rev. A*, **46** (1992) R1181.
[13] Grangier Ph., Poizat J. Ph., Grelu P., Castelli F., Lugiato L. A. and Sinatra A., *J. Mod. Opt.*, **41** (1994) 2241.
[14] Lambrecht A., Courty J. M. and Reynaud S., *J. Phys. II*, **6** (1996) 1.
[15] Lambrecht A., Giacobino E. and Reynaud S., *Atomic number fluctuations in a falling cold atom cloud*, to be published in *Quantum Semiclass. Opt.* (1996).
[16] Lambrecht A., Courty J. M., Reynaud S. and Giacobino E., *Appl. Phys. B*, **60** (1995) 129.
[17] Lambrecht A., Giacobino E. and Courty J. M., *Opt. Commun.*, **115** (1995) 199.
[18] Ketterle W., Davis K. B., Joffre M. A., Martin A. and Pritchard D. E., *Phys. Rev. Lett.*, **70** (1993) 2253.

La condensation de Bose-Einstein

4.1 L'expérience sur la condensation du Lithium

Après ma thèse, j'ai passé un an en stage post-doctoral à l'Institut Max-Planck pour l'Optique Quantique dans le groupe du Professeur T.W. Hänsch de 1995 à 1996. Pendant cette période, je me suis intéressée à l'étude expérimentale et théorique de la condensation de Bose-Einstein. Cet effet, qui venait d'être observé dans des milieux atomiques dilués[1,2], est une manifestation macroscopique de la statistique quantique des bosons.

Nous avons monté une expérience à Munich dans le but d'étudier d'une manière très détaillée les propriétés caractéristiques d'un condensat d'atomes de Lithium. Le premier objectif était de construire un dispositif permettant de piéger des atomes de Lithium à une densité et une température suffisantes pour atteindre la limite de la condensation de Bose-Einstein sans perdre trop d'atomes au cours de la préparation du condensat. Bien qu'à l'époque une expérience avec le Lithium ait déjà été réalisée dans un autre groupe de recherche[3], l'expérience restait particulièrement intéressante car le Lithium a une longueur de diffusion négative qui aurait théoriquement dû empêcher les atomes de former un condensat. De plus, la comparaison entre le Li^6 et le Li^7 devait permettre de distinguer l'effet des statistiques quantiques de type fermions et bosons.

Dans ce but, nous avons étudié des pièges magnétiques avec un gradient très important afin de confiner des atomes dans un volume très petit. Ces pièges étaient construits avec des aiguilles métalliques pointues. Les atomes de Lithium étaient tout d'abord piégés dans un piège magnéto-optique, puis transférés dans le piège magnétique. Ils devaient être ensuite soumis à une phase de refroidissement évaporatif.

Cette expérience n'a pas mené à la formation d'un condensat à cause de la limitation

1. M.H. Anderson, J.R. Ensher, M.R. Matthews, C.E. Wieman, and E.A. Cornell, *Science* **269**, 198 (1995)

2. K.B. Davis, M.-O. Mewes, M.R. Andrews, N.J. van Druten, D.S. Durfee, D.M. Kurn, and W. Ketterle, *Phys. Rev. Lett.* **75**, 3969 (1995)

3. C.C. Bradley, C.A. Sackett, J.J. Tollett, and R.G. Hulet, *Phys. Rev. Lett.* **75**, 1687 (1995)

en densité du nuage atomique dans le piège. Nous savons aujourd'hui que la durée de vie et la stabilité de ces condensats sont bien inférieures à celles d'un condensat avec un atome possédant une longueur de diffusion positive.

J'ai également participé à la construction d'une expérience sur la condensation des atomes de Rubidium. Cette expérience a abouti d'abord à la formation d'un condensat [4], puis à la réalisation d'un "laser à atomes" [5], bien après mon départ et je ne la détaillerai pas ici.

4.2 Les aspects thermodynamiques

Parallèlement à l'expérience décrite ci-dessus, j'ai mené une deuxième ligne de recherche concernant la condensation de Bose-Einstein en collaboration avec Gert-Ludwig Ingold de l'Université d'Augsbourg.

En particulier, nous avons étudié la condensation de Bose-Einstein dans un potentiel harmonique à une dimension, suite à une proposition d'expérience de condensation dans un tel système [6]. Pour ce système, les auteurs avaient trouvé une population macroscopique dans l'état fondamental et ils en avaient déduit l'existence d'un processus de condensation. Nous avons essayé de préciser les conditions nécessaires pour l'apparition d'un phénomène de condensation [7]. En effet, l'augmentation de la population de l'état fondamental ne donne pas une indication fiable, dans la mesure où elle n'est pas forcément accompagnée de signatures dans des grandeurs thermodynamiques. Dans ce cas, elle n'est pas associée à des propriétés de cohérence de l'ensemble des atomes.

Le cas du potentiel harmonique unidimensionnel présente une difficulté particulière. En effet, dans ce système, la limite thermodynamique n'est pas bien définie. Quand la fréquence propre du potentiel harmonique est fixée, la température critique diverge à la limite d'un nombre de particules infini. Il n'est donc pas évident de définir une transition de phase dans ce système. Pour contourner cette difficulté, nous avons étudié ce problème en analogie avec un puits de potentiel à deux dimensions. Les deux systèmes ont une densité d'état constante ce qui permet une comparaison quantitative. Par contre, dans le cas du puits bidimensionel, il a été démontré qu'aucun porcessus de condensation ne

4. T. Esslinger, I. Bloch, and T.W. Hänsch, *Phys. Rev.* **A 58**, R2664 (1998)
5. I. Bloch, T.W. Hänsch, and T. Esslinger, *Phys. Rev. Lett.* **82**, 3008 (1999)
6. W. Ketterle and N.J. van Druten, *Phys. Rev.* **A 54**, 656 (1996)
7. G. Ingold and A. Lambrecht, *Eur. Phys. J.* **D 1**, 29 (1998)

pouvait avoir lieu[8, 9].

Nous avons d'abord calculé la population dans l'état fondamental dans les deux systèmes en fonction de la température normalisée par la température critique. Les deux systèmes montrent le même comportement, à savoir une montée abrupte de la population de l'état fondamental pour un grand nombre de particules. Sachant qu'il n'y a pas de processus de condensation dans le puits de potentiel bidimensionel, il est évident que l'augmentation de la population de l'état fondamental n'est pas une indication suffisante.

Nous avons ensuite calculé la chaleur spécifique pour le potentiel harmonique unidimensionnel. Le résultat montre que la chaleur spécifique est une fonction monotone croissante de la température et qu'aucune signature d'une transition de phase n'est visible. Par conséquent, il n'y a pas condensation de Bose-Einstein dans ce système.

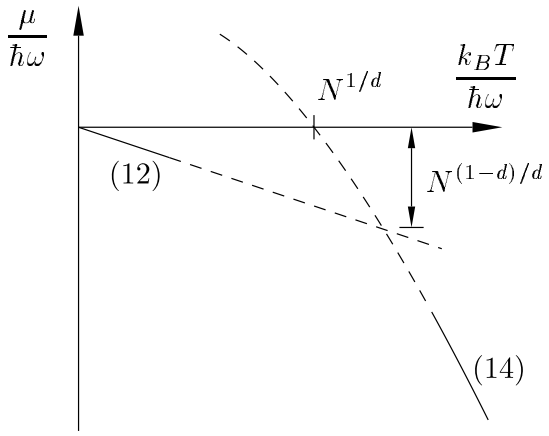

FIG. 4.1 – *Le potentiel chimique par mode d'oscillateur en fonction de la température normalisée. Les deux droites correspondent respectivement à la limite haute (14) et basse température (12) du potentiel chimique. Le zéro correspond à l'énergie de l'état fondamental.*

Nous avons finalement formulé un critère approprié pour savoir si, oui ou non, un processus de condensation de Bose-Einstein peut avoir lieu dans un potentiel harmonique de dimension entière arbitraire d. Une transition de phase a lieu seulement si le potentiel chimique est égal à l'énergie de l'état fondamental en-dessous de la température critique. On peut alors prouver l'impossibilité de la condensation de Bose-Einstein à une dimension en étudiant l'intersection entre la limite haute et basse température du potentiel chimique pour une dimension arbitraire. La figure 4.1 illustre l'argument. Les droites (12) et (14) correspondent respectivement aux limites basse et haute température.

Clairement, la valeur du potentiel chimique au point d'intersection dépend, pour toutes

8. S.R.Groot, G.J. Hooyman, and C.A. ten Seldam, *Proc. R. Soc. London* **A203**, 266 (1950)
9. R.M. Ziff, G. E. Uhlenbeck, and M. Kac, *Phys. Rep.* **32**, 169 (1977)

les dimensions $d > 1$, de l'inverse du nombre de particules et tend alors vers zéro dans la limite thermodynamique. Ceci permet une transition de phase à une température de l'ordre de $N^{1/d}$, en dessous de laquelle le potentiel chimique est égal à l'énergie de l'état fondamental. Dans le cas d'un potentiel harmonique unidimensionel, la valeur du potentiel chimique reste constante dans la limite thermodynamique ce qui exclut un processus de condensation. Les calculs et résultats de cette étude sont détaillés dans la publication ci-jointe.

4.3 Publication jointe

Reproduction de l'article "Thermodynamics of non-interacting bosons in low- dimensional potentials" G. Ingold and A. Lambrecht, *Eur. Phys. J.* **D 1**, 29 (1998).

Eur. Phys. J. D **1**, 29–32 (1998)

THE EUROPEAN PHYSICAL JOURNAL D

Thermodynamics of non-interacting bosons in low-dimensional potentials

Gert-Ludwig Ingold[1,a] and Astrid Lambrecht[2,b,c]

[1] Institut für Physik, Universität Augsburg, Memminger Str. 6, 86135 Augsburg, Germany
[2] Max-Planck-Institut für Quantenoptik, Hans-Kopfermann-Str. 1, 85748 Garching, Germany

Received: 17 February 1997 / Revised: 3 September 1997 / Accepted: 13 October 1997

Abstract. On the basis of a macroscopic ground state population it was argued recently that Bose-Einstein condensation should occur in a one-dimensional harmonic potential. We examine this situation by drawing analogies to bosons in a two-dimensional box, where the thermodynamic limit is well-defined. We show that in both systems although the ground state populations show sharp onsets at the critical temperature, the behaviour of the specific heat is analytic, which proves the absence of a phase transition in these systems.

PACS. 03.75.Fi Phase coherent atomic ensemble (Bose condensation) – 05.30.Jp Boson systems – 64.60.-i General studies of phase transitions

The experimental study of ultracold trapped Bose gases [1–3] has revived the interest in Bose-Einstein condensation in the regime of weak or even vanishing interaction. In these experiments the atoms are confined by external forces, which might be modelled by a three-dimensional harmonic potential. Recently it was suggested on the basis of results for the ground state population that in an effectively one-dimensional potential Bose-Einstein condensation should occur [4]. In the present paper we place the discussion of non-interacting bosons in a one-dimensional harmonic potential into a larger framework by drawing analogies to particles in a two-dimensional box with infinite walls, a system which has, in contrast to the former one, the advantage that a well-defined thermodynamic limit exists. Within this framework we address the conceptual problem whether a macroscopic ground state population is a sufficient indicator for Bose-Einstein condensation to appear or if in contrast, thermodynamic quantities have to be considered. In addition to the ground state population we study in particular the specific heat, calculated with a continuous density of states, which is permissible for large particle numbers. The result is confirmed by an analysis based on the discrete level structure.

Bose-Einstein condensation [5] is usually described within the grandcanonical ensemble where the average number of particles is given by

$$N = \int_0^\infty \mathrm{d}E \rho(E) \frac{z}{\exp(\beta E) - z}. \tag{1}$$

Here, $z = \exp(\beta\mu)$ is the fugacity with $\beta = 1/k_\mathrm{B}T$ and the chemical potential μ. The energy scale is chosen such that the minimum value of the d-dimensional external potential $U(\mathbf{r})$ equals zero. Then the classical density of states for particles of mass m

$$\rho(E) = \frac{1}{\Gamma(d/2)} \left(\frac{m}{2\pi\hbar^2}\right)^{d/2} \int \mathrm{d}V_\mathrm{cl} \left[E - U(\mathbf{r})\right]^{(d-2)/2}, \tag{2}$$

where the integration has to be taken over the classically accessible region, vanishes for negative energies. If $\rho(E) \to 0$ for small energies, N reaches a finite maximum even for the maximum value of the fugacity $z = 1$. Additional particles are then found in the ground state which is not included in the density of states (Eq. (2)). For a d-dimensional harmonic potential the density of states varies like E^{d-1} and therefore Bose-Einstein condensation is only expected for $d = 2$ and higher [6,7].

This approach has been criticized by various authors. For the three-dimensional harmonic potential it was shown that corrections to the density of states (Eq. (2)) lead to corrections to the Bose temperature, which are of order $N^{-1/3}$ [8]. Other work [9–13] has addressed the question whether there are effects due to the discreteness of the energy levels which is not included in equation (2). In this context, it was recently claimed that Bose-Einstein condensation can be found even in the case of a one-dimensional harmonic potential [4].

[a] e-mail: `gert.ingold@physics.uni-augsburg.de`
[b] *Present and permanent address*: Laboratoire Kastler Brossel, Université Pierre et Marie Curie, Ecole Normale Supérieure, Centre National de Recherche Scientifique, 4 place Jussieu, BP74, 75252 Paris cedex 05, France
[c] e-mail: `astrid@spectro.jussieu.fr`

The argument given by Ketterle and van Druten is as follows. The relative ground state occupation N_0/N is calculated by taking into account the discreteness of the energy levels. As an example, we show in Figure 1a results for particle numbers varying between $N = 10^2$ and $N = 10^7$ particles. The temperature is scaled with a critical temperature determined by [4]

$$N = \frac{k_\mathrm{B} T_\mathrm{c}}{\hbar\omega} \ln\left(\frac{2k_\mathrm{B} T_\mathrm{c}}{\hbar\omega}\right), \tag{3}$$

where $\hbar\omega$ is the energy level spacing. It can be seen that with increasing number of particles N, the crossover between finite and vanishing ground state occupation sharpens. This behaviour is similar to the three-dimensional case, where Bose-Einstein condensation occurs, and it is thus concluded that there is condensation even in one dimension.

However, in a one-dimensional harmonic potential with fixed frequency ω the critical temperature T_c diverges in the limit $N \to \infty$. It is therefore not obvious how a phase transition in such a system may be defined. Furthermore, a rescaling with T_c is then equivalent to widening the harmonic potential when increasing the particle number, *i.e.* lowering the oscillation frequency towards zero (*cf.* Eq. (3)).

We now address the question whether a macroscopic ground state population is a sufficient indicator to define Bose-Einstein condensation in this system. In this respect it is useful to consider another system with a constant density of states $\rho(E)$. From equation (2) we find for a two-dimensional box of length L

$$\rho(E) = \frac{mL^2}{2\pi\hbar^2}. \tag{4}$$

Here a proper thermodynamic limit $N, L \to \infty$, with constant density N/L^2, can be performed and the notion of phase transition is well defined. While $(2\pi\hbar^2/k_\mathrm{B}m)(N/L^2)$ provides the temperature scaling, either N or L^2 determine how closely the thermodynamic limit is approached. For the two-dimensional box it is generally accepted that, in contrast to the three-dimensional box, no phase transition occurs (see [9], where the authors derive this conclusion, although the specific heat for the two-dimensional box is not correctly reproduced [14]).

An analogy to the one-dimensional harmonic oscillator may be drawn by comparing its density of states $\rho(E) = 1/\hbar\omega$ to expression (4). The temperature scale is now given by $N\hbar\omega$ while the thermodynamic limit is reached either for $N \to \infty$ or $\hbar\omega \to 0$. For fixed frequency ω the limit $N \to \infty$ leads to a change in the temperature scale. A phase transition should therefore become apparent when rescaling the temperature with N. For later purposes we note that the dimensionless density for the two-dimensional box $N(\lambda_\mathrm{T}/L)^2$, where $\lambda_\mathrm{T} = (2\pi\hbar^2\beta/m)^{1/2}$ is the thermal de Broglie wavelength, corresponds to $N\beta\hbar\omega$ for the one-dimensional harmonic oscillator.

To check the analogy between the two systems, we have calculated the ground state population for the two-dimensional box using discrete energy levels. Following

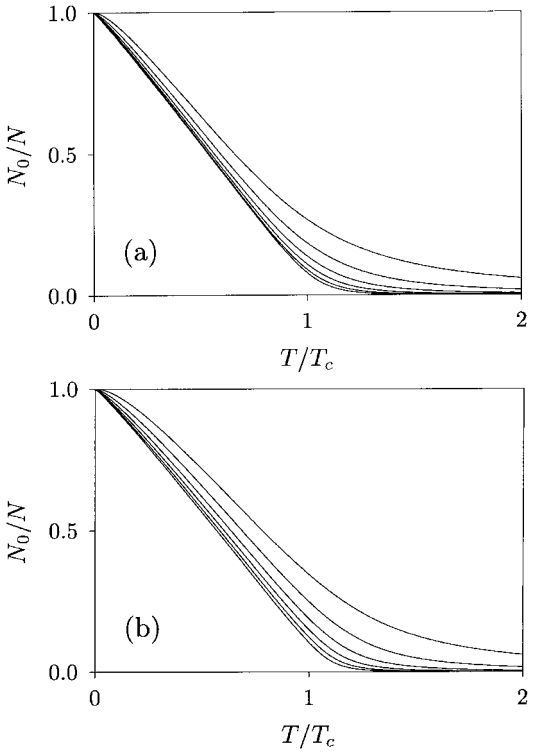

Fig. 1. Relative ground state occupation N_0/N (a) for the one-dimensional harmonic potential and (b) for the two-dimensional box as a function of temperature T scaled with the critical temperature T_c. The numerical results obtained by taking into account the discrete level structure correspond to $N = 10^2, 10^3, 10^4, 10^5, 10^6$, and 10^7 particles from the upper right to the lower left curve.

the reasoning of Ketterle *et al.* [4] we define a critical temperature *via* $N = 2(L/\lambda_{\mathrm{T,c}})^2 \ln(L/\lambda_{\mathrm{T,c}})$ and obtain the results shown in Figure 1b. Clearly, as in the case of a one-dimensional harmonic potential, the ground state population for large N shows a rather sharp transition to macroscopic values below the critical temperature. No qualitative difference in the behaviour of the two systems is visible. The definition of Bose-Einstein condensation *via* a macroscopic ground state population enters therefore in conflict with predictions for the two-dimensional box. For a good criterion for condensation one instead has to resort to thermodynamic quantities.

To this purpose we consider in particular the specific heat, which recently has become accessible experimentally [15]

$$C = \frac{\mathrm{d}}{\mathrm{d}T} \int_0^\infty \mathrm{d}E \rho(E) \frac{Ez}{\exp(\beta E) - z}. \tag{5}$$

Here C is expressed through the continuous density of states $\rho(E)$, which will prove to be sufficient for our purposes. Evaluating equation (5) with constant density of states $\rho = 1/\hbar\omega$ yields

$$\frac{C}{Nk_\mathrm{B}} = \frac{2}{N\beta\hbar\omega} \sum_{n=1}^{\infty} \frac{z^n}{n^2} + \frac{1}{N\hbar\omega} \frac{\ln(1-z)}{z} \frac{\mathrm{d}z}{\mathrm{d}\beta} \tag{6}$$

and for the fugacity we obtain from (1)

$$z = 1 - \exp(-\beta\hbar\omega N). \tag{7}$$

This expression is correct for high temperatures but breaks down when z becomes of the order of its zero temperature value $N/(N+1)$, which is the case at temperatures of the order of the critical temperature defined by equation (3). At these temperatures z almost takes the value of one and the difference to the approximation (7) is at most of order $1/N$. Although equation (7) could not be used to determine the ground state population at low temperatures, it allows us to obtain the correct result for the specific heat. Corrections of order $1/N$ to the fugacity are negligible in the first term on the right hand side of equation (6) whereas they are potentially dangerous in the logarithmic term. However in the temperature range of interest this term is strongly suppressed because $\mathrm{d}z/\mathrm{d}\beta$ becomes exponentially small.

With equation (7) the specific heat takes the form

$$\frac{C}{Nk_\mathrm{B}} = \frac{2}{y}\sum_{n=1}^{\infty}\frac{(1-\exp(-y))^n}{n^2} - \frac{y}{\exp(y)-1} \tag{8}$$

with $y = \beta\hbar\omega N$. The particle number N enters this result only through a linear rescaling of the specific heat and the temperature. A similar result has been derived for a canonical ensemble [12]. According to the above discussion the sum in equation (8) determines the low temperature behaviour of the specific heat which is then found to be

$$\frac{C}{Nk_\mathrm{B}} = \frac{\pi^2}{3}\frac{1}{y} = \frac{\pi^2 k_\mathrm{B}}{3N}\frac{1}{\hbar\omega}T. \tag{9}$$

In view of the analogy between the one-dimensional harmonic oscillator and the two-dimensional box the specific heat of the latter one then becomes

$$\left(\frac{C}{Nk_\mathrm{B}}\right)_{\mathrm{2dbox}} = \frac{\pi^2 k_\mathrm{B}}{3N}\frac{mL^2}{2\pi\hbar^2}T. \tag{10}$$

In Figure 2, expression (8) is depicted by the full line with its low temperature approximation (9). The dashed line shows the result of a numerical calculation for 10 particles in a one-dimensional harmonic potential taking into account the discreteness of the spectrum. Even for such small N, equation (8) gives a rather good approximation. For 100 or more particles the difference between the result for the one-dimensional harmonic oscillator based on the discrete level structure on one hand and equation (8) on the other hand becomes negligible. For the two-dimensional box the convergence of the calculation using discrete energies to the result for a constant density of states is somewhat slower due to the higher dimensionality of the system.

Thus for large particle numbers the form of the specific heat becomes independent of N and neither singularities build up in the thermodynamic limit $N \to \infty$ nor a maximum appears at the critical temperature like the one found in the result sketched in [9]. Furthermore, the limiting result (8) is analytic for finite temperatures and we conclude that, as in the two-dimensional box, there is no phase transition in a one-dimensional harmonic potential.

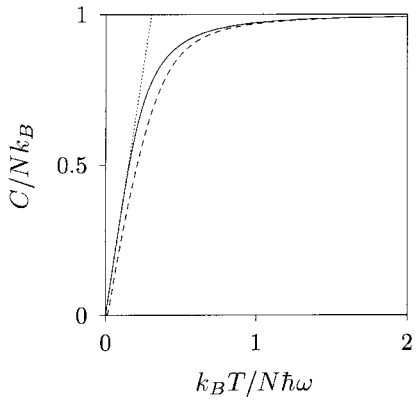

Fig. 2. Specific heat C of a Bose gas in a one-dimensional harmonic potential as a function of temperature T. The full line represents the result of a calculation with constant density of states with its low temperature approximation (dotted line), while the dashed line is for $N = 10$ particles taking into account the discrete level structure. For $N = 10$ equation (3) yields $k_\mathrm{B}T_\mathrm{c}/N\hbar\omega = 0.454$. Similar numerical results have been obtained in [12,13].

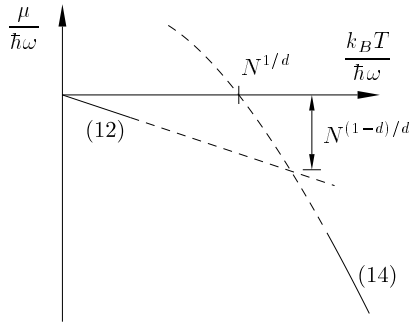

Fig. 3. Illustration of the reasoning leading to equation (15). The lines correspond to the upper bound of the chemical potential (12) and the high temperature approximation (14), respectively.

The difference between the behaviour of a non-interacting Bose gas in a one-dimensional and higher-dimensional harmonic potentials may also be understood in terms of discrete energy levels. An appropriate criterion for the possibility of Bose-Einstein condensation to occur is whether in the thermodynamic limit $N \to \infty$ the chemical potential equals the ground state energy below the critical temperature or not. In the following we will show that this criterion is not met in a one-dimensional harmonic potential. We start out with the average number of particles in a grand canonical description

$$N = \frac{1}{\exp(-\beta\mu)-1} + \sum_{n=1}^{\infty}\frac{g_n^{(d)}}{\exp[\beta(\hbar\omega n-\mu)]-1}, \tag{11}$$

where $g_n^{(d)}$ is the degeneracy of the n-th eigenlevel of the d-dimensional harmonic potential. The first term on the

right-hand-side of equation (11) represents the population of the ground state.

One derives an upper bound of the chemical potential at arbitrary temperatures by considering a situation where the excited states do not contribute to the number of particles

$$\frac{\mu}{\hbar\omega} \leq -\frac{1}{N}\frac{k_{\mathrm{B}}T}{\hbar\omega}. \tag{12}$$

Naturally this case coincides with the low temperature limit $\beta\hbar\omega \gg 1$. Chemical potential and temperature are taken with respect to the energy level spacing $\hbar\omega$ of the harmonic potential. This is the appropriate choice if ω is kept fixed in the thermodynamic limit.

For high temperatures the ground state population becomes very small and therefore $\beta|\mu| \gg 1$. We may then approximate expression (11) for the average particle number by

$$N = \exp(\beta\mu)\sum_{n=0}^{\infty} g_n^{(d)} \exp(-\beta\hbar\omega n) = \frac{\exp(\beta\mu)}{(1-\exp(-\beta\hbar\omega))^d}. \tag{13}$$

Except for very low particle numbers the high temperature regime implies $\beta\hbar\omega \ll 1$. The chemical potential is then found as

$$\frac{\mu}{\hbar\omega} = \frac{\ln\left[N(\beta\hbar\omega)^d\right]}{\beta\hbar\omega} \tag{14}$$

and equals zero at $k_{\mathrm{B}}T/\hbar\omega = N^{1/d}$. Since the ground state energy was taken to be zero, the high temperature result suggests that there might be Bose-Einstein condensation below a temperature $\hbar\omega N^{1/d}/k_{\mathrm{B}}$. A more detailed analysis leads to a prefactor of the order of one.

To exclude the existence of a phase transition in a one-dimensional harmonic potential, it is sufficient to consider the upper bound (12) for the chemical potential at its intersection with the high temperature expression (14). There the value of the chemical potential becomes (*cf.* Fig. 3)

$$\frac{\mu}{\hbar\omega} = -N^{(1-d)/d}. \tag{15}$$

For $d = 1$ this is of order one independently of the particle number N and one expects a smooth crossover at the intersection point. This behaviour forbids a phase transition in the one-dimensional case. On the other hand, for $d \geq 2$, the chemical potential at the intersection vanishes for $N \to \infty$ opening the possibility of a sharp transition at a temperature of order $N^{1/d}$, below which the chemical potential strictly equals the ground state energy. We thus recover the predictions of the theory based on the density of states (2).

In conclusion, by studying the specific heat and using an analogy with two-dimensional box systems we have shown that a macroscopic ground state population alone is not a sufficient indicator of a phase transition. In higher dimensional systems which show a condensation phenomenon a macroscopic ground state population is always accompanied by some signature in the specific heat or higher derivatives of the free energy. Their absence for the case of a one-dimensional harmonic potential leads us to conclude that no phase transition occurs in this system. The main interest of Bose-Einstein condensation lies in the particular coherence properties of condensates. Then the question arises to which extent the ground state population can give information about coherence. The results of this paper show that it might be necessary, maybe not sufficient, to carefully study thermodynamic quantities as well.

References

1. M.H. Anderson, J.R. Ensher, M.R. Matthews, C.E. Wieman, E.A. Cornell, Science **269**, 198 (1995).
2. C.C. Bradley, C.A. Sackett, J.J. Tollett, R.G. Hulet, Phys. Rev. Lett. **75**, 1687 (1995).
3. K.B. Davis, M.-O. Mewes, M.R. Andrews, N.J. van Druten, D.S. Durfee, D.M. Kurn, W. Ketterle, Phys. Rev. Lett. **75**, 3969 (1995).
4. W. Ketterle, N.J. van Druten, Phys. Rev. A **54**, 656 (1996).
5. F. London, Phys. Rev. **54**, 947 (1938).
6. V. Bagnato, D.E. Pritchard, D. Kleppner, Phys. Rev. A **35**, 4354 (1987).
7. V. Bagnato, D. Kleppner, Phys. Rev. A **44**, 7439 (1991).
8. S. Grossmann, M. Holthaus, Z. Naturforsch. **50a**, 921 (1995).
9. S.R. de Groot, G.J. Hooyman, C.A. ten Seldam, Proc. R. Soc. London Ser. A **203**, 266 (1950).
10. S. Grossmann, M. Holthaus, Z. Phys. B **97**, 319 (1995).
11. K. Kirsten, D.J. Toms, Phys. Rev. A **54**, 4188 (1996).
12. F. Brosens, J.T. Devreese, L.F. Lemmens, Solid St. Comm. **100**, 123 (1996).
13. T. Haugset, H. Haugerud, J.O. Andersen, Phys. Rev. A **55**, 2922 (1997).
14. R.M. Ziff, G.E. Uhlenbeck, M. Kac, Phys. Rep. **32**, 169 (1977).
15. J.R. Ensher, D.S. Jin, M.R. Matthews, C.E. Wieman, E.A. Cornell, Phys. Rev. Lett. **77**, 4984 (1996).

Effets mécaniques des fluctuations du vide

Depuis Octobre 1996, je suis chargée de recherche au CNRS au Laboratoire Kastler Brossel. Je travaille dans l'équipe "Fluctuations quantiques et relativité" de Serge Reynaud. Mes sujets de recherche sont essentiellement organisés autour des effets mécaniques des fluctuations du vide.

La théorie quantique a profondément changé notre conception de l'espace vide. En effet, même quand on a pompé toute la matière d'une enceinte fermée et qu'on a refroidi cette enceinte jusqu'au zéro de température pour éliminer le rayonnement du corps noir, il reste encore dans l'enceinte des fluctuations quantiques irréductibles de champ. Ces fluctuations, aussi appelées fluctuations du vide ou fluctuations de point zéro, correspondent à une énergie moyenne de $\hbar\omega/2$ par mode du champ de fréquence ω.

Les fluctuations du vide ont des conséquences physiques observables. Dans le domaine des forces macroscopiques en particulier, deux miroirs plans, parallèles, placés à une distance L l'un de l'autre dans le vide subissent une force attractive, la force de Casimir[1]. Elle est due à la pression de radiation des fluctuations du vide modifiées par la cavité que forment ces deux miroirs. Cette force, bien que faible, est maintenant mesurée avec une bonne précision. Comme je le présenterai dans la deuxième section de ce chapitre, l'accord entre les résultats expérimentaux et la théorie est satisfaisant pourvu que celle-ci prenne en compte aussi bien la réflexion imparfaite des miroirs utilisés dans les expériences que les corrections de température.

La pression de radiation du vide a aussi des conséquences physiques observables sur le mouvement d'un diffuseur dans le vide, où elle est responsable d'une force de réaction de rayonnement. Celle-ci tend à s'opposer au mouvement du diffuseur, dès que celui-ci suit un mouvement à accélération non-uniforme[2]. Ceci est une preuve, parmi d'autres, du fait que l'on ne peut pas oublier les effets des fluctuations du vide, y compris quand on étudie le mouvement mécanique d'objets macroscopiques.

1. H.B.G. Casimir, *Proc. Kon. Ned. Akad. Wetenshap* **51**, 793 (1948)
2. S.A. Fulling and P.C.W. Davies, *Proc. R. Soc. London* **A 348**, 393 (1976)

Les fluctuations du vide soulèvent des problèmes importants à l'interface entre théorie quantique d'une part, phénomènes gravitationnels d'autre part. En particulier, la densité d'énergie calculée dans la théorie quantique est une intégrale divergente et, même après la prise en considération d'une fréquence de coupure haute fréquence, elle est des ordres de grandeur plus grande que la densité d'énergie moyenne observée autour de nous par l'intermédiaire des phénomènes gravitationnels. Cette "catastrophe du vide", relevée dès 1916 par Nernst[3], reste aujourd'hui encore un problème non résolu, directement lié au "problème de la constante cosmologique"[4].

Il existe cependant des questions parfaitement bien définies dans ce domaine, auxquelles on peut apporter des réponses correctes dans le cadre théorique actuel, et qui ont des liens directs avec les principes généraux de la relativité d'Einstein tels que le principe d'équivalence ou le principe de relativité du mouvement.

5.1 Relativité du mouvement dans le vide quantique

La pression de radiation des fluctuations du vide est elle-même une quantité fluctuante. Tout diffuseur subit donc des fluctuations de force, de valeur moyenne nulle lorsqu'il est seul et immobile dans le vide. Lorsque le diffuseur se déplace dans le vide, l'équilibre entre les fluctuations de force des deux cotés du miroir est perturbé. Le miroir subit alors une force moyenne s'opposant à son mouvement. Comme dans le cas bien connu du mouvement Brownien, cette force motionnelle peut se comprendre comme l'effet cumulatif à long terme des fluctuations de force. Comme je vais le présenter maintenant, j'ai étudié cet effet motionnel pour des systèmes quantiques simples comme un miroir et une cavité en mouvement dans le vide.

5.1.1 Le rayonnement motionnel

Quand un miroir oscille dans le vide, la force de réaction de rayonnement tend à freiner son mouvement. Par conservation de l'énergie, le miroir émet des photons dans le vide. Cette radiation motionnelle met en évidence l'influence réciproque entre les fluctuations du vide et le mouvement mécanique.

Il existe une autre façon d'interpréter la force motionnelle. Lorsque le miroir oscille dans le vide, le couplage entre la pression de radiation des modes vides et le mouvement mécanique se traduit par un processus paramétrique. Ce processus, analogue à la

3. W. Nernst, *Verh. Deut. Phys. Ges.* **18**, 83 (1916)
4. R. Adler, B. Casey, and O.C. Jacob, *Am. J. Phys.* **63**, 620 (1995)

génération des états comprimés, crée des paires de photons. L'amortissement du mouvement du miroir, dû à la conservation de l'énergie, correspond exactement à la force motionnelle.

Ce rayonnement est bien sûr nul pour un mouvement à vitesse uniforme du miroir, par suite de l'invariance de Lorentz des fluctuations du vide. Si le miroir est en mouvement uniformément accéléré, le rayonnement émis est également nul. Ceci est dû à une symétrie plus large, qui est l'invariance conforme du vide électromagnétique. Le rayonnement induit par le mouvement n'apparaît que lorsque l'accélération dépend du temps, comme par exemple dans le cas d'une oscillation harmonique du miroir.

Ces résultats ont un grand intérêt conceptuel, parce qu'ils relient les propriétés dissipatives des fluctuations du vide et les symétries de la théorie électromagnétique[5,6]. Cependant, ces effets des fluctuations du vide n'ont pas été étudiés expérimentalement jusqu'à présent. La raison essentielle en est que les signatures mécaniques qui leur sont associées apparaissent comme de petites perturbations du mouvement de n'importe quel objet macroscopique. En effet, les forces correspondantes sont proportionnelles à $\hbar$ et sont donc difficiles à détecter. Par contraste, le nombre de photons émis, qui est donné par l'énergie rayonnée divisée par l'énergie d'un seul photon, ne dépend plus de $\hbar$. Du point de vue d'une réalisation expérimentale, cet argument favorise clairement la détection du rayonnement, d'autant plus qu'il existe des techniques très sensibles pour la détection de photons.

Le rayonnement émis par un miroir unique oscillant dans le vide est trop petit pour être observé expérimentalement avec les techniques actuelles. En vue d'une mise en évidence des effets dissipatifs du vide quantique, une idée très naturelle consiste alors à étudier le rayonnement induit par le mouvement d'une cavité ayant une grande finesse[7]. Cette idée permet de bénéficier d'une exaltation résonnante du rayonnement motionnel. Les calculs effectués auparavant ne traitaient que le cas irréaliste d'une cavité construite avec des miroirs parfaits. J'ai effectué des calculs permettant d'évaluer de manière quantitative l'influence de la finesse de la cavité. Par rapport au cas d'un miroir unique oscillant dans le vide, la situation de la cavité présente deux différences. Tout d'abord, la cavité a des fréquences de résonances pour lesquelles le rayonnement motionnel est amplifié par la finesse de la cavité. Le spectre du rayonnement est changé en conséquence. Les photons sont émis à des fréquences de résonance de la cavité. On peut distinguer deux modes de

5. M.T. Jaekel, A. Lambrecht, and S. Reynaud, in "Vacuum", eds. E. Gunzig and S. Diner (Plenum, à paraître)

6. S. Reynaud, A. Lambrecht, C. Genet, and M.T. Jaekel, *C.R. Acad. Sci. Paris* **2 IV**, 1287 (2001)

7. A. Lambrecht, M.T. Jaekel, and S. Reynaud, *Phys. Rev. Lett.* **77**, 615 (1996)

rayonnement. Pour un mouvement oscillatoire qui module la longueur mécanique de la cavité, celle-ci rayonne à des fréquences multiples paires de la fréquence d'oscillation. Mais la cavité rayonne aussi quand elle oscille de façon à ce que sa longueur reste constante. Dans ce cas, le rayonnement est émis à des fréquences multiples impaires de la fréquence mécanique. Ce dernier mouvement ressemble à l'oscillation d'un miroir unique dans la mesure où la cavité se déplace dans le vide sans référence autre que le vide lui-même.

5.1.2 Sonoluminescence

Dans ce contexte, je me suis aussi intéressée à une explication du phénomène de la sonoluminescence[8]. Une bulle d'air qu'on fait imploser à l'aide d'une onde sonore émet un rayonnement intense au moment où son diamètre est minimal. Il a été proposé que l'émission du rayonnement soit un effet dissipatif des fluctuations du vide[9]. En estimant le nombre de photons émis par la bulle, j'ai trouvé qu'une bulle qui se déplace à la vitesse du son émet un nombre de photons environ 10^{28} fois plus petit que le flux de photon observé expérimentalement. Autrement dit, pour pouvoir expliquer les observations expérimentales à l'aide de l'effet dissipatif des fluctuations du vide, il serait nécessaire que la surface de la bulle bouge à 100 fois la vitesse de la lumière[10]. La raison de ces résultats décevants est que la bulle est une très mauvaise "cavité" avec une finesse de l'ordre de 1.

Actuellement, l'ensemble des informations expérimentales disponibles favorise une description de la sonoluminescence comme un phénomène dû au chauffage adiabatique de la bulle lors de son collapse qui produirait l'ionisation partielle du gaz dans la bulle et l'émission thermique de rayonnement par les particules chargées[11].

5.1.3 Traitement non-perturbatif du rayonnement motionnel

Les premiers calculs que j'ai effectués correspondaient à un traitement linéarisé de l'interaction entre le champ et le mouvement. Depuis, j'ai développé une description plus rigoureuse qui prend en compte les effets non-linéaires en même temps que les pertes de la cavité. Cette description permet d'abord de tester la validité des résultats déjà obtenus. De plus, elle permet d'identifier des signatures particulières du rayonnement motionnel qui pourraient servir dans une expérience à le distinguer des effets parasites.

8. D.F. Gaitan, L.A. Crum, C.C. Church, and R.A. Roy, *J. Acoust. Soc. Am.* **91**, 3166 (1992)
9. C. Eberlein, *Phys. Rev. Lett.* **76**, 3842 (1996)
10. A. Lambrecht and S. Reynaud, *Phys. Rev. Lett.* **78**, 2267 (1997)
11. M.P. Brenner, S. Hilgenfeldt, and D. Lohse, *Rev. Mod. Phys.* **74**, 425 (2002)

Lors de chaque réflexion sur un des deux miroirs, le champ subit deux effets. Premièrement, il acquiert un déphasage dû au mouvement des miroirs. Deuxièmement, il est mélangé au champ du vide entrant dans la cavité. Dans le cas réaliste où la vitesse des miroirs est faible devant la vitesse de la lumière, le déphasage lors d'une seule réflexion crée deux bandes latérales sur le champ qui sont décalées de la fréquence centrale par la fréquence de l'oscillation mécanique. La prochaine réflexion produit de nouvelles bandes latérales sur ce champ déjà transformé lors de la première réflexion. Ces processus se répètent et le déphasage sur le champ s'accumule pendant le grand nombre d'aller-retours qu'effectue le champ dans la cavité avant de s'en échapper. L'accumulation est d'autant plus importante que la finesse de la cavité est élevée.

Par conséquent, le calcul quantique du champ dans la cavité et du champ rayonné à l'extérieur de la cavité est assez complexe. En particulier, un calcul numérique du champ par itération n'est possible que pour une cavité fermée mais ce cas ne présente aucun intérêt en vue d'une réalisation expérimentale. Nous avons trouvé une façon analytique d'itérer l'effet des réflexions multiples du champ sur les miroirs en mouvement. Le calcul analytique des fonctions de corrélations et du spectre de rayonnement se réduit alors à des manipulations de matrices. Sans entrer dans le détail des calculs, j'expose ci-dessous les résultats les plus importants obtenus ainsi[12]. Les articles reproduits à la fin de cette section décrivent les calculs d'une façon plus détaillée.

On peut définir une vitesse effective des miroirs qui dépend du produit de la vitesse maximale des miroirs par la finesse de la cavité. Bien que la vitesse mécanique des miroirs soit très petite devant la vitesse de la lumière dans toute situation réaliste, la *vitesse effective* peut approcher la vitesse de la lumière pour une cavité de haute finesse. Dans ce cas, le traitement linéarisé du rayonnement perd sa validité. Trois nouveaux effets apparaissent.

Le premier est une mise en forme temporelle du champ qui se concentre dans des impulsions émises périodiquement par la cavité. La figure 5.1 montre la densité d'énergie émise par la cavité en fonction des cycles d'oscillation pour trois vitesses effectives normalisées par la vitesse de la lumière. Pour une faible vitesse effective, le rayonnement varie de façon sinusoïdale c'est à dire linéairement en fonction de l'excitation mécanique. Par contre, pour une vitesse effective proche de la vitesse de la lumière, le champ est émis dans des impulsions. Cette variation temporelle du champ permet des densités d'énergie très élevées dans des fenêtres temporelles étroites et régulièrement espacées et pourrait être exploitée dans une réalisation expérimentale.

12. A. Lambrecht, M.T. Jaekel, and S. Reynaud, *Eur. Phys. J.* **D 3**, 95 (1998)

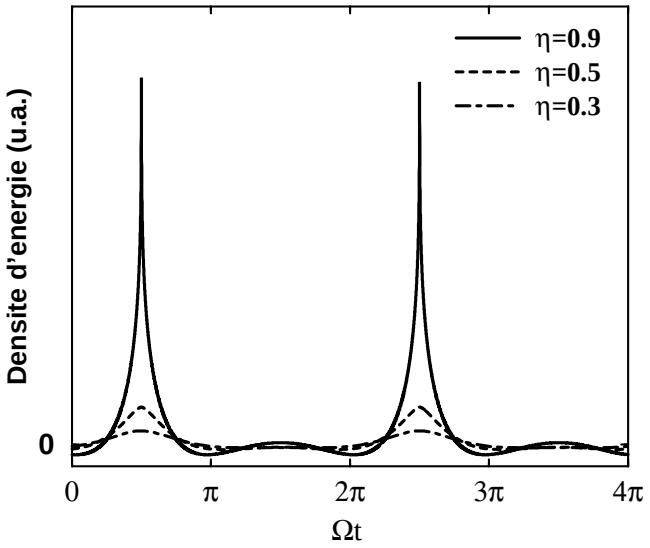

FIG. 5.1 – *La densité d'énergie émise par la cavité vers l'extérieur en fonction des cycles d'oscillations pour trois vitesses effectives normalisées par la vitesse de la lumière (paramètre η). Quand η s'approche de l'unité, le champ est émis dans des impulsions étroites et régulièrement espacées.*

Le deuxième effet est une multiplication de fréquence qui a lieu dans le couplage opto-mécanique entre fluctuations du vide et mouvement mécanique. La figure 5.2 montre le spectre de rayonnement émis par la cavité. Par suite des conditions de résonance dans le couplage opto-mécanique entre le mouvement des miroirs et les fluctuations du vide, les photons sont émis à des fréquences précises correspondant aux modes de la cavité. Ces pics de résonances sont d'autant plus fins et plus hauts que la finesse de la cavité est élevée. Des photons peuvent être émis par la cavité à des fréquences plus élevées que la fréquence d'excitation mécanique des miroirs. De plus, aucun photon n'est émis à des fréquences multiples de la fréquence d'oscillation mécanique. Le spectre en nombre de photons émis forme en effet des arches entre deux fréquences multiples entières de la fréquence d'oscillation. Ces caractéristiques sont très différentes de celles des effets parasites et pourraient donc servir à identifier le rayonnement motionnel dans une expérience.

Le troisième nouvel effet est l'existence d'une divergence de la densité d'énergie lorsque la vitesse effective approche la vitesse de la lumière. Ceci correspond en fait à un seuil d'oscillation du système. En dessous de ce seuil, la cavité amplifie l'effet dissipatif des fluctuations du vide, mais les pertes subies par le champ lors des réflexions sur les miroirs sont plus importantes que l'amplification par le mouvement des miroirs. En dessus du seuil par contre, l'amplification dépasse les pertes subies par le champ et le système entre dans un régime de croissance exponentielle. Sans calcul supplémentaire, on s'attend à ce

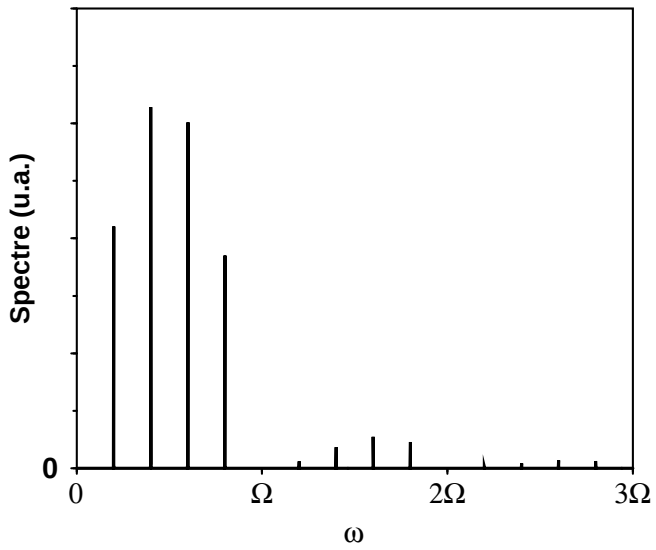

FIG. 5.2 – *Le spectre de rayonnement émis par la cavité pour $\eta = 0.9$. Les pics dans lesquels les photons sont émis correspondent aux fréquences de résonance de la cavité. Le spectre a éte calculé pour une cavité oscillant à $\Omega = 3\pi/L$. Le rayonnement est non seulement émis à des fréquences plus petites, mais aussi plus grandes que Ω ce qui met en évidence un processus de multiplication de fréquence. Aucun photon n'est émis aux fréquences multiples entières de Ω.*

que la cavité émette des impulsions d'une intensité nettement plus élevée qu'en dessous du seuil par analogie avec l'oscillateur paramétrique optique.

5.1.4 Effet de la température

Afin de se rapprocher d'une situation expérimentale, je me suis aussi intéressée à l'influence de la température sur les effets dissipatifs des fluctuations du vide. A toute température finie, les fluctuations du vide sont accompagnées de fluctuations thermiques. Celles-ci subissent également des transformations dues à la diffusion du champ sur les miroirs en mouvement. J'ai donc étudié les signatures des effets thermiques pour la cavité en mouvement avec l'approche non-perturbative présentée ci-dessus[13].

L'effet de mise en forme temporelle du champ se rencontre également dans un champ thermique. En particulier, la cavité oscillant dans un champ thermique émet des impulsions d'autant plus intenses que la température du champ est elevée. Ce calcul m'a permis de déterminer la température en dessous de laquelle le rayonnement motionnel est dû à

13. A. Lambrecht, M.T. Jaekel, and S. Reynaud, *Europhys. Lett.* **43**, 147 (1998)

l'effet dissipatif des fluctuations du vide et non pas à une transformation d'un champ thermique. Pour une oscillation dans le domaine des GHz, une température de l'ordre de 10 mK serait nécessaire pour assurer que l'effet observé est dû aux fluctuations du vide. Cet exemple est illustré sur la figure 5.3.

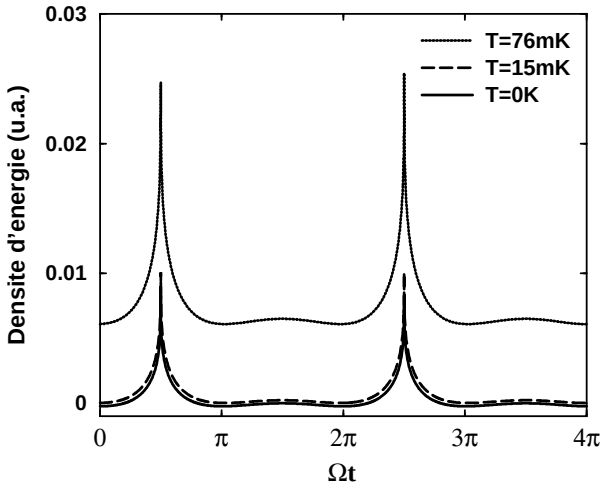

FIG. 5.3 – *La densité d'énergie émise par la cavité vers l'extérieur en fonction des cycles d'oscillation pour trois températures différentes. A une température jusqu'à environ 15 mK, le rayonnement est essentiellement dû aux fluctuations du vide. Pour des températures supérieures, l'effet dissipatif est dû au champ thermique.*

5.1.5 Ordres de grandeur

A cause de ses implications fondamentales, il serait très intéressant de mettre en évidence expérimentalement l'effet mécanique dissipatif des fluctuations des vides et d'étudier ses caractéristiques. Le rayonnement motionnel émis par un seul miroir vibrant dans le vide est bien trop petit pour être observable. Par contre, en utilisant une cavité de haute finesse une mise en évidence ne paraît pas impossible, si on peut résoudre certaines difficultés.

Pour profiter d'une amplification résonnante du rayonnement dans une cavité de haute finesse, il faudrait exciter une oscillation des miroirs à quelques GHz. Afin d'accéder au régime non-linéaire où les effets de formation d'impulsions et de multiplication de fréquences apparaissent, la vitesse des miroirs devrait être de l'ordre d'une dizaine de cm/s avec une amplitude d'oscillation de l'ordre de 10^{-11}m. Dans ce cas, la cavité émettrait un flux d'environ 10 photons par seconde à l'extérieur. Un tel flux est mesurable dans le domaine des fréquences micro-ondes. Notamment en astronomie, il existe des détecteurs avec un bon rendement quantique qui peuvent compter quelques photons par seconde. La

vitesse des miroirs demandée est également compatible avec une réalisation expérimentale dans la mesure où elle est beaucoup plus petite que la vitesse du son dans des matériaux typiques comme le quartz ou la silice, ce qui exclut les problèmes de rupture de matériaux lors de l'excitation. La difficulté réside dans l'excitation mécanique d'un tel mouvement mécanique à des fréquences très élévées. Ceci nécessiterait l'application de forces considérables aux miroirs. Tous les mécanismes d'excitation, que ce soit par pression de radiation modulée au GHz, par effet piézo-électrique ou par des ondes accoustiques de surface, emploient des champs électromagnétiques. Une forte excitation produirait alors du rayonnement parasite qu'il faudrait savoir distinguer du rayonnement motionnel. Les signatures évoquées plus haut pourraient jouer un rôle essentiel pour permettre de distinguer l'effet recherché et le rayonnement parasite. De plus, comme l'a montré l'étude des effets thermiques, il faudrait faire l'expérience à une très basse température, de l'ordre de 10 mK. La difficulté de l'expérience vient du fait qu'il faudrait satisfaire toutes ces conditions simultanément en réunissant des technologies très performantes de domaines différents.

Plusieurs autres voies sont possibles. On peut penser à faire l'expérience à température ambiante, ce qui augmenterait considérablement l'ordre de grandeur du rayonnement émis. On pourrait également se servir d'autres effets physiques pour produire une oscillation apparente du miroir pour le vide électromagnétique (effet d'indice, effet de peau, materiaux photorefractifs,...). Une telle expérience ne donnerait plus de renseignements directs sur l'effet dissipatif du vide, mais sa réalisation serait beaucoup plus facile.

5.1.6 Publications jointes

Reproduction de l'article "Motion induced radiation from a vibrating cavity", A. Lambrecht, M.T. Jaekel, and S. Reynaud, *Phys. Rev. Lett.* **77**, 615 (1996)

Motion Induced Radiation from a Vibrating Cavity

Astrid Lambrecht,[1] Marc-Thierry Jaekel,[2] and Serge Reynaud[3]
[1]*Max-Planck-Institut für Quantenoptik and Ludwig-Maximilians-Universität München, Hans-Kopfermann-Strasse 1, D-85748 Garching, Germany*
[2]*Laboratoire de Physique Théorique de l'Ecole Normale Supérieure, Université de Paris-Sud, Centre National de la Recherche Scientifique, 24 rue Lhomond, F-75231 Paris Cedex 05, France*
[3]*Laboratoire Kastler Brossel, Ecole Normale Supérieure, Université Pierre et Marie Curie, Centre National de la Recherche Scientifique, 4 place Jussieu, F-75252 Paris Cedex 05, France*
(Received 21 December 1995)

We study the radiation emitted by a cavity moving in vacuum. We give a quantitative estimate of the photon production inside the cavity as well as of the photon flux radiated from the cavity. A resonance enhancement occurs not only when the cavity length is modulated but also for a global oscillation of the cavity. For a high finesse cavity the emitted radiation surpasses radiation from a single mirror by orders of magnitude. [S0031-9007(96)00676-X]

PACS numbers: 03.70.+k, 12.20.Ds, 42.50.Lc

Vacuum field fluctuations exert radiation pressure forces on any scatterer placed in empty space. For two mirrors at rest in vacuum, this effect has been known for a long time as the Casimir effect [1]. It has more recently been recognized that dynamical counterparts of this static force appear for moving scatterers. For some types of motion, the field does not remain in the vacuum state, but photons are produced through nonadiabatic processes [2]. Because of energy conservation, the scatterers' motion then has to be damped out, and this damping may be associated with dissipative radiation reaction forces.

Motion induced effects of vacuum radiation pressure do not require the presence of two mirrors but already exist for a single mirror moving in vacuum. In this case, the radiation reaction force is known to arise as soon as the mirror has a nonuniform acceleration [3]. The effects of radiation from a moving mirror and the associated radiation reaction force raise intriguing questions with respect to the standard mechanical description of motion. They imply that dissipative effects are associated with the motion of mirrors in vacuum, although this motion has no further reference than vacuum itself. They thus seem to challenge the principle of relativity of motion. It would therefore be very important to obtain experimental evidence of these dissipative processes associated with motion in vacuum. However, vacuum radiation pressure scales as Planck's constant $\hbar$ and produces therefore only small mechanical perturbations for any macroscopic mirror, so that the feasibility of an experimental demonstration of motion induced dissipation is usually considered to lie out of reach of present technology.

The aim of the present Letter is to show that quantitative figures are greatly improved when the attention is focused onto the emission of radiation from an empty high finesse cavity oscillating in vacuum. Indeed, the number of emitted photons is the ratio of the radiated energy to the photon energy and thus scales as $\hbar^0$. This argument clearly supports a detection of optical rather than mechanical signatures of motion induced dissipation. Furthermore, a cavity configuration should allow one to take advantage of resonance enhancement effects.

Motion induced radiation can be interpreted using analogies with optical parametric processes. It is well known that the cavity field is parametrically excited when the mechanical cavity length is modulated at a frequency equal to an even integer multiple of the fundamental optical resonance frequency. If the cavity field is initially in the vacuum state, this excitation leads to a squeezed vacuum state [4] which differs from the pure vacuum state and, in particular, contains photons. Compared to the situation with a single oscillating mirror, radiation is resonantly enhanced in this cavity configuration. More strikingly, a resonant enhancement also exists when the cavity oscillates as a whole, with its mechanical length kept constant, at frequencies equal to odd integer multiples of the fundamental optical resonance frequency. Motional radiation is in this case reminiscent of photon emission from a single oscillating mirror, however, with the difference that it is enhanced by the cavity finesse.

A number of calculations has been devoted to the energy buildup inside a cavity with perfect mirrors [5]. However, these calculations do not provide satisfactory answers to the previously discussed questions. They do not consider the photons radiated by the cavity since the latter is treated like a closed system. Even for the photons produced inside the cavity, the hypothesis of perfect mirrors amounts to disregarding the important problem of finite lifetime of photons inside the cavity. In this Letter, in contrast, we study the configuration of a cavity built with partly transmitting mirrors. The cavity thus appears as an open system able to radiate into the free field vacuum. At the same time, the influence of the cavity finesse may be quantitatively evaluated.

For simplicity, we limit ourselves here to two-dimensional space-time calculations. As is well known from the analysis of squeezing experiments, the trans-

verse structure of the cavity modes does not change appreciably the results obtained from this simplified model. Each transverse mode is correctly described by a two-dimensional model as soon as the size of the mirrors is larger than the spot size associated with the mode. The two-dimensional model thus corresponds to a conservative estimate where one transverse mode is efficiently coupled to the moving mirrors. A more precise evaluation for a realistic configuration should take diffraction into account and would probably lead to a result obtained by multiplying the two-dimensional result by the Fresnel number, i.e., the number of efficiently coupled transverse modes [6].

Before studying the cavity configuration, we consider briefly the case of a single moving mirror and calculate the photon flux as well as the spectrum of the emitted radiation. To derive the radiation, we use general arguments associated with scattering theory, without specific assumptions on the form of the interaction between mirror and field. This approach does not rely on a detailed microscopic analysis and is therefore applicable to any type of mirror as long as its internal dissipation is negligible. We disregard the recoil of the mirror which is supposed to have a macroscopic mass. To specify the scattering properties of the mirror, we introduce column matrices $\Phi[\omega]$ which contain the components at a given frequency ω of the free fields propagating in opposite directions,

$$\Phi(\omega) = \sqrt{\frac{\hbar}{2(\omega)}} \begin{bmatrix} \theta(\omega) a_{+,\omega} + \theta(-\omega) a^{\dagger}_{+,-\omega} \\ \theta(\omega) a_{-,\omega} + \theta(-\omega) a^{\dagger}_{-,-\omega} \end{bmatrix}. \quad (1)$$

Field components with positive or negative frequencies correspond, respectively, to annihilation ($a_{\pm,\omega}$) and creation ($a^{\dagger}_{\pm,\omega}$) operators (θ is the Heaviside step function). The transformation from the input field Φ_{in} to the output one Φ_{out} is described by a unitary S matrix which contains the transmission and reflection amplitudes $s(\omega)$ and $r(\omega)$ at a given frequency

$$\Phi_{\text{out}}[\omega] = \begin{bmatrix} s[\omega] & r[\omega] \\ r[\omega] & s[\omega] \end{bmatrix} \Phi_{\text{in}}[\omega]. \quad (2)$$

The scattering of the field on a motionless mirror does not change the field frequency, and the vacuum state is then preserved, as a consequence of unitarity.

When the mirror is moving, the frequency of the field is changed by the scattering process, and the S matrix now describes this frequency change,

$$\Phi_{\text{out}}[\omega] = \int \frac{d\omega'}{2\pi} S[\omega, \omega'] \Phi_{\text{in}}[\omega']. \quad (3)$$

Assuming that the incoming field is in the vacuum state, one obtains the following expression for the number N of photons radiated into vacuum by the moving mirror

$$N = \int_0^{\infty} \frac{d\omega}{2\pi} \int_0^{\infty} \frac{d\omega'}{2\pi} n[\omega, \omega'],$$

$$n[\omega, \omega'] = \frac{\omega}{\omega'} \operatorname{Tr} (S[\omega, -\omega'] S[\omega, -\omega']^{\dagger}). \quad (4)$$

$n[\omega, \omega']$ is the spectral density which describes the number of particles present in the output field. Photon creation from vacuum is associated with a scattering process from a negative frequency $-\omega'$ to a positive frequency ω. The radiation has to be summed over the two output ports as indicated by the trace Tr.

When the S matrix is evaluated in a first order expansion in the displacement, which is valid for small displacements in which we are interested here, the spectral density $n[\omega, \omega']$ is proportional to the square modulus of the frequency component $\delta q[\omega + \omega']$ of the displacement

$$n[\omega, \omega'] = \frac{\omega \omega'}{c^2} \gamma[\omega, \omega'] |\delta q[\omega + \omega']|^2,$$

$$\gamma[\omega, \omega'] = 2(1 - s[\omega] s[\omega'] + r[\omega] r[\omega'] + 1 - s[\omega]^* s[\omega']^* + r[\omega]^* r[\omega']^*). \quad (5)$$

This expression results from a linear approximation of the motional perturbation of the field, but it is valid without any restriction on the motion's frequency. It is directly connected to the general relation which exists between the motional perturbation of the scattering matrix and the radiation pressure force exerted upon the mirror [7].

In the following, we consider the case of a mirror following a harmonic motion at a frequency Ω. Since we expect the radiation of photons to be proportional to time, we focus our attention on a harmonic motion of amplitude a during a time T,

$$\delta q(t) = 2a \cos(\Omega t), \qquad 0 < t < T. \quad (6)$$

For a long oscillation time T, we find the number N of radiated photons to be defined per unit time,

$$\frac{N}{T} = \frac{a^2}{c^2} \int_0^{\Omega} \frac{d\omega}{2\pi} \omega(\Omega - \omega) \gamma[\omega, \Omega - \omega]. \quad (7)$$

This result is similar to the expression one would obtain for the number of photons spontaneously emitted by an atom coupled to vacuum fluctuations, calculated with Fermi's golden rule. Here the emission is generated by the parametric coupling of the mirror's mechanical motion to vacuum radiation pressure rather than by the coupling of the atomic dipole to the vacuum field. Hence, photons are emitted through a two-photon parametric process rather than through a one-photon process. As is well known, spontaneous emission is not accompanied by absorption processes because vacuum is the field ground state. Here the same property entails that photons are only emitted at frequencies ω and ω' smaller than the frequency Ω of the mechanical motion. Each parametric process corresponds to the emission of two photons carrying away an energy $\hbar\Omega = \hbar(\omega + \omega')$, so that the radiated energy may be obtained as $\frac{1}{2} N \hbar \Omega$. This energy corresponds exactly to the work supplied by the mirror against the radiation reaction force, in absence of other dissipative mechanisms. This consistency between mechanical dissipation and optical radiation is ensured by expression (7) where N appears to be proportional to

the noise spectrum at frequency Ω of the fluctuations of vacuum radiation pressure experienced by the mirror [7].

In the limiting case of a nearly perfect mirror ($s \to 0; r \to -1$), we obtain a simplified expression for the number of radiated photons

$$\frac{N}{T} = \frac{8a^2}{c^2}\int_0^{\Omega}\frac{d\omega}{2\pi}\,\omega(\Omega-\omega) = \frac{2a^2\Omega^3}{3\pi c^2}\,,$$
$$N = \frac{\Omega T}{6\pi}\left(\frac{v}{c}\right)^2, \qquad v = 2\Omega a. \tag{8}$$

Expression (8) for N is a product of two dimensionless factors, namely, the number of mechanical oscillation periods during the time T and the square of the maximal velocity v of the mirror divided by the velocity of light c. A characteristic feature of motion induced radiation, which could be used in an experiment to distinguish it from spurious effects, is the parabolic shape of its spectral density with a maximum at $\omega = \Omega/2$.

The derivation of motion induced radiation is similar in the case of two moving mirrors. Assuming the two mirrors follow a harmonic motion at the same frequency Ω with respective amplitudes a_i ($i = 1, 2$), we deduce the number of photons radiated per unit time to be

$$\frac{N}{T} = \sum_{ij}\frac{a_i a_j}{c^2}\int_0^{\Omega}\frac{d\omega}{2\pi}\,\omega(\Omega-\omega)\gamma_{ij}[\omega,\Omega-\omega]. \tag{9}$$

As in the case of a single mirror, the functions γ_{ij} already appear in the evaluation of motional forces, and they have been studied previously [8]. We introduce here simplifying assumptions allowing one to obtain analytical expressions for the motional radiation. In the frequency range $[0, \Omega]$ one can in a good approximation assume the reflection coefficients r_1 and r_2 of the two mirrors to be real and frequency independent. In the following we are concentrating on the most interesting case where the cavity has a high finesse which implies that both r_1 and r_2 are close to unity. Since the functions $\gamma_{ij}[\omega, \omega']$ exhibit resonances when one of the emission frequencies ω or ω' corresponds to a cavity mode, we will keep the reflection coefficients, which appear in their denominators and thus determine their resonant behavior. In contrast, we will set to unity the reflection coefficients acting only as weighting factors in the numerators. With these assumptions the functions γ_{ij} only depend on the product $r_1 r_2$ of the reflection coefficients which we denote

$$r_1 r_2 = e^{-2\rho}, \qquad \rho \ll 1\,, \tag{10}$$

where $1/\rho$ measures the cavity finesse. They then read

$$\gamma_{11}[\omega,\omega'] = \gamma_{22}[\omega,\omega'] = 4 + 4D_+[\omega]D_+[\omega'], \qquad \gamma_{12}[\omega,\omega'] = \gamma_{21}[\omega,\omega'] = -4D_-[\omega]D_-[\omega'],$$
$$D_+[\omega] = \frac{\sinh(2\rho)}{\cosh(2\rho)-\cos(2\omega\tau)} = \sum_{k=-\infty}^{\infty}\frac{\rho}{\rho^2+(\omega\tau-k\pi)^2}\,, \tag{11}$$
$$D_-[\omega] = \frac{2\sinh(\rho)\cos(\omega\tau)}{\cosh(2\rho)-\cos(2\omega\tau)} = \sum_{k=-\infty}^{\infty}\frac{(-1)^k\rho}{\rho^2+(\omega\tau-k\pi)^2}\,.$$

τ is the time of flight of a photon from one mirror to the other. With the exception of the first term in γ_{11}, all terms contain denominators clearly associated with the presence of the cavity.

We can now calculate the emitted photon number by performing the integration (9) for the various Lorentzian components of the spectrum. Using the assumption of a high finesse cavity we find

$$\frac{N}{T} = \frac{\Omega^3(a_1^2+a_2^2)}{3\pi c^2} + \sum_{k,k'=1}^{\infty}\frac{N_{k,k'}}{T}\,,$$
$$\frac{N_{k,k'}}{T} = \frac{1}{\tau}\,\frac{k\pi}{c\tau}\,\frac{k'\pi}{c\tau}\,\frac{4\rho[a_1-(-1)^{k+k'}a_2]^2}{4\rho^2+(\Omega\tau-k\pi-k'\pi)^2}\,. \tag{12}$$

The photon flux outside the cavity can also be written by resumming the contributions of all modes,

$$\frac{N}{T} = \frac{\Omega^3}{3\pi c^2}(a_1^2+a_2^2) + \frac{\Omega}{6\pi c^2}\left(\Omega^2-\frac{\pi^2}{\tau^2}\right)\frac{\sinh(2\rho)\,(a_1+a_2)^2}{\cosh(2\rho)+\cos(\Omega\tau)} + \frac{\Omega}{6\pi c^2}\left(\Omega^2-\frac{\pi^2}{\tau^2}\right)\frac{\sinh(2\rho)\,(a_1-a_2)^2}{\cosh(2\rho)-\cos(\Omega\tau)}\,. \tag{13}$$

The first term in these expressions is a nonresonant contribution coming from direct reflection of vacuum fluctuations on both sides of the cavity. All other terms describe resonances of the motional radiation occurring when the mechanical excitation frequency Ω is close to an integer multiple of the fundamental optical resonance frequency π/τ. $N_{k,k'}$ describes parametric emission of radiation into the optical modes of frequencies $k\pi/\tau$ and $k'\pi/\tau$. Compared to the result obtained for a single mirror, the radiated photon flux is enhanced by a resonance factor which is essentially the cavity finesse. For the lowest mechanical resonance at $\Omega = 2\pi/\tau$, only one intracavity mode is excited ($k = k' = 1$). This corresponds to the situation studied in most works on intracavity field buildup [5]. In

the more general frame developed in the present Letter, higher resonance frequencies exist, giving rise to several emission peaks. The emission peaks all have the same spectral width given by the cavity finesse, and their relative intensities reproduce a parabolic spectrum, as the one obtained for a single moving mirror, however, with a large resonant enhancement. The information contained in the set of peaks can again be used to distinguish motion induced radiation from spurious effects.

In Eq. (12), even modes $\Omega = 2\pi/\tau, 4\pi/\tau, \ldots$ appear as elongation modes which correspond to a periodic modulation of the mechanical cavity length. In contrast, odd modes $\Omega = 3\pi/\tau, 5\pi/\tau, \ldots$ are excited by a global translation of the cavity with its length kept constant. The latter effect is thus reminiscent of radiation of a single oscillating mirror, since the cavity moves in vacuum without any further reference than vacuum itself. However, radiation is now enhanced by the cavity finesse. These two kinds of vibration modes, which appear to be contrasted in a mechanical point of view, have been obtained in a unified manner in our scattering approach which deals with the field bouncing back and forth in the cavity. The basic reason for this similar description within the scattering formalism is that the optical length as seen by the field varies in the same way for both kinds of modes, although the mechanical cavity length is modulated in one case and constant in the other one.

To estimate the stationary number of photons inside the cavity, we may use a simple balance argument. Each photon has a probability 4ρ of escaping from the cavity during each round-trip time 2τ. As we know the photon flux emitted by the cavity per unit time, we can deduce the number of photons $\mathcal{N}_{k,k'}$ produced by the oscillation in a pair of cavity modes,

$$\mathcal{N}_{k,k'} = \frac{k\pi}{c\tau}\,\frac{k'\pi}{c\tau}\,\frac{2[a_1 - (-1)^{k+k'}a_2]^2}{4\rho^2 + (\Omega\tau - k\pi - k'\pi)^2}\,. \quad (14)$$

So far we have given a quantitative estimate for the number N of radiated photons as well as for the number $\mathcal{N}$ of photons produced inside the cavity. The model of a cavity with partly transmitting mirrors allows us to evaluate now the resonance enhancement factor in terms of the cavity finesse. A mechanical excitation at exact resonance leads to the following orders of magnitude for N and $\mathcal{N}$:

$$N \simeq \frac{\Omega T}{2\pi}\,\frac{v^2}{c^2}\,\frac{1}{\rho}\,, \qquad \mathcal{N} \simeq \frac{v^2}{c^2}\,\frac{1}{\rho^2}\,, \quad (15)$$

where v measures either the sum or the difference of the peak velocity of the vibrating mirrors, depending on the mode parity. We may emphasize that not only the number of photons inside the cavity, but also the number of radiated photons, diverge at the limit of perfectly reflecting mirrors where the finesse of the optical and mechanical resonances goes to infinity. This shows that the simple model which treats the cavity as a closed system misses important physical phenomena.

To be more specific about the orders of magnitude, let us recall that we have assumed the input fields to be in the vacuum state. This assumption requires the number of thermal photons per mode to be smaller than 1 in the frequency range of interest ($\hbar\omega < k_B\Theta$ with k_B the Boltzmann constant and Θ the temperature). Low temperature technology thus points to experiments using small mechanical structures with optical resonance frequencies as well as mechanical oscillation frequencies in the GHz range. In this frequency range, the finesse of a superconducting cavity can reach 10^9 [9]. A peak velocity $v \simeq 1$ m/s, corresponding to an amplitude in the nm range, would thus be sufficient to obtain a radiated flux of 10 photons per second outside and a stationary number of 10 photons inside the cavity. It is important to emphasize that the peak velocity considered in the present analysis is only a small fraction of the typical sound velocity in materials so that fundamental breaking limits do not oppose these numbers. The photons may be detected outside the cavity by performing sensitive photon-counting detection of the radiated flux. Inside the cavity the state of the field could be probed with the help of Rydberg atoms [9]. Therefore, if a technique is found to excite a vibrating motion with the above characteristics, the challenge of an experimental observation of motional radiation in vacuum can be taken up.

We would like to thank M. Devoret, D. Estève, T.W. Hänsch, S. Haroche, P.A. Maia Neto, and J.-M. Raimond for useful discussions.

[1] H. B. G. Casimir, Proc. K. Ned. Akad. Wet. **51**, 793 (1948); G. Plunien, B. Müller, and W. Greiner, Phys. Rep. **134**, 87 (1986).
[2] G. T. Moore, J. Math. Phys. (N.Y.) **11**, 2679 (1970).
[3] S. A. Fulling and P. C. W. Davies, Proc. R. Soc. London A **348**, 393 (1976).
[4] E. Giacobino and C. Fabre, Appl. Phys. B **55**, 189 (1992).
[5] C. K. Law, Phys. Rev. Lett. **73**, 1931 (1994); V. V. Dodonov, A. B. Klimov, and V. I. Man'Ko, Phys. Lett. A **142**, 511 (1989); **149**, 225 (1990); V. V. Dodonov, Phys. Lett. A **207**, 126 (1995); see also references therein.
[6] P. A. Maia Neto and S. Reynaud, Phys. Rev. A **47**, 1639 (1993).
[7] M. T. Jaekel and S. Reynaud, Quantum Opt. **4**, 39 (1992).
[8] M. T. Jaekel and S. Reynaud, J. Phys I (France) **2**, 149 (1992).
[9] G. Rempe, F. Schmidt-Kaler, and H. Walther, Phys. Rev. Lett. **64**, 2783 (1990); M. Brune, F. Schmidt-Kaler, A. Maali, J. Dreyer, E. Hagley, J.-M. Raimond, and S. Haroche, Phys. Rev. Lett. **76**, 1800 (1996).

Reproduction de l'article "Frequency up-converted radiation from a cavity moving in vacuum", A. Lambrecht, M.T. Jaekel, and S. Reynaud, *Eur. Phys. J.***D 3**, 95 (1998)

Eur. Phys. J. D **3**, 95–104 (1998)

THE EUROPEAN PHYSICAL JOURNAL D

Frequency up-converted radiation from a cavity moving in vacuum

A. Lambrecht[1,a], M.T. Jaekel[2], and S. Reynaud[1]

[1] Laboratoire Kastler Brossel[b], Université Pierre et Marie Curie, case 74, 4 place Jussieu, 75252 Paris Cedex 05, France
[2] Laboratoire de Physique Théorique de l'École Normale Supérieure[c], 24 rue Lhomond, 75231 Paris Cedex 05, France

Received: 10 December 1997 / Received in final form: 27 March 1998 / Accepted: 27 March 1998

Abstract. We calculate the photon emission of a high finesse cavity moving in vacuum. The cavity is treated as an open system. The field initially in the vacuum state accumulates a dephasing depending on the mirrors motion when bouncing back and forth inside the cavity. The dephasing is not linearized in our calculation, so that qualitatively new effects like pulse shaping in the time domain and frequency up-conversion in the spectrum are found. Furthermore we predict the existence of a threshold above which the system should show self-sustained oscillations.

PACS. 42.50.Lc Quantum fluctuations, quantum noise, and quantum jumps – 03.70.+k Theory of quantized fields – 12.20.Ds Specific calculations

Vacuum field fluctuations exert radiation pressure on scatterers in vacuum. For a pair of mirrors at rest this effect is well known as Casimir effect [1]. When a mirror is moving radiation pressure of vacuum fluctuations leads to a dissipative force which opposes itself to the mirrors motion. This force is known to arise as soon as the mirror has a non-uniform acceleration [2]. Accordingly the electromagnetic field remains not in the vacuum state but photons are emitted by the scatterer into vacuum [3]. Radiation from a moving mirror and the associated radiation reaction force imply that dissipative effects are associated with the motion of mirrors in vacuum, although this motion has no further reference than vacuum itself. Since these effects challenge the principle of relativity of motion in vacuum, it would be very important to obtain experimental evidence for them and to study their characteristics in detail.

Motion-induced radiation can be interpreted as a result of dephasing of vacuum fields depending on the mirrors motion. The order of magnitude of the dephasing is expected to be the ratio between the mirror's velocity v and the speed of light c. For most conceivable motion of a macroscopic object, the velocity v cannot greatly exceed the sound velocity and is thereby much slower than that of light. This is why motion-induced radiation is very small for a single mirror oscillating in vacuum. This conclusion holds for perfectly reflecting mirrors as well as for partly transmitting ones.

A number of works have been devoted to photon production inside the cavity built with a pair of perfectly reflecting mirrors moving in vacuum [4–7]. However no predictions can be made for the amount of radiation emitted outside the cavity when the resonator is treated as a closed system. In contrast the resonant enhancement is found to be determined by the cavity finesse when the cavity is treated as an open system [8] from which the photons can escape. Motion induced radiation, that is photon emission outside a cavity oscillating in vacuum is resonantly enhanced by the cavity finesse when compared to the radiation from a single oscillating mirror. The resonant enhancement occurs when the mechanical frequency is a multiple of the lowest cavity mode. Even and odd multiples correspond respectively to breathing modes, where the mechanical cavity length changes periodically, and to translation modes, where the cavity moves as a whole [9]. The latter effect reminds radiation from a single mirror inasmuch as vacuum fluctuations are the only reference for the cavity motion. However the order of magnitude of photon emission may greatly exceed the one from a single mirror. From an experimental point of view the cavity is so far the most interesting system to look for an experimental observation of dissipative effects of vacuum fluctuations.

Inside a cavity the field undergoes many reflections before leaving the cavity through one of the mirrors. The number of round-trips of the field is roughly given by the cavity finesse. In loose terms, one may define an effective velocity where the physical velocity v normalized by the speed of light is multiplied by the number of round-trips inside the cavity. Effective velocity and thus motion-induced radiation become the larger the higher is the cavity finesse. The effective velocity is no longer a material

[a] e-mail: `astrid@spectro.jussieu.fr`
[b] Laboratoire de l'École Normale Supérieure et de l'Université Pierre et Marie Curie associé au CNRS
[c] Laboratoire du CNRS associé à l'École Normale Supérieure et à l'Université Paris-Sud

velocity and may therefore approach the speed of light. In contrast to the single mirror's case, qualitatively new effects are expected, such as the formation of a pulse bouncing back and forth in the cavity [6,7]. Since the pulse duration is shorter than the time of flight through the cavity, the radiation spectrum should also contain various frequencies corresponding to higher-order cavity modes and thus exceeding the mechanical frequency.

These effects cannot be obtained with a linear treatment as the one used in [9]. In such a treatment the field scattering is supposed to be linear in the mirrors motion. The field-mirror interaction corresponds to a coupling of the vacuum field radiation pressure, which is quadratic in the field, to the mirrors mechanical motion. Photons are thus emitted in pairs. In the linear regime the generation of motion-induced radiation is analogous to a parametric process during which the mechanical excitation is transformed into a pair of photons. Due to energy conservation the sum of their frequencies equals the oscillation frequency. Therefore motion-induced photons are only emitted at frequencies smaller than the excitation frequency. The linear assumption is correct as long as the total field dephasing due to interaction with the moving reflector remains small. The field dephasing from one reflection scales with the mirrors velocity over the speed of light. The linear assumption is always satisfied for a single macroscopic mirror.

However for a cavity the crucial parameter is the effective velocity and the total field dephasing can become important for a high finesse cavity. As a consequence we expect frequency multiplication to occur which generates frequencies larger than the mechanical excitation frequency. The linear treatment, which predicts the emission frequencies to be smaller than the oscillation frequency, then looses its validity and has to be replaced by a treatment which fully accounts for a large field dephasing produced through successive reflections of the field onto the mirrors. This treatment will be called non-linear in the following although the scattering is still linear in the field.

The aim of the present paper is to give a treatment of the radiation emitted by a cavity moving in vacuum which takes into account both the effect of accumulated field dephasing and the open character of the cavity. In particular we will study the explicit dependence of motional radiation on the two experimentally accessible parameters, the mirrors velocity and the cavity finesse. We will first introduce general calculation techniques for a single mirror and for a cavity moving in vacuum with an arbitrary motion. We will then concentrate on a particular motion, the harmonic oscillation of the mirrors, which allows to evaluate in closed analytical form the correlation functions of the radiation through a special parametrization of the motion. We will give expressions for the time-dependent radiated energy as well as the frequency-dependent radiation spectrum.

1 Single mirror moving in vacuum

Neglecting all effects related to polarizations, the electromagnetic field Φ is considered as a scalar function of one space variable, t and x, and will be written as a sum of two counterpropagating components φ and ψ which are functions of two light-cone variables u and v

$$\begin{aligned} \Phi(t,x) &= \varphi(u) + \psi(v) \\ u &= t - x, \qquad v = t + x. \end{aligned} \tag{1}$$

For the sake of simplicity, the velocity of light is set to unity. We limit ourselves here to two-dimensional space-time calculations. As is well-known from the analysis of squeezing experiments [10], the transverse structure of the cavity modes does not change appreciably the results obtained from this simplified model. Each transverse mode is correctly described by a two-dimensional model as soon as the size of the mirrors is larger than the spot size associated with the mode. The two-dimensional model thus corresponds to a situation where one transverse mode is efficiently coupled to the moving mirrors.

We now represent the mirror's motion either by a function $x = q(t)$ associated with the trajectory or as a monotonous function $v = V(u)$ relating the light cone variables u and v of the light rays intersecting on the mirror's trajectory. A propagation component φ_{out} of the output field can then be written as a function of the input fields φ_{in} and ψ_{in} and of the function V

$$\begin{aligned} \varphi_{out} &= \sqrt{R}\psi_{in} \circ V + \sqrt{T}\varphi_{in} \\ T &= 1 - R \\ (h \circ g)(u) &= h(g(u)). \end{aligned} \tag{2}$$

The symbol $\circ$ represents the composition law for functions. The coefficients $\sqrt{R}$ and $\sqrt{T}$ are the reflection and transmission amplitudes describing scattering upon the mirror. For the sake of simplicity, we have assumed these coefficients to be real and frequency independent.

We now recall the standard calculation of the energy radiated into vacuum by the moving mirror [2]. The input fields are supposed to be in the vacuum state and characterized by the correlation function

$$\langle \varphi_{in}(u)\varphi_{in}(\bar{u})\rangle = -\frac{\hbar}{4\pi}\ln|u-\bar{u}| - \frac{i\hbar}{8}\varepsilon(u-\bar{u}). \tag{3}$$

The first term corresponds to the anticommutator and is state-dependent whereas the second term gives the commutator contribution and is state-independent. Since ε is the sign function, it is clear that the field commutator remains unchanged under the transformation (2) where u is replaced by a monotonous function $V(u)$. The change of the correlation function between the input and output field is given by the following function which depends on the field anticommutators only

$$\begin{aligned} C(u,\bar{u}) &= \langle \varphi'_{out}(u)\varphi'_{out}(\bar{u})\rangle - \langle \varphi'_{in}(u)\varphi'_{in}(\bar{u})\rangle \\ &= -\frac{\hbar R}{4\pi}\left(\frac{V'(u)V'(\bar{u})}{(V(u)-V(\bar{u}))^2} - \frac{1}{(u-\bar{u})^2}\right). \end{aligned} \tag{4}$$

Throughout the paper, the prime signifies a derivative of a function with respect to its argument. The energy density $e_u(u)$ radiated per unit time is given by the function $C(u, \bar{u} = u)$ evaluated at coinciding points through a point splitting regularization procedure [2]

$$e_u(u) = C(u,u) = -\frac{\hbar R}{24\pi}\mathcal{S}V(u)$$
$$\mathcal{S}V = \frac{V'''}{V'} - \frac{3}{2}\left(\frac{V''}{V'}\right)^2. \tag{5}$$

The function $\mathcal{S}V$ is the Schwarzian derivative of V. No radiation is emitted when the reflector has a uniform acceleration, which corresponds to a vanishing Schwarzian derivative $\mathcal{S}V$. The total energy radiated by the moving mirror can then be obtained by integrating the energy density over u. In the following, we will concentrate on the particular case of an oscillatory motion of mechanical frequency Ω. In this case the energy E_u radiated per period is read as

$$E_u = \int_0^{\frac{2\pi}{\Omega}} e_u(u)\mathrm{d}u. \tag{6}$$

In order to characterize the radiation we have also to describe its spectral properties. The radiation spectrum may be represented as a density of photons obtained from the Fourier transform of the two point function $C(u, \bar{u})$. We will turn to its description later on.

2 Cavity moving in vacuum

The vacuum field is defined on both sides of the cavity as in the previous section. The relation between input and output fields is a generalization of (2) which corresponds to the standard Fabry-Perot theory

$$\varphi_{out} = -\sqrt{R_2}\psi_{in}\circ V_{-1} + \sqrt{R_1}T_2\sum_{n\geq 0} r^n \psi_{in}\circ V_n$$
$$+\sqrt{T_1}\sqrt{T_2}\sum_{n\geq 0} r^n \varphi_{in}\circ U_n$$
$$T_1 = 1-R_1,\ T_2 = 1-R_2,\ r = \sqrt{R_1}\sqrt{R_2} = e^{-2\rho}. \tag{7}$$

The reflection and transmission amplitudes of the two mirrors are related through unitarity conditions. The coefficient r determines the attenuation factor of the field on a single cavity round-trip. It can also be written as a function of the cavity losses ρ. Throughout the paper we will use ρ when we consider the experimentally interesting case of a high finesse cavity with $\rho \ll 1$. In the more general case the reflection coefficient r will be used. The functions U_n and V_n represent the light cone variables associated with the various input rays which are transformed into the output light ray u by the cavity. When the cavity is at rest they are given by simple relations

$$U_n(u) = u - 2nL$$
$$V_n(u) = u - (2n+1)L. \tag{8}$$

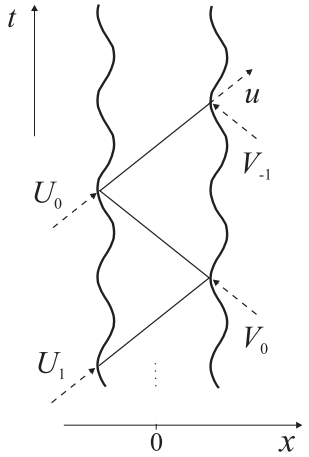

Fig. 1. Space-time diagram of on arbitrary field trajectory bouncing back and forth inside the cavity. Both mirrors are supposed to follow a harmonic motion. Light rays are indicated by null lines, *i.e.* straight lines making a 45°-angle with the time and space axis.

The length L of the cavity is measured as a time of flight between the two mirrors; the two mirrors are supposed to be located at $x = \pm L/2$ respectively; the ray V_{-1} represents the particular case where the field has been directly reflected back by the first encountered mirror without entering the cavity.

We may deduce the field emitted by the vibrating cavity through the same expression (7) as for the motionless cavity, but with functions U_n and V_n now given by the procedure sketched in Figure 1. The functions U_n and V_n corresponding to the various light rays in Figure 1 are built up through a functional iteration,

$$U_n = f_{2n} \qquad V_n = f_{2n+1}$$
$$f_{-1} = g \qquad f_0 = I$$
$$f_{2n} = g^{-1}\circ f_{2n-1} \qquad f_{2n+1} = h\circ f_{2n} \tag{9}$$

where I is the identity function ($I(u) = u$), while the two functions h and g^{-1}(inverse of g) represent the trajectories of the mirrors

$$x = q_1(t) \Longrightarrow v = h(u)$$
$$x = q_2(t) \Longrightarrow v = g(u) \Rightarrow u = g^{-1}(v). \tag{10}$$

The function f_{2n} results from n successive compositions of the function $g^{-1}\circ h$. This construction is quite analogous to the one described in [7], but it is written here such that it may be applied to an open cavity.

In a linear treatment [9] the total field dephasing remains small. At every reflection the field acquires a dephasing due to the mirrors motion $2q_i(t), (i = 1, 2)$. In this case the composition of functions (9) is reduced to the summation of the mirrors motion. The accumulated dephasing after M roundtrips inside the cavity is now seen to be simply M times the dephasing due to a single

roundtrip. The scattered field then has a temporal variation which reproduces the mirrors motion. With these approximations the results of the linear treatment are recovered.

However, if the field undergoes a great number of roundtrips inside the cavity, the total dephasing does not remain small and a linearization is not valid anymore. The dephasing has then to be calculated through the general composition law (9). Following the same procedure as for the single mirror, we calculate the density of energy $e_u(u)$ radiated to the right through the two-point correlation function defined as in (4) by letting $\bar{u}$ come to coincidence with u. As all functions now depend on a single parameter u, we omit this parameter in the expression for the energy density

$$e_u = -\frac{\hbar}{4\pi}\left\{\frac{R_2}{6}\mathcal{S}f_{-1} - 2T_2\sum_{n\geq 0} r^{n+1}\frac{f'_{-1}f'_{2n+1}}{(f_{-1}-f_{2n+1})^2} + \frac{T_2^2R_1}{6}\sum_{n\geq 0} r^{2n}\mathcal{S}f_{2n+1} + \frac{T_1T_2}{6}\sum_{n\geq 0} r^{2n}\mathcal{S}f_{2n} + T_1T_2\sum_{n\neq m\geq 0} r^{n+m}\frac{f'_{2n}f'_{2m}}{(f_{2n}-f_{2m})^2} + T_2^2R_1\sum_{n\neq m\geq 0} r^{n+m}\frac{f'_{2n+1}f'_{2m+1}}{(f_{2n+1}-f_{2m+1})^2}\right\}. \quad (11)$$

Compared to the radiated energy density of a single mirror (5), we now find a sum of Schwarzian derivatives corresponding to different numbers n of round-trips inside the cavity, as well as new terms arising from the interference between light rays having undergone a different number of roundtrips.

The derivatives appearing in the upper equation are iteratively deduced from each other through relations (9) and the chain rules associated with derivation of composed functions

$$(g\circ h)' = h'\ g'\circ h$$
$$\mathcal{S}(g\circ h) = \mathcal{S}h + h'^2\,(\mathcal{S}g)\circ h. \quad (12)$$

In the general case of arbitrary motions of the two mirrors, the various relations which have been written in the present section allow to compute the energy density radiated by a cavity built with partly transmitting mirrors.

3 Harmonic motions and periodic orbits

From now on we focus our attention on configurations which have been shown to be the most efficient ones to generate motion-induced radiation [9] and which furthermore allow us to put the problem in a simpler form.

We consider that the two mirrors follow harmonic motions at such a frequency that the motion-induced effects, *i.e.* motional radiation and motional force, are resonantly enhanced by the multiple interference taking place inside the cavity. The frequency Ω of the harmonic motion is thus supposed to be such that ΩL is a multiple of π

$$\Omega L = K\pi. \quad (13)$$

The amplitudes of the two motions are supposed to have the same absolute value with either opposite or identical signs depending on the parity of the integer number K

$$\Omega q_1(t) = -\frac{K\pi}{2} - \beta\sin\left(\Omega t - \frac{(K+1)\pi}{2}\right)$$
$$\Omega q_2(t) = \frac{K\pi}{2} - \beta\sin\left(\Omega t + \frac{(K+1)\pi}{2}\right)$$
$$\beta = \mathrm{th}(\alpha). \quad (14)$$

We have written the two equations of motion in terms of dimensionless numbers. In particular, one distinguishes two parameters α and β. β represents the ratio between the maximal velocity of the mirrors and the velocity of light while α plays the role of a rapidity which will be found to add up through successive reflections when one considers the composed motion of both mirrors.

When K is an even number, the upper equations describe a situation where the two mirrors are oscillating such that the length of the cavity changes periodically. In the opposite case, the cavity performs a global oscillation with its length kept constant. The two cases will be called even and odd modes respectively in the following. A cavity motion corresponding to an odd mode is reminiscent of motion-induced radiation from a single oscillating mirror, but in addition here the radiation is resonantly enhanced inside the cavity. These statements follow from the linearized approach [9] but we expect a similar behavior to take place in the full treatment developed in the present paper.

There exist periodic orbits such that the optical length seen by the field bouncing back and forth in the cavity is the same on successive round-trips despite the motion of the mirrors [7]. These orbits correspond to particular values $\tilde{u}$ of the light-cone variable u such that the iteration procedure leads to expressions similar to the ones obtained when the mirrors are at rest (*cf.* (8)). Although definition (9) of f_p is different depending on whether p is even or odd, the periodic orbits generalize the usual resonance condition of the Fabry-Perot theory

$$f_p(\tilde{u}) = \tilde{u} - pL. \quad (15)$$

They therefore give rise to a constructive interference effect, analogous to that occurring for a motionless cavity. Since the light rays corresponding to a periodic orbit encounter the mirrors at the same position after an arbitrary number of round-trips, the composition (9) of motions leads to a simple power law for the derivatives evaluated after n roundtrips as well as for the Schwarzian derivatives

$$f'_p(\tilde{u}) = e^{2p\alpha}$$
$$\mathcal{S}f_p(\tilde{u}) = \mathcal{S}f(\tilde{u})\frac{1-e^{4p\alpha}}{1-e^{4\alpha}}. \quad (16)$$

There exist two sets of periodic orbits which correspond to opposite values of α in (16). These two periodic orbits attract (respectively repel) the neighboring trajectories, when $e^{4\alpha}$ is greater (respectively smaller) than unity. Only the attractive orbit is expected to give rise to a large enhancement of the motional radiation.

In expression (11) of the energy density the Schwarzian derivative (16) is multiplied by the squared reflection coefficient after n roundtrips r^{2n}. Summation over the number of roundtrips leads then to a geometric progression of $r^{2n}e^{8n\alpha}$. The first factor represents the attenuation of the energy density associated with the cavity losses through the two mirrors. The second one accounts for the parametric amplification of the field associated with the mirrors' motion. As a consequence, the energy density takes large values when the parametric amplification compensates the losses. In fact, a divergence of the energy density should occur when $re^{4\alpha}$ approaches unity. This corresponds exactly to the oscillation threshold of a mechanically excited parametric amplifier. Let us notice that the approach developed in the present paper does not remain valid above this threshold.

We have focussed our attention here on the case where periodic orbits correspond to light rays meeting the two mirrors at their mean positions, respectively $-L/2$ and $L/2$. There exist more general situations where the light rays meet the mirrors at other positions [7] which will not be considered here. Notice that the particular case studied in the present paper is interesting from an experimental point of view since it corresponds to the maximum value of the parameter α for motions having a given frequency and a given amplitude.

In the following, we will restrict our attention to the cases of practical interest where the physical velocity of the mirror remains small when compared to the velocity of light. As discussed in the Introduction, this condition is always met for macroscopic mirrors. It implies that a single reflection produces a small dephasing on the field and, thereby, small radiation effects. Precisely, this means that the quantity $\mathcal{S}f$ which appears in (16) has an extremely small value while the factor $e^{2\alpha}$ is very close to unity. It follows that a large number n of roundtrips is needed to obtain a factor $e^{2n\alpha}$ differing appreciably from unity and therefore giving rise to a noticeable radiation. We show now that this assumption permits to perform the functional iteration in an analytical manner.

The crucial point is that the functional iteration (9) may in this case be restricted to the sub-space of periodic functions h corresponding to homographic relations between the phases $e^{i\Omega u}$ and $e^{i\Omega h(u)}$

$$e^{i\Omega h(u)} = \frac{ae^{i\Omega u}+b}{b^* e^{i\Omega u}+a^*} \Longrightarrow A(h) = \begin{pmatrix} a & b \\ b^* & a^* \end{pmatrix} \qquad (17)$$

a and b are two complex constants and a^* and b^* their complex conjugates which can be gathered in a matrix $A(h)$ associated with the function h. Attention may be restricted to matrices having a determinant equal to unity. In the sub-space of functions (17), the composition of two functions merely corresponds to a product of their corresponding matrices.

$$A(h \circ g) = A(h)A(g). \qquad (18)$$

Rigorously speaking, the function (17) does not correspond to sinusoidal trajectories (14) but rather to specific trajectories already considered by Law for dealing with photon production inside a closed cavity [6]

$$\begin{aligned} a = e^{i\phi_a}\mathrm{ch}\alpha, \qquad b = e^{i\phi_b}\mathrm{sh}\alpha \\ \sin(\Omega q - \phi_a) = -\beta \sin(\Omega t - \phi_b) \end{aligned} \qquad (19)$$

where the reduced velocity β gives the mirrors velocity compared to the speed of light. Variations of the phase factors ϕ_a and ϕ_b amount to displacements of the trajectory along the space and time axis. At the limit of small velocities however, the trajectory (19) is reduced to an ordinary sinusoidal motion (14)

$$\beta \ll 1 \Longrightarrow \Omega q = \phi_a - \beta \sin(\Omega t - \phi_b). \qquad (20)$$

The difference between the two motions scales as the cube β^3 of velocity and is therefore extremely small for realistic motions of macroscopic mirrors. The effect of the trajectory (19) is thus indistinguishable from the effect of the sinusoidal motion for a single reflection.

If one considers two oscillating mirrors, the two functions h and g, corresponding to the first and second mirror, are associated with two matrices $A(h)$ and $A(g)$ respectively. The matrix components are chosen to fit equations (14) of motion of the two mirrors

$$\begin{aligned} A(h) &= \begin{pmatrix} (-i)^K \mathrm{ch}\alpha & i^{K+1}\mathrm{sh}\alpha \\ (-i)^{K+1}\mathrm{sh}\alpha & i^K \mathrm{ch}\alpha \end{pmatrix} \\ A(g) &= \begin{pmatrix} i^K \mathrm{ch}\alpha & (-i)^{K+1}\mathrm{sh}\alpha \\ i^{K+1}\mathrm{sh}\alpha & (-i)^K \mathrm{ch}\alpha \end{pmatrix}. \end{aligned} \qquad (21)$$

As the composition of the two functions corresponds to a product of their matrices, the composition law naturally produces a homographic function when the number of reflections becomes large. This essential feature will be used in the following to compute the temporal and spectral characteristics of motional radiation from purely algebraic manipulations of the associated matrices. In particular, the functions f_p in equation (9) corresponding to successive reflections of the field inside the cavity are obtained through matrix multiplication

$$A_p = \begin{pmatrix} (-i)^{Kp}\mathrm{ch}p\alpha & i^{2K+1}(-i)^{Kp}\mathrm{sh}p\alpha \\ (-i)^{2K+1}i^{Kp}\mathrm{sh}p\alpha & i^{Kp}\mathrm{ch}p\alpha \end{pmatrix}. \qquad (22)$$

The discrepancy between the composed functions built on the two motions (14) and (19) does not affect the results if $\beta \ll 1$. More precisely, the difference between the composed functions f_p built on the two motions (14) and (19) remains of the order of β^2 when the number of iterations increases.

4 Pulse shaping

In the following, we will analyze the case of a single mirror following a trajectory (17) with an arbitrary velocity parameter α. Although the hypothesis of a large rapidity α is not realistic for a single mirror, it can be used as a model for the composition of a large number of round trips inside the cavity. We will then come to the full treatment of the cavity where interferences have also to be accounted for.

The derivative $h'(u)$ may be written from (17) as

$$h'(u) = \frac{1}{\left|a + be^{-i\Omega u}\right|^2} \tag{23}$$

$h'(u)$ oscillates between the extremal values $\exp(\pm 2\alpha)$ which correspond to physical velocities of the mirror $\pm\beta$. For homographic functions (17), the Schwarzian derivative has the simple form

$$\mathcal{S}h = \frac{\Omega^2}{2}\left(1 - h'^2\right). \tag{24}$$

The total energy radiated to the right by a single mirror is then obtained by averaging the energy density (5) over one oscillation period

$$E_u = \frac{\hbar R \Omega}{12} \mathrm{sh}^2\alpha. \tag{25}$$

This energy does not saturate when the parameter α increases although the velocity scales as thα and remains smaller than the velocity of light. The radiated energy is always greater than the squared velocity $\mathrm{th}^2\alpha$ which was the value suggested by the linear treatment [9]. However it is impossible to obtain appreciable radiation with a single oscillating mirror for velocities small compared to the speed of light. In the realistic case of a mirror moving at a small velocity the radiated energy as well as the number of emitted photons scale with α^2.

We come now to the energy density radiated by an oscillating cavity, assuming that a large number of roundtrips is necessary to compensate the small velocity of the mirrors and thus get a noticeable radiation. The energy density e_u may be obtained from (11) by using the following properties of the Schwarzian derivative of f_p and of the first-order derivative f'_p respectively

$$\begin{aligned} \mathcal{S}f_p &= \frac{\Omega^2}{2}\left(1 - f_p'^2\right) \\ f'_p &= \frac{1}{\mathrm{ch}2p\alpha + (-1)^K \mathrm{sh}2p\alpha \sin\Omega u}. \end{aligned} \tag{26}$$

To plot the energy density for different linear and nonlinear regimes we introduce effective quantities

$$\begin{aligned} \alpha_{eff} &= 2\alpha/\rho \\ \beta_{eff} &= \mathrm{th}(\alpha_{eff}). \end{aligned} \tag{27}$$

The effective rapidity α_{eff} is given by the roundtrip value of the rapidity multiplied by the cavity finesse ρ^{-1}. In contrast to the mechanical velocity v normalized by the speed of light, which has to remain much smaller than 1 in any physical situation, the corresponding effective velocity β_{eff} can become an important fraction of the speed of light when the field undergoes a large number of reflections inside the cavity. The maximal value of the effective reduced velocity is limited to $\beta_{eff} \sim 0.76$ by the divergence of the energy density at $\alpha_{eff} = 1$. This value corresponds indeed to the threshold $re^{4\alpha} = 1$ which has already been mentioned previously for the periodic orbits.

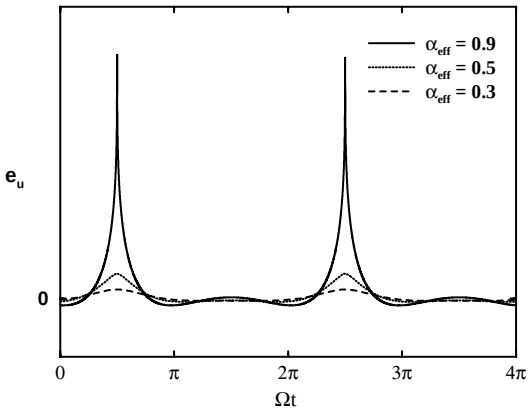

Fig. 2. Energy density emitted to the right by the cavity as a function of time for different effective rapidities α_{eff} and $r = 0.99$. The top line of the frame corresponds to $10^{-3}\hbar\Omega^2$. With increasing values of the effective rapidity the energy starts to concentrate in pulses emitted periodically by the cavity. The pulses become very sharp close to the threshold of oscillation $\alpha_{eff} = 1$.

The variation of the energy density for different parameters α_{eff} is presented in Figure 2. In the linear regime where $\alpha_{eff} \ll 1$ the temporal variation of the emitted energy is sinusoidal. When α_{eff} increases the energy concentrates in pulses which are periodically emitted by the cavity. This pulse shaping becomes the more pronounced, the width of the pulses the smaller, the larger becomes the effective rapidity and thus the accumulated field dephasing.

In the same manner as for the single mirror the total energy radiated by the cavity is computed by averaging the energy density over one oscillation period $2\pi/\Omega$. As previously we will restrict our attention to a realistic case, where the mirrors velocity is small which justifies the use of the homographic relations. In this case we may replace the differences of functions in the denominators of (11) by their motionless values (8). Higher order contributions decrease with the inverse of their squared order. The sums over the number of roundtrips can then be performed and we find the following expression for the energy radiated to

the right

$$E_u = \frac{\hbar\Omega R_2}{12}\mathrm{sh}^2\alpha + \frac{\hbar\Omega T_2}{48}\left(\zeta_u(\alpha)+\zeta_u(-\alpha)-2\right) - \frac{\hbar\Omega T_2}{8\pi^2K^2}\Big(\xi(\alpha)(\zeta_u(\alpha)-e^{-2\alpha}) + \xi(-\alpha)(\zeta_u(-\alpha)-e^{2\alpha})\Big)$$

$$\zeta_u(\alpha) = \frac{(1-e^{-4\rho})e^{2\alpha}+T_1(1-e^{2\alpha})}{1-e^{4(\alpha-\rho)}}$$

$$\xi(\alpha) = \sum_{l=1}^{\infty}\frac{e^{2l(\alpha-\rho)}}{l^2\mathrm{ch}2\alpha l}. \quad (28)$$

The energy E_v radiated to the left can be obtained from the above formula by interchanging the indices 1 and 2 of the reflection and transmission coefficients. The total energy radiated in both directions is then evaluated as the sum of the two contributions

$$E = E_u + E_v. \quad (29)$$

The total radiated energy would diverge for $\alpha = \rho$. However this limit is not reached as the energy density already diverges when $2\alpha/\rho$ approaches unity. The reason for this difference is simply that the widths of the various contributions to the energy density decrease when the number of roundtrips n increases, so that the contribution to the integrated energy increases less rapidly than the peak value of the energy density. As a consequence, the divergence of the peak density occurs before the divergence of the integrated energy. We remind here that our calculation does not remain valid above the oscillation threshold. Still it may be expected that a large amount of radiation is emitted above threshold.

For experimental reasons one might also be interested in the amount of energy stored inside the cavity. Let us first remark that inside the cavity the fields propagating to the right and to the left are not independent from each other due to the boundary conditions. All intracavity quantities thus contain the field components of both directions and are obtained as the sum of the two contributions. Having this argument in mind the intracavity energy, integrated over the cavity length $L = K\pi/\Omega$, is then with the same notations as above found to be

$$\mathcal{E} = \frac{\hbar\Omega K}{48}\left(\zeta(\alpha)+\zeta(-\alpha)-2\right) - \frac{\hbar\Omega}{8\pi^2K}\left(\xi(\alpha)\zeta(\alpha)+\xi(-\alpha)\zeta(-\alpha)-2\xi(0)\right)$$

$$\zeta(\alpha) = \frac{1}{2}(\zeta_u(\alpha)+\zeta_v(\alpha)). \quad (30)$$

The energy density is here directly expressed with respect to the static Casimir energy which is recovered when the cavity is motionless [2]. This result is due to the fact that the vacuum outside and inside the cavity is not the same but differs exactly by this amount of energy.

In order to obtain an appreciable value for the radiated energy if the cavity is moving at a small velocity, it is necessary to consider a high finesse cavity $\rho \ll 1$, keeping in mind that the finesse should be limited by the condition $\alpha_{eff} < 1$. Using these assumptions equations (29, 30) may be approximated as follows by expanding separately the common denominator and numerators

$$E \approx \frac{\hbar\Omega}{6}\alpha^2 + \frac{\hbar\Omega}{6}\left(1-\frac{1}{K^2}\right)\frac{\rho\alpha^2}{\rho^2-\alpha^2}$$

$$\mathcal{E} \approx \frac{\hbar\Omega}{24}\left(K-\frac{1}{K}\right)\frac{\alpha^2}{\rho^2-\alpha^2}$$

$$\alpha \leq \frac{\rho}{2} \ll 1. \quad (31)$$

The first term in the radiated energy is due to the field which is directly reflected by the two mirrors without entering the cavity. This term corresponds to the expression for motion-induced radiation from a single perfectly reflecting mirror. The second term has its origin in the field which has traversed the cavity and thus accumulated a much more important dephasing than the singly reflected field. Neglecting α^2 in the denominator leads to the linear result presented in [9]. The linear approximation is found to be rigorously valid if the rapidity is much smaller than the cavity losses ($\alpha \ll \rho$). Furthermore the present treatment allows us to calculate motion-induced radiation when the field dephasing becomes large due to accumulation on a large number of reflections. Equations (31) have a range of validity extending up to the threshold $\alpha_{eff} = 1$.

The intracavity energy contains only the term corresponding to the field which has entered the cavity. Its expression can also be deduced from the radiated energy through a detailed balance argument, which goes as follows [9]: the energy inside the cavity can be obtained from the radiated energy by multiplying it by two factors $\Omega/(2\pi)$ and $2L/(4\rho)$. The first factor is due to the fact that the radiated energy is the energy density integrated over one oscillation period. During one roundtrip of duration $2L$ each photon has the probability 4ρ - corresponding to the energy transmission coefficient of the two mirrors - to escape from the cavity. The present non-linear evaluation of the intracavity energy gives indeed the same result as the balance argument in the limiting case of a high finesse cavity (*cf.* Eqs. (31)). However, as equations (28, 30) show the balance argument is not true for a cavity with arbitrary reflection and transmission coefficients. A remarkable consequence of equations (31) is that the non-linear calculation is necessary as soon as the number of photons inside the cavity becomes of the order of unity.

Interesting remarks can be made concerning the particular case $K = 1$. Clearly equations (31) show that for a high finesse cavity no enhancement of photon production inside the cavity can be obtained when the mechanical excitation frequency equals the lowest cavity mode ($K = 1$) in accordance with results in references [5,6]. In this case the energy E radiated by the cavity corresponds to the one emitted by a single mirror and the motional intracavity energy vanishes. However, in the general case of arbitrary cavity finesse motion-induced photons are also found for the $K = 1$ mode (*cf.* Eq. (30)). The key point is

that as far as classical light rays are concerned the mode $K = 1$ behaves like all other modes [7]. However the field dephasing and thus motion-induced radiation is not only determined by the behavior of the light rays but also by the cavity which plays the part of a filtering function and suppresses photons at zero frequency. As a consequence of the coupling to radiation pressure photons are not emitted singly but in pairs. Thus motion-induced radiation is enhanced by the cavity if all photons are emitted into a cavity mode, the sum of their frequencies being equal to the mechanical oscillation frequency. In order to fulfill this condition when the cavity oscillates with the frequency of the lowest cavity mode photons have to be emitted at zero frequency. The cavity suppresses those photons the more efficiently the higher is the cavity finesse. Thus motion-induced photons for the $K = 1$ mode can be found in the bad cavity limit but not in the high finesse limit.

Coming back to the general case, we emphasize that equations (31) remain valid up to the threshold $\rho = 2\alpha$, when the cavity finesse ρ^{-1} is increased with the amplitude of motion kept constant. Below this value motion-induced radiation is amplified inside the cavity, but the cavity losses exceed the amplification gain. As expressions (31) are monotonous in ρ their maximum values are thus reached at threshold. In this regime we then find a maximum of the radiated energy which depends linearly on ρ. Comparing this value to the maximum energy emitted by a single oscillating mirror shows a gain of the order of the cavity finesse by considering a cavity instead of a single mirror. The cavity is thus a much more favorable system to produce motion-induced radiation than a single mirror. Furthermore if one increases the cavity finesse above its threshold value the roundtrip amplification of the field due to the mirrors motion should exceed the cavity losses and the system should enter a regime of exponential amplification. Without further calculations we then expect the oscillating cavity to emit photon pulses of much higher intensity above threshold than below.

5 Frequency up-conversion

We now turn to the calculation of the radiation spectrum where we will proceed as previously by first studying the case of a single moving mirror and afterwards the one of the oscillating cavity.

The scattering field equation (2) writes in Fourier space

$$\begin{aligned}\varphi_{out}[\nu] &= \sqrt{T}\varphi_{in}[\nu] \\ &\quad +\sqrt{R}\int d\bar{\nu}\frac{\Omega}{2\pi}\psi_{in}[\bar{\nu}]\int du e^{i\Omega(\nu u+\bar{\nu}V(u))} \\ \nu &= \frac{\omega}{\Omega}, \qquad \bar{\nu} = \frac{\bar{\omega}}{\Omega}\end{aligned} \tag{32}$$

where we have introduced the reduced frequencies $\bar{\nu}$ and ν normalized with respect to the mechanical frequency Ω. The field dephasing of the output field is determined by $V(u)$ and thus associated with the mirrors position $Q(u)$ which is easily calculated from (17)

$$\Omega Q\,(u) = \Omega\frac{V(u)-u}{2} = \mathrm{arctg}\left(\frac{\beta\cos\Omega u}{1+\beta\sin\Omega u}\right)\cdot \tag{33}$$

$e^{2i\bar{\nu}Q(u)}$ is a periodic function and can thus be developed into a Fourier series with discrete coefficients γ_m

$$e^{2i\bar{\nu}\Omega Q(u)} = \sum_m \gamma_m[\bar{\nu}]e^{-im\Omega u} \tag{34}$$

which will determine the radiation spectrum. If the mirrors motion were sinusoidal these Fourier coefficients would be given by Bessel functions of different orders. We have now to evaluate these coefficients for a homographic trajectory (19).

To this aim, we first write the field dephasing (34) as

$$e^{2i\Omega\bar{\nu}Q(u)} = \left(\frac{1+i\beta e^{-i\Omega u}}{1-i\beta e^{i\Omega u}}\right)^{\bar{\nu}}\cdot \tag{35}$$

The Fourier coefficients (34) may be rewritten in terms of an hypergeometric series[1]

$$\begin{aligned}\gamma_m[\bar{\nu}] &= (-i)^{m+2}\,\frac{\bar{\nu}}{\pi}\sin(\pi\bar{\nu})\,G_m\,(\bar{\nu},\beta) \\ G_m\,(\nu,\beta) &= \beta^m\sum_{l\geq 0}\frac{\Gamma\,(\nu+l)\,\Gamma\,(m-\nu+l)}{\Gamma(m+1+l)}\frac{\beta^{2l}}{l!}\cdot\end{aligned} \tag{36}$$

The radiation spectrum, that is the spectral density of the photon number per unit time and defined for positive frequencies, is then given by [9]

$$\begin{aligned}n_\nu &= R\sum_{m\geq\nu}\frac{\nu}{m-\nu}|\gamma_m[m-\nu]|^2 \\ &= R\frac{\sin^2(\pi\nu)}{\pi^2}\sum_{m>\nu}\nu\,(m-\nu)\,|G_m\,(\nu,\beta)|^2\,.\end{aligned} \tag{37}$$

The total energy may be recovered as the integral of the spectrum as well as the integral of the energy density. The radiation spectrum vanishes for all values ν equal to a natural number, that is for all frequencies ω equal to a multiple of Ω. The spectrum thus decomposes into a succession of arches, each limited by two successive multiples of the excitation frequency.

The upper expression corresponds to reflection upon a single moving mirror. In order to get the spectral distribution of radiation from the cavity, we now have to take into account the interferences between light rays having undergone different number of reflections inside the cavity. We proceed in the same manner as in the case of a single moving mirror by splitting the function f_p into two parts. The first part is linear in the parameter u while the

[1] The coefficient $G_m(\nu,\beta)$ is directly related to the hypergeometric function $F(\nu, m-\nu; m+1; \beta^2)$ defined for instance in [11]. We have also used property 8.334 of the Γ-function in the same reference.

second one Q_p is induced by the motion and harmonic like the mirrors' motion

$$f_p(u) = u - pL + 2Q_p(u)$$

$$\Omega Q_p(u) = \mathrm{arctg}\left(\frac{\beta_p \cos \Omega u}{1 + \beta_p \sin \Omega u}\right)$$

$$\beta_p = (-1)^K \mathrm{th}\,(p\alpha)\,. \tag{38}$$

The round-trip dephasing $2L$ corresponds to the case of periodic orbits so that the function Q_p vanishes at these points. The periodic function $e^{2i\bar{\nu}Q_p}$ can be developed into a Fourier series with coefficients now depending on the number of round trips p. We proceed as previously to find the Fourier coefficients

$$\gamma_{m,p}[\bar{\nu}] = \int_0^{\frac{2\pi}{\Omega}} \frac{\Omega}{2\pi} du\; e^{im\Omega u} e^{iK\pi\bar{\nu}p} e^{2i\Omega\bar{\nu}Q_p(u)}$$

$$= (-i)^{m+2}\,\bar{\nu}\frac{\sin(\pi\bar{\nu})}{\pi} e^{iK\pi\bar{\nu}p} G_m(\nu, \beta_p) \tag{39}$$

and the radiation spectrum

$$n_\nu = \frac{\sin^2(\pi\nu)}{\pi^2} \sum_{m>\nu} \nu\,(m-\nu)$$
$$\times \left\{ \left| \sqrt{R_1}T_2 \sum_{n\geq 0} r^n e^{-2i\pi K\nu(n+1)} G_m(\nu, \beta_{2n+1}) \right.\right.$$
$$\left. - \sqrt{R_2} G_m(\nu, \beta_{-1}) \right|^2$$
$$\left. + T_1 T_2 \left| \sum_{n\geq 0} r^n e^{-2i\pi K\nu n} G_m(\nu, \beta_{2n}) \right|^2 \right\}. \tag{40}$$

Let us mention that we recover the predictions of the linearized treatment for a motion with a small velocity by keeping only the lowest-order term $m = 1$ in the hypergeometric series. The spectrum is then parabolic and found to be restricted to the frequency range corresponding to the first arch [9].

Figure 3 shows the radiation spectrum for an effective rapidity $\alpha_{eff} = 0.9$ near the threshold of parametric oscillation. The spectrum shown here is plotted for a cavity oscillating globally at a frequency of $\Omega = 3\pi/L$. This means that the cavity performs three oscillations during one roundtrip of the field inside the cavity. The dashed line was obtained by putting formally $K = 0$ in equation (40) which eliminates the phase factors responsible for the interferences. It may be interpreted as the spectrum of radiation emitted by a single oscillating mirror averaged over the effective velocity. Clearly photons can be created by higher-order harmonics of the motion as well as by the fundamental one as soon as the effective velocity becomes appreciable compared to the speed of light. As a striking consequence, photons are radiated at frequencies higher than the mechanical frequency Ω. A process of frequency up-conversion thus exists in the opto-mechanical coupling between vacuum fluctuations and mechanical motion of scatterers. A corresponding situation is found for a single oscillating mirror (dashed line) which is however not realistic as it would imply a mirror's mechanical velocity appreciable compared to the speed of light. The use of a cavity allows to reproduce the same spectral density within the bandwidth of the cavity resonance lines for realistic mirrors' velocities. A second striking feature is that no photons are emitted at frequencies equal to multiple integers of the excitation frequency Ω neither by a single oscillating mirror nor by a vibrating cavity.

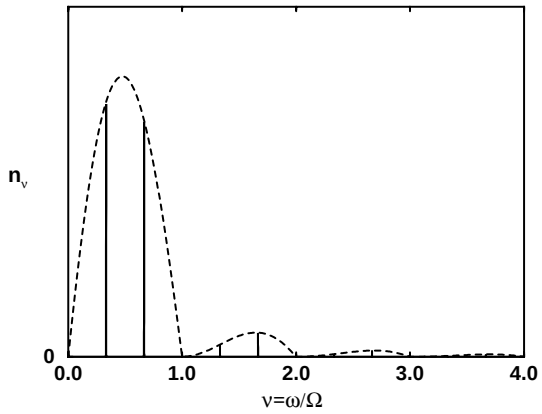

Fig. 3. Spectrum of the radiation emitted by the cavity for $\alpha_{eff} = 0.9$ and a reflection coefficient of $r = 0.99$. The top line of the frame corresponds to $\alpha_{eff}^2/4$. The peaks correspond to cavity resonance frequencies. The spectrum is plotted for a cavity oscillating globally at a mechanical frequency $\Omega = 3\pi/L$. The dashed line constitutes the envelope of the spectrum. It was obtained by averaging the spectrum of a single mirror over the effective velocities corresponding to different number of roundtrips. Photons are created at frequencies higher than the mechanical oscillation frequency through frequency up-conversion in the opto-mechanical coupling between vacuum fluctuations and the mirrors motion. Furthermore the radiation spectrum vanishes for frequencies equal to a multiple integer of the mechanical excitation frequency.

When comparing the cavity radiation spectrum to expression (37) corresponding to a single mirror, a difference is the emergence of peaks typical of cavity resonances. In fact, the interferences between the pathes corresponding to different numbers n of round-trips are essentially determined by the factors $r^n e^{-2in\pi K\nu}$ and $r^n e^{-2i\pi K\nu(n+1)}$. The propagation dephasing after one round-trip is $e^{2i\pi K\nu}$ where K is the order of the mechanical frequency as compared with the fundamental resonance frequency of the cavity. It follows that the peaks are apparent at frequencies equal to an integer multiple of K^{-1}, as shown in Figure 3 with $K = 3$. Their shape is Lorentzian for a high finesse cavity. The width of each peak is given by the inverse of the cavity finesse. The number of peaks fitting into the interval $[0, \Omega]$ corresponds to the order K of the excited cavity mode compared to the mechanical frequency.

6 Discussion

In this paper we have presented a non-linear calculation of motion-induced radiation from a cavity taking fully into account the accumulation of dephasing through successive reflections of the field on partly transmitting mirrors. This approach confirms the main results of the linearized treatment which was previously used and makes it possible to specify its range of validity. Furthermore the non-linearity due to the accumulative field dephasing produces particular signatures of motion-induced radiation which cannot be calculated within the linear approximation.

In the experimentally relevant case where the mirrors move with a velocity small compared to the speed of light the emitted photon number from a single mirror moving in vacuum scales with its squared velocity. Compared to this situation motion-induced radiation from an oscillating cavity is enhanced by the cavity finesse. For high finesse cavities as they exist for instance in the microwave-regime this enhancement brings motion-induced radiation within reach of an experimental observation. This clearly proves the cavity to be a much more favorable system for the generation of motion-induced radiation.

In addition the present calculation shows that the linear approach is valid when the effective rapidity, given by the mirrors' physical velocity multiplied by the cavity finesse, is much smaller than 1. We have given here expressions having a much larger range of validity.

In order to measure motion-induced radiation it is necessary to dispose of signatures which permit to distinguish vacuum radiation from spurious effects. The present calculation has allowed to identify two quantities showing signatures which could serve to this aim, the temporal variation of the radiated energy density and the spectral density of the emitted photon number.

We have studied the emitted energy density as a function of different effective rapidities. With increasing effective rapidity the energy starts to concentrate in pulses which are emitted periodically into vacuum by the cavity. These pulses become the higher and the sharper the more the effective rapidity approaches its threshold value. The energy density diverges when the single-reflection rapidity equals half of the cavity losses during one roundtrip ($\alpha = \rho/2$). The characteristic temporal variation which allows high energy densities in regularly spaced and narrow time windows might be exploited in an experimental observation.

The spectrum of motion-induced radiation shows several remarkable features. First photons may be radiated at frequencies higher than the mechanical frequency Ω in contrast to the prediction of the linear treatment. A process of frequency up-conversion thus takes place in the opto-mechanical coupling between vacuum fluctuations and mechanical motion of scatterers. Second the spectrum always vanishes for all multiple integers of the mechanical oscillation frequency. Due to the opto-mechanical resonance condition motion-induced radiation is furthermore only predicted at particular frequencies corresponding to fractions of the mechanical oscillation frequency. These signatures are different from pick-up effects and could serve to identify motion-induced radiation.

So far we have discussed the behavior of the system in a regime where the cavity amplifies the dissipative effects of vacuum fluctuations. However, as a consequence of the divergence of the energy density there exists a threshold above which the system will show self-sustained oscillations in analogy with an optical parametric oscillator [10]. This regime is reached if the cavity finesse is increased above its threshold value. The amplification of motion-induced radiation should then exceed the cavity losses. It is to be expected that in this regime the cavity will emit photon pulses with much larger intensity than below threshold. If it were possible to reach this regime experimentally an observation of motion-induced radiation as well as of its characteristics could be achieved more easily. It might thus also be interesting to calculate the radiated energy and the spectrum above threshold. The question then arises which are the mechanisms limiting the amplification of radiation in this regime.

In conclusion, these results confirm the idea that it might be possible to show experimental evidence of the dissipative effects of motion in quantum vacuum.

We thank M. Brune, M. Devoret, D. Estève, S. Haroche, J.-M. Raimond and C. Urbina for fruitful discussions.

References

1. H.B.G. Casimir, Proc. K. Ned. Akad. Wet. **51**, 793 (1948).
2. S.A. Fulling, P.C.W. Davies, Proc. R. Soc. London A **348**, 393 (1976).
3. G.T. Moore, J. Math. Phys. **11**, 2679 (1970).
4. V.V. Dodonov, A.B. Klimov, V.I. Man'Ko, Phys. Lett. A **142**, 511 (1989).
5. V.V. Dodonov, Phys. Lett. A **207**, 126 (1995); see also references therein.
6. C.K. Law, Phys. Rev. Lett. **73**, 1931 (1994).
7. C.K. Cole, W.C. Schieve, Phys. Rev. **52**, 4405 (1996).
8. M.T. Jaekel, S. Reynaud, J. Phys. I France **1**, 1395 (1991).
9. A. Lambrecht, M.T. Jaekel, S. Reynaud, Phys. Rev. Lett. **77**, 615 (1996).
10. S. Reynaud, A. Heidmann, E. Giacobino, C. Fabre, Progress in Optics *XXX*, edited by E. Wolf (1992) pp. 1-85.
11. I.S. Gradshteyn, I.M. Ryzhik, *Tables of Integrals, Series, and Products*, 5th edn., edited by A. Jeffrey, Eq. 9.100.

5.2 La force de Casimir

La force de Casimir, prédite par Henrik Casimir en 1948[14], est une force attractive qui s'exerce entre deux miroirs au repos dans le vide. Pour deux miroirs parfaitement réfléchissants, à température nulle, elle ne dépend que de la géométrie, à savoir la surface et la séparation des miroirs, et des constantes fondamentales, la vitesse de la lumière et la constante de Planck. Elle a donc un caractère remarquablement universel contrairement aux forces de van der Waals qui lui sont apparentées mais qui dépendent explicitement de la charge électronique.

Cependant, jusqu'à une période récente, elle n'avait été mesurée qu'avec une précision médiocre. Depuis 1997, plusieurs nouvelles expériences ont été développées aux Etats-Unis[15, 16, 17, 18], en Suède[19] et en Italie[20]. Les résultats expérimentaux obtenus explorent des distances entre 20 nm et quelques micromètres et affichent une précision au niveau du pourcent. Cette précision expérimentale permet de tester la théorie quantique des champs de façon détaillée.

5.2.1 Motivations

La mesure de la force de Casimir et la comparaison entre résultats expérimentaux et théoriques à haute précision sont principalement motivées par deux raisons. Tout d'abord, toute définition opérationnelle du vide nécessite la définition d'une enceinte délimitant un espace vide et la force de Casimir est précisément la manifestation physique des fluctuations du vide lorsqu'on les enferme dans une enceinte. Il est alors important de tester la force de Casimir de façon quantitative en tant que prédiction fondamentale de la théorie quantique des champs. Par exemple, sa dépendence en température est encore discutée au niveau théorique et elle n'a pas encore été vérifiée expérimentalement avec une précision suffisante.

D'autre part, l'analyse des caractéristiques de la force de Casimir est largement motivée par les mesures très précises de force qui se développent à des distances entre le nanomètre et le micromètre. L'objectif de ces mesures est de tester la gravité newtonienne à courte

14. H.B.G. Casimir, *Proc. Kon. Ned. Akad. Wetenshap* **51**, 793 (1948)
15. S.K. Lamoreaux, *Phys. Rev. Lett.* **78**, 5 (1997)
16. U. Mohideen and A. Roy, *Phys. Rev. Lett.* **81**, 4549 (1998)
17. A. Roy, C. Lin, and U. Mohideen, *Phys. Rev.* **D 60**, 111101 (1999)
18. B.W. Harris, F. Chen, and U. Mohideen, *Phys. Rev.* **A 62**, 052109 (2000)
19. Th. Ederth, *Phys. Rev.* **A 62**, 062104 (2000)
20. G. Bressi, G. Carugno, R. Onofrio, and G. Ruoso, *Phys. Rev. Lett.* **88**, 041804 (2002)

distance[21], en particulier pour la recherche de nouvelles forces de type Yukawa prévues par les modèles théoriques d'unification et ayant des portées comprises entre le nanomètre et le millimètre[22, 23, 24], ou par la recherche de dimensions supplémentaires compactes éventuelles qui se manifesteraient aussi par de nouvelles forces[25]. La comparaison à haute précision entre les forces de Casimir mesurée et calculée donne des domaines d'exclusion pour les paramètres de ces faibles forces qui sont à ce jour les plus restrictives pour des portées inférieures à 100 μm.

Notons enfin que la force de Casimir joue un rôle très important dans les nouveaux domaines des micromachines et des nanostructures. Les systèmes microélectromécaniques (MEMS), qui sont des senseurs et actuateurs microscopiques très perfomants, contiennent des éléments à des distances micrométriques voire nanométriques. Comme il a été démontré expérimentalement par F. Capasso au Lucent Technologies[26], la force de Casimir influence considérablement le comportement statique et dynamique du système. Elle se manifeste par exemple par le déplacement des fréquences propres du système ou par l'apparition d'hystéresis ou de bistabilité. C'est une raison de plus de la mesurer précisément.

Pour toutes ces situations différentes, il faut tenir compte dans le calcul théorique des conditions expérimentales réelles. Casimir avait calculé la force entre deux miroirs plans parallèles, parfaitement réfléchissants, à température nulle. Evidemment cette situation idéalisée n'est jamais réalisée dans une expérience. Pour calculer la force de Casimir dans une expérience réelle, il faut tenir compte de la réponse optique des miroirs qui dépend de la fréquence, de la température à laquelle se fait la mesure, de la géométrie et de l'état de surface des miroirs.

Dans la suite, j'exposerai la méthode que nous avons développée pour inclure dans le calcul de la force deux effets expérimentaux importants, à savoir la réflectivité imparfaite des miroirs et la température, à laquelle l'expérience est faite.

5.2.2 La force de Casimir par la théorie des réseaux optiques

Nous avons développé une nouvelle méthode de calcul de la force de Casimir dans le but de pouvoir caractériser des situations expérimentales réelles[27]. Nous avons utilisé la théorie

21. E. Fischbach and C. Talmadge, *The Search for Non-Newtonian Gravity* (AIP Press,1998)
22. G. Carugno, Z. Fontana, R. Onofrio, and C. Rizzo, *Phys. Rev.* **D 55**, 6591 (1997)
23. J.C. Long, H.W. Chan, and J.C. Price, *Nucl. Phys.* **B 539**, 23 (1999)
24. M. Bordag, B. Geyer, G.L. Klimchitskaya, and V.M. Mostepanenko, *Phys. Rev.* **D 60**, 055004 (1999)
25. E. Fischbach and D. E. Krause, *Phys. Rev. Lett.* **82**, 4753 (1999)
26. H.B. Chan, V.A. Aksyuk, R.N. Kleiman, D.J. Bishop, and F. Capasso, *Science* 291, 1941 (2001)
27. C. Genet, A. Lambrecht, and S. Reynaud, en cours de préparation

des réseaux optiques, dans laquelle l'influence des miroirs sur le champ électromagnétique est décrite par des matrices de diffusion ou des matrices de transfert. Les coefficients de réflexion obéissent à des propriétés physiques de causalité, de stabilité et de transparence à haute fréquence. Ces propriétés, qui sont naturellement respectées par tout miroir réel, permettent de déduire une expression pour la force de Casimir sans aucune divergence. De plus, notre méthode présente l'avantage de pouvoir décrire facilement des systèmes composés par empilement de systèmes simples. Par exemple, il est possible de décrire un miroir multicouche en empilant les couches de matériaux différents. Ceci correspond à une simple multiplication des matrices de transfert.

Il a été suggéré d'augmenter la force de Casimir en utilisant une cavité confocale et des miroirs résonnants[28]. Nous avons appliqué notre méthode pour interpréter une expérience de mesure de la force de Casimir qui était destinée à profiter de cette prédiction en utilisant des miroirs diélectriques ayant un coefficient de réflexion à bande étroite. A l'aide des propriétés de causalité et de passivité des miroirs, j'ai montré que la force de Casimir était proportionnelle à la largeur en fréquence du coefficient de réflexion, c'est à dire d'autant plus petite que la bande de fréquence est étroite, en contradiction avec les suggestions qui avaient été faites. De plus, ce calcul a permis de montrer que la force de Casimir entre deux miroirs réels est toujours plus petite que la force entre deux miroirs parfaits[29].

5.2.3 La conductivité des miroirs

Les miroirs utilisés dans les nouvelles expériences sont métalliques et la force de Casimir est affectée de façon appréciable par la conductivité finie des métaux. En effet, un métal ordinaire est un réflecteur quasi-parfait à basse fréquence mais un mauvais réflecteur à haute fréquence. La conductivité finie change alors la force de Casimir pour les courtes distances entre les deux miroirs, typiquement en dessous du micromètre. J'ai étudié cet effet en détail pour les métaux utilisés dans les expériences, à savoir l'aluminium, le cuivre et l'or. La figure 5.4 illustre le résultat. Elle montre la force réelle entre les deux miroirs par rapport à la force idéale calculée par Casimir en fonction de la distance entre les miroirs. A grande distance, la réflectivité des miroirs est déterminée surtout par les basses fréquences. Les miroirs métalliques sont alors presque parfaitement réfléchissants et la force réelle correspond à la force idéale. Par contre, à courte distance, la réflectivité à haute fréquence domine et les miroirs métalliques sont de mauvais réflecteurs. La force de

28. E. Iacopini, *Phys. Rev.* **A 48**, 129 (1993)
29. A. Lambrecht, M.T. Jaekel, and S. Reynaud, *Phys. Lett.* **A 225**, 188 (1997)

Casimir est réduite par un facteur qui atteint 50% à une distance typique de 100 nm.

Ces résultats théoriques montrent l'importance cruciale d'un traitement complet de l'influence de la réflectivité des miroirs sur la force de Casimir dans une comparaison quantitative entre la théorie et les résultats expérimentaux[30].

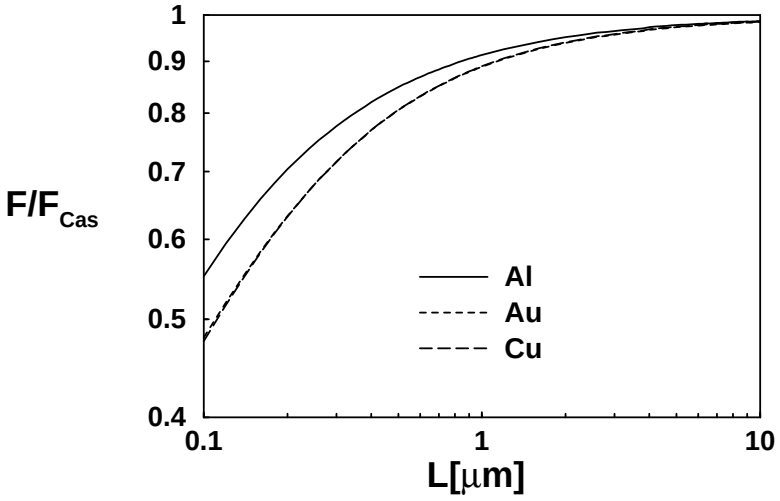

FIG. 5.4 – *La force de Casimir F entre miroirs métalliques par rapport à la force idéale F_{Cas} en fonction de la distance entre les miroirs pour les trois métaux Al (courbe en traits pleins), Au (tirets courts) et Cu (tirets longues).*

Le calcul de la force de Casimir entre deux miroirs métalliques a également permis de résoudre une difficulté rencontrée dans la mesure de la force de Casimir effectuée en 1997 par S.K. Lamoreaux[31]. Celui-ci prédisait une force différente entre deux miroirs en cuivre et entre deux miroirs en or, ce qui produisait un désaccord considérable dans la comparaison des mesures expérimentales avec les prédictions théoriques. Mes calculs ont montré que la force de Casimir était presque la même pour les deux métaux[32], en accord avec l'expérience.

5.2.4 L'effet de la température

Avec Cyriaque Genet, qui a effectué sa thèse sous ma co-responsabilité de septembre 1999 à juillet 2002, nous avons calculé les corrections venant du fait que les expériences sont faites à température ambiante. En fait, il faut traiter en même temps l'effet de conductivité et la correction thermique. Contrairement à l'effet de conductivité qui est important à haute fréquence, les fluctuations thermiques deviennent importantes à basse fréquence,

30. A. Lambrecht and S. Reynaud, *Eur. Phys. J.* **D 8**, 309 (2000)
31. S.K. Lamoreaux, *Phys. Rev. Lett.* **78**, 5 (1997); erratum dans *Phys. Rev. Lett.* **81**, 5475 (1998)
32. A. Lambrecht and S. Reynaud, Phys. Rev. Lett. 84, 5672 (2000)

c'est à dire à des distances relatives entre les miroirs au dessus de quelques micromètres. Pour cette raison, ces deux corrections avaient toujours été calculées séparément, mais ceci constituait évidemment une approximation.

Dans le cas où la conductivité est décrite par un modèle plasma, nous avons effectué le calcul simultané des deux corrections, qui est assez compliqué. La figure 5.5 montre le résultat de nos calculs, à savoir l'influence de la température sur la force de Casimir entre miroirs parfaits (courbe pointillée) en comparaison avec l'effet de la conductivité des miroirs métalliques à température nulle (courbe en tirets) et l'influence des deux corrections prises en compte simultanément (courbe en traits pleins)[33]. Les paramètres du modèle plasma ont été choisis pour décrire des miroirs en cuivre ou en or.

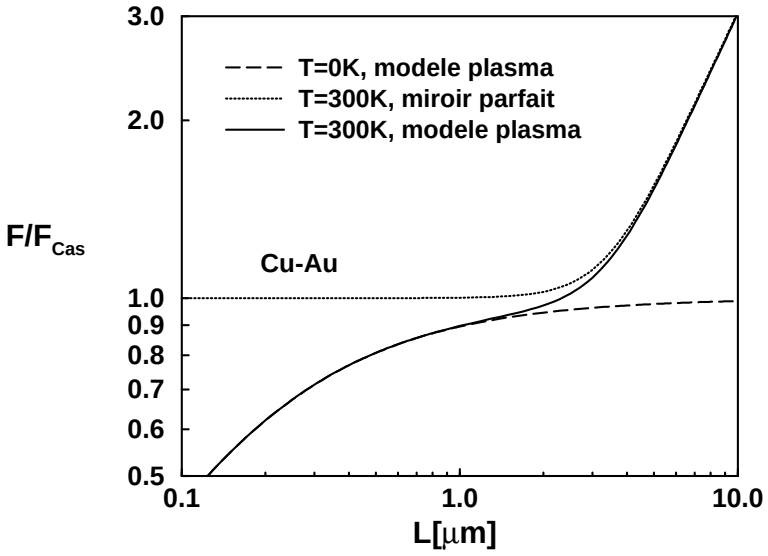

FIG. 5.5 – *La force de Casimir F par rapport à la force idéale F_{Cas} en fonction de la distance entre les miroirs. La courbe pointillée est calculée pour des miroirs parfaits à température ambiante, la courbe en tirets montre l'influence de la conductivité modélisée par un modèle plasma à température nulle. La courbe en traits pleins illustre l'effet simultané des deux corrections.*

Nous avons pu montrer que l'approximation qui consiste à évaluer séparément les deux corrections n'était pas correcte à une précision de l'ordre du pourcent. Nous avons aussi donné une nouvelle estimation de l'effet combiné qui est facile à calculer mais néanmoins beaucoup plus précise que l'approximation utilisée auparavant[34].

Le traitement des miroirs métalliques dissipatifs à température non nulle a donné

33. C. Genet, A. Lambrecht, and S. Reynaud, *Phys. Rev.* **A 62**, 012110 (2000)
34. C. Genet, A. Lambrecht, and S. Reynaud, *Int. J. Mod. Phys.* **A 17**, 761 (2002)

lieu récemment à une discussion polémique[35, 36, 37, 38, 39, 40, 41, 42]. En effet, la formulation dite de Lifshitz, qui est souvent utilisée, peut donner des résultats erronés. Cela arrive si les coefficients de réflexion ont des discontinuités, ce qui est précisément le cas pour la polarisation transverse électrique d'un miroir métallique dissipatif décrit par un modèle de Drude. Notre formulation de la force de Casimir n'est pas sensible à ces discontinuités et donne le résultat correct dans tous les cas[43]. Ceci est important pour une comparaison entre théorie et expérience.

5.2.5 Publications jointes

Reproduction de l'article "Casimir force between metallic mirrors", A. Lambrecht and S. Reynaud, *Eur. Phys. J.* **D8**, 309 (2000)

35. M. Bordag, B. Geyer, G.L. Klimchitskaya, and V.M. Mostepanenko, *Phys. Rev. Lett.* **85**, 503 (2000)
36. M. Boström and Bo E. Sernelius, *Phys. Rev. Lett.* **84**, 4757 (2000)
37. V.B. Svetovoy and M.V. Lokhanin, *Mod. Phys. Lett.* **A 15**, 1013 (2000)
38. S.K. Lamoreaux, Comment on [36], *Phys. Rev. Lett.* **87**, 139102 (2001)
39. Bo E. Sernelius, Reply to [38], *Phys. Rev. Lett.* **87**, 139101 (2001)
40. M. Boström and Bo E. Sernelius, Comment on [35], *Phys. Rev. Lett.* **87**, 259101 (2001)
41. M. Bordag, B. Geyer, G.L. Klimchitskaya, and V.M. Mostepanenko, Reply to [40], *Phys. Rev. Lett.* **87**, 259102 (2001)
42. G.L. Klimchitskaya, *Int. J. Mod. Phys.* **A 17**, 751 (2002)
43. C. Genet, A. Lambrecht, and S. Reynaud, en cours de préparation

Eur. Phys. J. D **8**, 309–318 (2000)

THE EUROPEAN PHYSICAL JOURNAL D

EDP Sciences

Casimir force between metallic mirrors

A. Lambrecht[a] and S. Reynaud

Laboratoire Kastler Brossel[b], Campus Jussieu, case 74, 75252 Paris Cedex 05, France

Received 30 July 1999

Abstract. We study the influence of finite conductivity of metals on the Casimir effect. We put the emphasis on explicit theoretical evaluations which can help comparing experimental results with theory. The reduction of the Casimir force is evaluated for plane metallic plates. The reduction of the Casimir energy in the same configuration is also calculated. It can be used to infer the reduction of the force in the plane-sphere geometry through the "proximity theorem". Frequency dependent dielectric response functions of the metals are represented either by the simple plasma model or, more accurately, by using the optical data known for the metals used in recent experiments, that is Al, Au and Cu. In the two latter cases, the results obtained here differ significantly from those published recently.

PACS. 03.70.+k Theory of quantized fields – 12.20.Ds Specific calculations – 42.50.Lc Quantum fluctuations, quantum noise, and quantum jumps

1 Introduction

The Casimir force experienced by reflectors placed in vacuum is a macroscopic mechanical consequence of quantum fluctuations of electromagnetic fields [1]. Despite its relatively small magnitude, it has been observed in a number of "historic" experiments [2–5]. A much better experimental precision has been reached in recent experiments [6,7] which should now allow for an accurate comparison with theory. Clearly this requires not only a detailed control of the experiments but also a careful theoretical estimation of the various corrections corresponding to the differences between real experiments and the idealized Casimir situation.

The present paper is focussed on the estimation of corrections associated with the non ideal behavior of metallic reflectors. Additional corrections due to the effect of non-zero temperature and the geometry of the cavity have also to be mastered before an agreement of experimental results with theoretical expectations can be claimed. A general discussion of the corrections to Casimir formulas is presented in the next section. In particular, we recall how the Casimir force measured in the plane-sphere geometry may be inferred from the Casimir energy in the plane-plane geometry by using the so-called "proximity theorem".

We then focus attention on our main topic which is the evaluation of the reduction factor of Casimir force and Casimir energy for plane metallic plates in the limit of a large surface. We first compute the reduction factors obtained when describing the dielectric functions with a plasma model. This computation covers the whole range of distances large or small with respect to the plasma wavelength. The analytical expression of the force in the limit of small distances is also derived.

The plasma model is not a good description of the dielectric constant at low frequencies because it ignores the relaxation of electrons responsible for optical response of metals. This is why we also investigate the Drude model which accounts for this relaxation. We finally discuss in detail a more accurate description of the dielectric constant based on the optical data known for the metals. We concentrate on the three metals, aluminium, gold and copper, used in recent experiments and give the reduction factors for the whole range of experimentally explored distances. For Au and Cu, we obtain results differing significantly from recently published ones [8].

2 Corrections to the Casimir formula

In the original point of view [1], the Casimir effect is derived from the change of the total energy of vacuum due to the presence of two plane perfect reflectors. In this global approach, the Casimir energy is the part $E_{\rm C}$ of vacuum energy depending on the plate separation L

$$E_{\rm C} = A\frac{\hbar c\pi^2}{720L^3}\cdot \tag{1}$$

This energy is proportional to the surface A of the reflectors in the limit of a large surface, the Planck constant $\hbar$ and the speed of light c. The Casimir force $F_{\rm C}$ between the

[a] e-mail: lambrecht@spectro.jussieu.fr

[b] Unité de l'École Normale Supérieure, de l'Université Pierre et Marie Curie, et du Centre National de la Recherche Scientifique.

two reflectors is then derived from this position dependent energy

$$F_{\rm C} = -\frac{{\rm d}E_{\rm C}}{{\rm d}L} = A\frac{\hbar c\pi^2}{240L^4}\cdot \tag{2}$$

Being proportional to the surface, it defines a pressure which depends only on the distance L and the two fundamental constants $\hbar$ and c. Conventions of sign have been chosen so that both numbers (1, 2) are positive with the significance that the Casimir force is attractive and the Casimir energy is a binding energy.

In contrast with this global point of view, the Casimir force may also be understood as a local quantity, namely the radiation pressure exerted upon mirrors by vacuum fluctuations which are modified by the presence of the reflectors. This local approach makes it much easier to deal with corrections of Casimir formulas (1, 2). In a remarkable work, Lifshitz gave a general formula for the Casimir force between two plane plates characterized by their dielectric response functions [9]. In particular his formula accounts for the finite reflectivity of metallic mirrors and it was used to deduce a first order correction for the plasma model of metals [10]. Since the dielectric constant is large at frequencies smaller than the plasma frequency $\omega_{\rm P}$, the Casimir formula is recovered at distances larger than the plasma wavelength

$$\lambda_{\rm P} = \frac{2\pi c}{\omega_{\rm P}}\cdot \tag{3}$$

At frequencies larger than $\omega_{\rm P}$ in contrast, the mirror has a poor reflectivity so that the force is reduced with respect to (2) at distances of the order of the plasma wavelength $\lambda_{\rm P}$ which lies in the sub-μm range. The force may thus be written in terms of a factor $\eta_{\rm F}$ which measures the reduction of the force with respect to the case of perfect mirrors

$$F = \eta_{\rm F} F_{\rm C}. \tag{4}$$

The expression of the reduction factor is read at long distances as [11,12]

$$\eta_{\rm F} \simeq 1 - \frac{8}{3\pi}\frac{\lambda_{\rm P}}{L} \quad \Leftarrow \quad \frac{\lambda_{\rm P}}{L} \ll 1. \tag{5}$$

In the following we will also introduce a reduction factor $\eta_{\rm E}$ for the Casimir energy E

$$E = \int_L^\infty F\,(x)\,{\rm d}x = \eta_{\rm E} E_{\rm C}. \tag{6}$$

The Lifshitz formula also contained thermal corrections to the Casimir effect usually studied at zero temperature. These corrections are significant at distances larger than or of the order of a typical length [9]

$$\lambda_{\rm T} = \frac{\hbar c}{k_{\rm B} T} \tag{7}$$

where $k_{\rm B}$ is the Boltzmann constant and T the temperature. At room temperature this length is of the order of a few μm. Hence thermal corrections become significant for distances for which the mirrors can be considered as nearly perfect reflectors. Well-established estimations of thermal corrections for perfect mirrors may thus be used to evaluate the effect of temperature [12–14]. This effect is found to be negligible at distances smaller than 1 μm and to become dominant at distances larger than 5 μm [7,15].

The Lifshitz formula has been derived for plane plates in the limit of large transverse surface and large longitudinal optical depth. But recent experiments have been performed in a plane-sphere geometry which makes easier the control of geometry and, in particular, the precise control of the distance between plates [6,7]. Furthermore, mirrors are often built as multilayered structures rather than as single plates with a large optical depth. Finally the roughness of the metal/vacuum interfaces may also play an important role. These features have to be taken into account in an accurate estimation.

We will not present a detailed analysis of the geometrical effects in this paper. It is however worth recalling that the Casimir force in the plane-sphere geometry is usually estimated from the so-called "proximity theorem". Basically this theorem amounts to evaluating the force by adding the contributions of various distances as if they were independent. In the plane-sphere geometry the force $F_{\rm pt}$ evaluated from the proximity theorem is thus read as [16–19]

$$F_{\rm pt} = 2\pi R E = 2\pi R \eta_{\rm E} E_{\rm C} \tag{8}$$

where R is the radius of the sphere and E the Casimir energy evaluated in the plane-plane configuration for the same distance L, this distance being defined as the distance of closest approach in the plane-sphere geometry. Hence, the reduction factor $\eta_{\rm E}$ for the Casimir energy evaluated in the plane-plane configuration in (6) can be used to infer the reduction factor for the force measured in the plane-sphere geometry through the proximity theorem.

At this point we have to emphasize that our calculations are intended to provide a reliable estimation of the Casimir force and energy between two metal plates in the plane-plane geometry. Clearly, they do not give any indication of the degree of reliability of the proximity theorem. Since it is well-known that the Casimir force is not an additive quantity one cannot but question an estimation based on an addition procedure [20]. Precisely, one can hardly admit that the proximity theorem provides reliable estimations at the level of accuracy which is now aimed at, that is the % level. As already discussed, these problems are not the main task of this paper which is focussed on the effect of imperfect reflection of metallic mirrors. The same remarks apply to another aspect of the geometry, that is the roughness effect which has also been found to play a significant role [19,21].

3 The description of mirrors

As predicted by Casimir in his founding article [1] the divergences associated with the infiniteness of vacuum

energy do not play a real role in the estimation of the Casimir effect thanks to a general physical reason: real mirrors are certainly transparent at the limit of infinite frequencies. This idea was implemented in the Lifshitz theory [9] and it has a much broader range of validity. Real mirrors may always be characterized by frequency dependent reflectivity amplitudes which provide a finite expression for Casimir energy as soon as general properties of unitarity, causality and high-frequency transparency are accounted for [22]. Dispersive optical response functions necessarily include dissipation mechanisms so that incoming electromagnetic fields and additional Langevin fluctuations coming from matter have to be treated simultaneously [23]. The description of mirrors through well-behaved reflectivity amplitudes [22] automatically includes a proper description of these fluctuations [24].

The two mirrors form a Fabry-Perot cavity which enhances or decreases field fluctuations depending on whether their frequency is resonant or not with cavity modes. This modulation of intracavity energy of vacuum fluctuations, integrated over frequencies and incidence angles corresponding to the various modes, is responsible for the Casimir force [22]. Using causality properties, the force can be written as an integral over imaginary frequencies and wavevectors [9]. After these transformations, the Casimir force may be written in terms of a reduction factor (4) which takes the following form adapted from [22]

$$\eta_{\rm F} = \frac{120}{\pi^4}\int_0^\infty {\rm d}K\, K^2 \int_0^K {\rm d}\Omega \sum_p \frac{r_p^2}{{\rm e}^{2K}-r_p^2}$$
$$K=\kappa L \qquad \Omega=\omega\frac{L}{c} \tag{9}$$

r_p denotes the reflection amplitude for one of the two mirrors and a given polarization p. This notation is a shorthand for $r_p\left({\rm i}\omega,{\rm i}\kappa\right)$ where ${\rm i}\omega$ is the imaginary frequency and ${\rm i}\kappa$ the imaginary wavevector along the longitudinal direction of the Fabry-Perot cavity. Ω and K stand for the frequency and wavevector measured in dimensionless units with the help of the cavity length L. The reflection amplitudes are supposed to be identical for the two mirrors. Otherwise r_p^2 has to be replaced by the product of the two amplitude reflection coefficients.

In the limit of perfect mirrors $\left(r_p^2=1\right)$ the Casimir formula (2) is recovered ($\eta_{\rm F}=1$). In the general case, the factor $\eta_{\rm F}$ measures the reduction of the force between real mirrors with respect to the case of perfect mirrors. We may also write a reduction factor (6) for the Casimir energy

$$\eta_{\rm E} = -\frac{180}{\pi^4}\int_0^\infty {\rm d}K\, K \int_0^K {\rm d}\Omega \sum_p \log\left(1-r_p^2{\rm e}^{-2K}\right). \tag{10}$$

Let us stress again that the expressions (9, 10) give only the corrections to Casimir force and energy associated with the finite conductivity of metallic plates. They correspond to plane reflecting plates at the limit of a large surface, assume a null temperature and disregard the problem of roughness. As discussed in the previous section, the factor $\eta_{\rm E}$ may be used to infer the force in the plane-sphere geometry through the proximity theorem.

Assuming furthermore that the metal plates have a large optical thickness, the reflection coefficients r_p correspond to the ones of a mere vacuum-metal interface [25]

$$r_\perp = -\frac{\sqrt{\omega^2\left(\varepsilon\left({\rm i}\omega\right)-1\right)+c^2\kappa^2}-c\kappa}{\sqrt{\omega^2\left(\varepsilon\left({\rm i}\omega\right)-1\right)+c^2\kappa^2}+c\kappa}$$
$$r_{||} = \frac{\sqrt{\omega^2\left(\varepsilon\left({\rm i}\omega\right)-1\right)+c^2\kappa^2}-c\kappa\varepsilon\left({\rm i}\omega\right)}{\sqrt{\omega^2\left(\varepsilon\left({\rm i}\omega\right)-1\right)+c^2\kappa^2}+c\kappa\varepsilon\left({\rm i}\omega\right)} \tag{11}$$

r_p still stands for $r_p\left({\rm i}\omega,{\rm i}\kappa\right)$ and $\varepsilon\left({\rm i}\omega\right)$ is the dielectric constant of the metal evaluated for imaginary frequencies. Taken together, the relations (9, 11) reproduce the Lifshitz expression for the Casimir force [9]. We however emphasize that (9) can be used to go beyond the Lifshitz expression since it allows one to deal with more general mirrors than those considered in (11).

As an example we consider mirrors built as metallic slabs having a finite thickness. For a given polarization, we denote by ρ the reflection coefficient (11) corresponding to a single vacuum/metal interface and we write the reflection amplitude r for the slab of finite thickness through a Fabry-Perot formula

$$r=\rho\frac{1-{\rm e}^{-2\delta}}{1-\rho^2{\rm e}^{-2\delta}},$$
$$\delta=\frac{D}{c}\sqrt{\omega^2\left(\varepsilon\left({\rm i}\omega\right)-1\right)+c^2\kappa^2}. \tag{12}$$

This expression has been written directly for imaginary frequencies. The parameter δ represents the optical length in the metallic slab and D the physical thickness. The single interface expression (11) is recovered in the limit of a large optical thickness $\delta\gg 1$. With the plasma model, this condition just means that the thickness D is larger than the plasma wavelength $\lambda_{\rm P}$.

In order to discuss recent experiments it may be useful to write the reflection coefficients for multilayer mirrors. For example one may consider two-layer mirrors with a layer of thickness D of a metal A deposited on a large slab of metal B in the limit of large thickness. The reflection formulas are then obtained as in [26] but accounting for oblique incidence. The equations (9, 10) may then be calculated for the two-layer mirrors. This could help to obtain more accurate estimations for the experiments as soon as physical characteristics of the two-layer mirrors are precisely known. In the present paper we use reflection amplitudes (11) which are well adapted to a general discussion since they depend on a smaller number of parameters.

4 Plasma and Drude model

We will now evaluate the reduction factor for the Casimir force when the frequency dependent dielectric function may be represented by the plasma or Drude model.

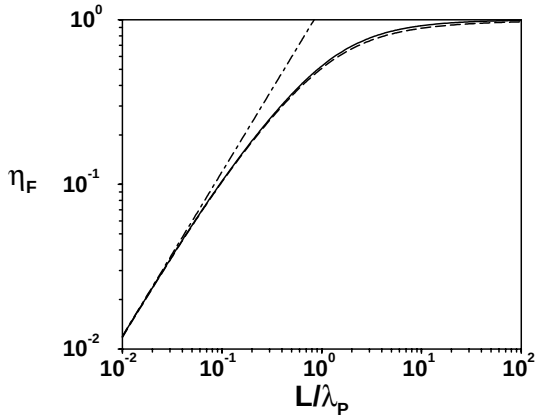

Fig. 1. Reduction of the Casimir force compared to the force between perfect mirrors, when the finite conductivity may be described by a plasma model (solid line) or a Drude model (dashed line) with a ratio $\gamma/\omega_{\rm P}$ equal to 4×10^{-3}. The difference due to the relaxation parameter has only a small effect on the calculation of the Casimir force. The dotted-dashed line corresponds to the short distance asymptotic behavior.

We begin with the plasma model where the quantities $\varepsilon(\omega)$ and $\varepsilon(\mathrm{i}\omega)$ are represented as follows

$$\varepsilon(\omega) = 1 - \frac{\omega_{\rm P}^2}{\omega^2},$$
$$\varepsilon(\mathrm{i}\omega) = 1 + \frac{\omega_{\rm P}^2}{\omega^2}. \tag{13}$$

Using expressions (11, 13) it is possible to obtain the reduction factor (9) defined for the Casimir force through numerical integrations. The result is drawn in Figure 1, as a function of the dimensionless parameter $L/\lambda_{\rm P}$, that is the ratio between the distance L and the plasma wavelength $\lambda_{\rm P}$. As expected the Casimir formula is reproduced at large distances ($\eta_{\rm F} \to 1$ when $L/\lambda_{\rm P} \gg 1$). At distances smaller than $\lambda_{\rm P}$ in contrast, a significant reduction factor is obtained. This factor $\eta_{\rm F}$ scales as $L/\lambda_{\rm P}$ at the limit of small distances. This means that the whole expression (4) of the Casimir force is a power law which undergoes a change of exponent when the distance L crosses the plasma wavelength $\lambda_{\rm P}$ characterizing the optical response of metals. This is quite analogous to the crossover discovered by Casimir and Polder for the variation of van der Waals force with respect to the interatomic distance [27].

An asymptotic law of variation for $\eta_{\rm F}$ varying as $L/\lambda_{\rm P}$ at small distances has been proposed repeatedly since Lifshitz [9]. We have been able to derive from (9, 11, 13) a precise value for the coefficient appearing in this law

$$L \ll \lambda_{\rm P} \quad \to \quad \eta_{\rm F} = \alpha \frac{L}{\lambda_{\rm P}}$$
$$\alpha = \frac{30}{\pi^2} \int_0^\infty \mathrm{d}K \; \mathrm{e}^{-\frac{3K}{4}} \left(\frac{K^2}{\sqrt{\sinh\frac{K}{2}}} - \frac{K^2}{\sqrt{\cosh\frac{K}{2}}} \right)$$
$$\simeq 1.193. \tag{14}$$

This implies a similar behavior for the reduction factor $\eta_{\rm E}$ with a different proportionality coefficient

$$L \ll \lambda_{\rm P} \quad \to \quad \eta_{\rm E} = \frac{3}{2}\alpha \frac{L}{\lambda_{\rm P}}\cdot \tag{15}$$

Hence, $\eta_{\rm E}$ is larger than $\eta_{\rm F}$ at short distances, which means a less important reduction with respect to the case of perfect mirrors. The asymptotic law (14) valid at short distances, taken with its equivalent (5) at large distances, is an important feature of the variation of $\eta_{\rm F}$ with L which is not obeyed by the approximants which have been used to discuss recent experimental results [8,15]. These approximants are compared with the exact expression of the reduction factor for the plasma model in Appendix A.

As already discussed, the plasma model does not provide a good description of the dielectric response of metals. The main reason is that the dielectric function $\varepsilon(\omega)$ is real in (13) and, therefore, does not account for any dissipative mechanism. A much better representation of the dielectric function corresponding to the optical response of conduction electrons is the Drude model [28]

$$\varepsilon(\omega) = 1 - \frac{\omega_{\rm P}^2}{\omega(\omega + \mathrm{i}\gamma)}$$
$$\varepsilon(\mathrm{i}\omega) = 1 + \frac{\omega_{\rm P}^2}{\omega(\omega + \gamma)}. \tag{16}$$

This model describes not only the plasma response of conduction electrons with $\omega_{\rm P}$ still interpreted as the plasma frequency but also their relaxation, γ being the inverse of the electronic relaxation time.

The relaxation parameter γ is much smaller than the plasma frequency. For Al, Au, Cu in particular, we will find in the next section values for the ratio $\gamma/\omega_{\rm P}$ of the order of 4×10^{-3}. Hence relaxation plays a significant role in the modeling of the dielectric constant only at frequencies where the latter is much larger than unity. Stated in different words, it has to be taken into account only when the metallic mirror behaves as a nearly perfect reflector. This suggests that the relaxation will not have a large influence on the Casimir effect. This qualitative argument is confirmed by the result of a numerical integration reported in Figure 1. With a value of $\gamma/\omega_{\rm P}$ equal to 4×10^{-3}, that is of the order of the real values obtained for Al, Au, Cu, the variation of $\eta_{\rm F}$ remains smaller than 2%. It thus plays a marginal role at the level of accuracy aimed at but it is easy and safer to take it into account.

5 Real metals

For metals like Al, Au, Cu, the dielectric constant departs from the Drude model when interband transitions are reached, that is when the photon energy reaches a few eV. Hence, a more precise description of the dielectric constant, taking into account the known data on optical properties of these metals, has to be used for evaluating the force in the sub-μm range.

The dielectric response function for real frequencies may be written in terms of real and imaginary parts ε' and ε'' obeying general causality relations

$$\varepsilon(\omega) = \varepsilon'(\omega) + \mathrm{i}\varepsilon''(\omega)$$
$$\varepsilon'(\omega) - 1 = \frac{2}{\pi}\mathcal{P}\int_0^\infty \frac{x\varepsilon''(x)}{x^2-\omega^2}\mathrm{d}x. \tag{17}$$

Causality relations also allow one to obtain the dielectric constant at imaginary frequencies $\varepsilon(\mathrm{i}\omega)$ from the function $\varepsilon''(x)$ evaluated at real frequencies x, that is also the oscillator strength characterizing the material [29]

$$\varepsilon(\mathrm{i}\omega) - 1 = \frac{2}{\pi}\int_0^\infty \frac{x\varepsilon''(x)}{x^2+\omega^2}\mathrm{d}x. \tag{18}$$

When discussing optical data, we will measure frequencies either in eV or in rad/s, using the equivalence 1 eV = 1.537×10^{15} rad/s.

The values of the complex index of refraction, measured through different optical techniques, are tabulated as a function of frequency in several references [30–32]. Optical data may vary from one reference to another. Available data do not cover the whole frequency range and they have to be extrapolated. These two problems may cause variations of the results obtained for $\varepsilon(\mathrm{i}\omega)$ and, therefore, for the Casimir force. This is why we explain in detail how we proceed from the input, the optical data, to the output of the process, the reduction factors for Casimir force and energy.

Figure 2 shows the values for $\varepsilon''(\omega)$ as a function of frequency ω for the three metals Al, Au and Cu. All data are taken from [30,31] with a frequency range 0.04−1000 eV for Al and 0.1−1000 eV for Au and Cu. A large number of points is available in these sources so that the interpolation between these points does not raise any difficulty. However the data have to be extrapolated at low frequencies to increase the domain over which the integrations are performed. At energies around 0.1 eV the optical properties are quite well-described by the contribution of conduction electrons. Hence data available at these energies may be nicely fitted with a Drude model. For Al the corresponding Drude parameters are given in [30] as $\omega_\mathrm{P} = 11.5$ eV and $\gamma = 50$ meV. For Au and Cu there are not enough optical data at low frequencies to permit a determination of the two parameters ω_P and γ separately. Here we use additional information namely the estimation of ω_P coming from solid state physics [28,29]. Precisely we write

$$\omega_\mathrm{P}^2 = \frac{4\pi N e^2}{m^*} = \frac{Nq^2}{\varepsilon_0 m^*}$$
$$N = ZN_\mathrm{a} \tag{19}$$

where N is the number of conduction electrons per unit volume, that is also the product of the number Z of electrons per atom by the atomic number density N_a, q is the charge of electron and m^* is the effective mass of conduction electrons. This mass is different of the mass m of free electrons. The same correction may be described as

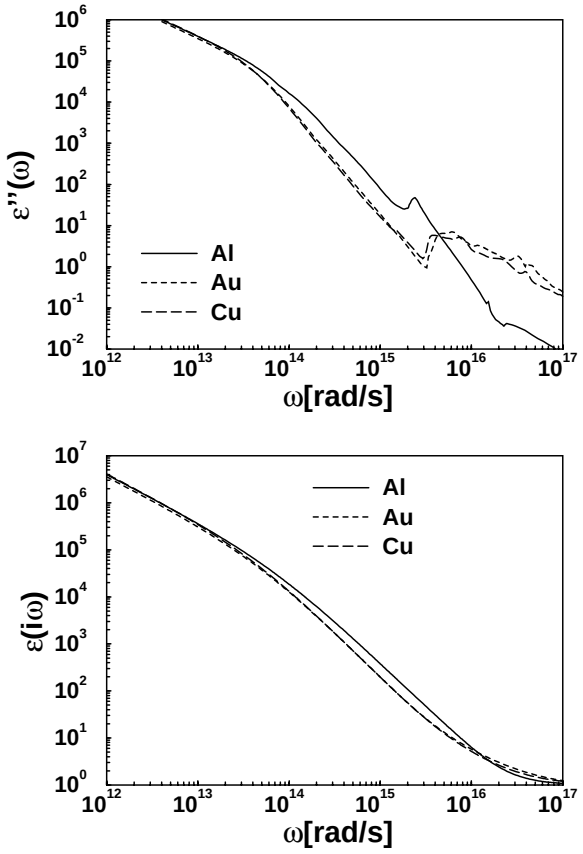

Fig. 2. The imaginary part of the dielectric constant as a function of real frequency (upper graph) and the dielectric constant as function of imaginary frequency (lower graph) for Al (solid line), Au (dotted line) and Cu (dashed line). At low frequencies the data fit a Drude model corresponding to the contribution of conduction electrons. Peaks in the imaginary part of the dielectric function correspond to deviations from the Drude model associated with interband transitions.

a change of the effective number of conduction electrons per atom from Z to Z^*. We keep the former description, use $Z = 1$ for Cu and Au, and choose for effective masses of conduction electrons the values $m^*/m \simeq 1$ for Au and $m^*/m \simeq 1.45$ for Cu [33,34]. With these assumptions we obtain nearly equal values for the plasma frequency of Au and Cu, $\omega_\mathrm{P} = 9.0$ eV. This corresponds to a plasma wavelength of 136 nm for Au and Cu, to be compared with the plasma wavelength of 107 nm for Al. Then the optical data of [30] allow us to deduce the relaxation parameter γ fitting the low energy data points with a Drude model. We obtain in this manner $\gamma = 35$ meV for Au and $\gamma = 30$ meV for Cu. These values correspond respectively to $\gamma/\omega_\mathrm{P} = 3.8 \times 10^{-3}$ and $\gamma/\omega_\mathrm{P} = 3.3 \times 10^{-3}$ to be compared to $\gamma/\omega_\mathrm{P} = 4.4 \times 10^{-3}$ for Al. Note that we have given deliberately all the numerical values in this paragraph with a limited accuracy since slightly different values could have been obtained as well, starting from different sources or using different criteria for choosing the values. This problem of extrapolation of optical data

at low frequencies is certainly a cause for systematical errors in the estimation of the Casimir force.

The dielectric constant for imaginary frequencies $\varepsilon(\mathrm{i}\omega)$ is then obtained by numerical integration of relation (18). Of course, the integration cannot be performed over the whole range $[0, \infty]$ of frequencies so that we have to give details about the integration procedure. We are mainly interested in experimentally explored plate separations in the range $0.1-10$ μm. These separations correspond to frequencies in the range $0.1-10$ eV. We thus need reliable values for $\varepsilon(\mathrm{i}\omega)$ with ω ranging from 10^{-4} to 10^{3} eV. To this aim we have to integrate (18) over real frequencies covering a still broader range $10^{-6}-10^{4}$ eV. In order to test the integration procedure we have varied the integration range by half an order of magnitude which changed the result by less than 1%. The curves obtained for the three metals are shown in the lower graph of Figure 2. In particular the curves for Au and Cu are nearly identical over the whole range of frequencies.

The Casimir force and energy are then calculated by numerical integration of equations (9, 10). The integration range is chosen as $10^{-4}-10^{3}$ eV in order to evaluate the Casimir force for plate separations in the range $0.1-10$ μm. The same test of the integration procedure has been performed leading to an error less than 1.5% for η_{F} and 2% for η_{E}. The limit of perfect reflectors has been reproduced with an error less than 1%. Figure 3 shows the reduction of the Casimir force and energy between metallic mirrors with respect to perfectly reflecting mirrors for the three metals. The force is reduced when going from Al to Au and has nearly the same value for Au and Cu. This directly reflects the behavior of the dielectric constants $\varepsilon(\mathrm{i}\omega)$ which decrease along the same series in Figure 2. As already discussed in the previous section the reduction η_{E} is less pronounced than η_{F}.

We give in the following table a few numerical values for the reduction factors η_{F} and η_{E} for the three metals at three typical distances.

	Al	Au	Cu
η_{F} [0.1 μm]	0.55	0.48	0.48
η_{E} [0.1 μm]	0.63	0.55	0.55
η_{F} [0.5 μm]	0.85	0.81	0.81
η_{E} [0.5 μm]	0.88	0.85	0.85
η_{F} [3.0 μm]	0.96	0.96	0.96
η_{E} [3.0 μm]	0.97	0.97	0.97

(20)

We remind once again that η_{E} is the reduction factor for energy between two plane mirrors, that is also the estimate of reduction factor for the force in the plane-sphere geometry. From our analysis the factors η_{F} and η_{E} turn out to be the same for Au and Cu. Incidentally, as the dielectric constants of Au and Cu are nearly the same, mirrors built with a layer of Au on a slab of Cu would not lead to different results. This seems to solve a difficulty in the analysis of experimental results of [6]. The values obtained here for Al at 0.1 μm and Cu at 0.5 μm correspond to those found in [8]. But significant differences appear for Au at 0.5 μm where we find values of η_{F} and η_{E} exceeding by 23% and 18% respectively the values given in [8]. Furthermore the agreement between our result for Cu at 0.5 μm and the one in [8] appears to be an accidental crossing between two curves having quite different behaviors as functions of distances. Since these differences have important consequences for the comparison of experimental results with theory, we discuss them in detail in Appendix B.

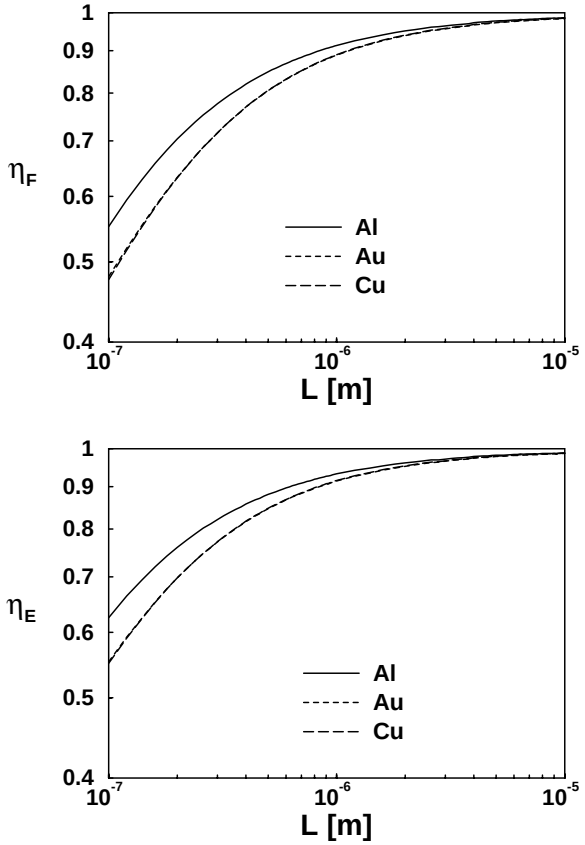

Fig. 3. Reduction of the Casimir force (upper graph) and energy (lower graph) between metallic reflectors with respect to perfectly reflecting mirrors as a function of their distance L. The three curves correspond to Al (solid line), Au (dotted line) and Cu (dashed line).

6 Conclusion

The Casimir force has now been experimentally explored at distances in the sub-μm range and the reduction of the force due to finite conductivity of metals has been observed. For an accurate comparison of the experimental results with theory, it is necessary to dispose of precise theoretical expectations.

In this paper we have presented a detailed analysis of the influence of the imperfect reflection on the Casimir force between two plane metallic plates. In particular,

we have given a precise evaluation of the reduction factor for metals used in recent experiments, that is Al, Au and Cu. This factor becomes significant at distances smaller than 1 μm and it reaches values of about 50% for the smallest explored distances.

The reduction factor $\eta_{\rm E}$ calculated in the present paper for the energy between plane plates can be used to infer the reduction factor for the force in the plane-sphere geometry if the proximity theorem is trusted. However the accuracy of this theorem is not known. Other corrections have also to be taken into account. Thermal corrections are significant at distances larger than a few μm but have not been seen in the experiment where these distances were explored [6]. The roughness corrections are also expected to play an important role [19,21].

In these conditions it is premature to claim that a good agreement has been reached between experiments and theory. It is worth developing new experiments using either the same techniques or different ones [35,36]. More work is also needed on the theoretical side, in particular for obtaining more reliable estimations of the effect of geometry and roughness on the Casimir force. Such efforts are certainly worthwhile not only because of the interest of reaching conclusions on the Casimir force but also for making it possible to control its effect when studying small short range forces [37–40].

We wish to thank Ephraim Fischbach, Marc-Thierry Jaekel, David Koltick, Vladimir Mostepanenko and Roberto Onofrio for stimulating discussions.

Appendix A: The plasma corrections

In this appendix we compare the reduction factor $\eta_{\rm F}$ evaluated for the Casimir force from expressions (9, 11) using the plasma model (13) with different approximants which have been used to discuss recent experimental results (see for example [8,15,19]).

The exact result is the solid line of Figure 1 reproduced as the solid line in Figure 4. Its behavior at long distances ($L \gg \lambda_{\rm P}$) corresponds to the known development [18]

$$\eta_{\rm A} = 1 - \frac{8}{3\pi}\frac{\lambda_{\rm P}}{L} + \frac{6}{\pi^2}\left(\frac{\lambda_{\rm P}}{L}\right)^2 \qquad (A.1)$$

drawn as long dashes A in Figure 4. Another interpolation formula may be deduced from this behavior as [18]

$$\eta_{\rm B} = \left(1 + \frac{11}{6\pi}\frac{\lambda_{\rm P}}{L}\right)^{-\frac{16}{11}} . \qquad (A.2)$$

This formula, drawn as short dashes B in Figure 4, presents the advantage of being positive at all distances and also being a monotonic function of distance, two important features of the exact result. However it fails to reproduce the asymptotic variation of $\eta_{\rm F}$ at small distances (compare with (14)). Another approximant, obtained by developing $\eta_{\rm B}$ at the fourth order in $\lambda_{\rm P}/L$, has sometimes been used [15]

$$\eta_{\rm C} = \eta_{\rm A} - \frac{38}{3\pi^3}\left(\frac{\lambda_{\rm P}}{L}\right)^3 + \frac{931}{9\pi^4}\left(\frac{\lambda_{\rm P}}{L}\right)^4 . \qquad (A.3)$$

It is drawn as the dotted-dashed line C in Figure 4. On the whole, Figure 4 clearly shows that all these approximants fail to reproduce the correct behavior at distances smaller than the plasma wavelength $\lambda_{\rm P}$.

Incidentally an interesting approximant may be defined by the following formula

$$\eta_{\rm U} = \frac{1}{1 + \frac{8}{3\pi}\frac{\lambda_{\rm P}}{L}} . \qquad (A.4)$$

It fits the known behavior of the exact result at the first-order, but not the second-order one, in $\lambda_{\rm P}/L$. It is proportional to $L/\lambda_{\rm P}$ at small distances as the correct result (14). Moreover the coefficient $3\pi/8$ has a value 1.178 very close to the proportionality coefficient $\alpha \simeq 1.193$ appearing in (14), the relative difference being of the order of 1%. Hence, $\eta_{\rm U}$ may be considered as a uniform approximant reproducing the variation of $\eta_{\rm F}$ over the whole range of distances. It reproduces the exact result everywhere with an error of at most 5%. This precision is however not sufficient for it to be used in the place of the correct result.

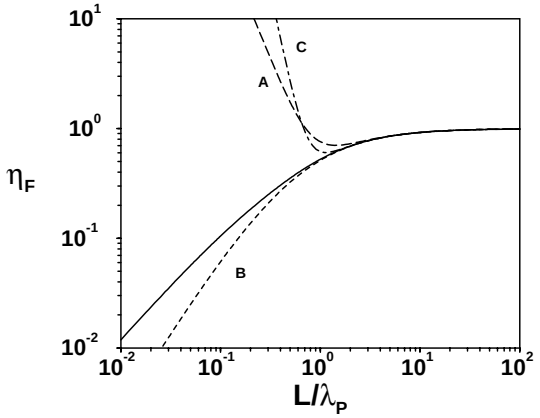

Fig. 4. Reduction factor $\eta_{\rm F}$ for the Casimir force as a function of the ratio $L/\lambda_{\rm P}$ when the finite conductivity is described by a plasma model (solid line). This curve is compared to different approximants (dashed lines) used in the literature and described in the text. These approximants are reasonable at large distances but depart from the exact result when $L/\lambda_{\rm P}$ approaches unity.

Appendix B: The case of copper

In this appendix, we compare the reduction factors $\eta_{\rm F}$ and $\eta_{\rm E}$ obtained for copper from the computations of the present paper and those of [8]. Both derivations are based on the same procedure which we have already described

in the text. Optical data taken from different references agree reasonably well between each other. We however point out that quite different techniques are used here and in [8] for interpolating between available data and extrapolating at low frequencies and that these differences are responsible for significant deviations in the behaviors of $\eta_{\rm F}$ and $\eta_{\rm E}$ as functions of the plate separation.

The upper graph of Figure 5 shows three different plots of the imaginary part of the dielectric constant. The first one is the one explained in the present paper with data points taken from [30,31] (diamonds) and extrapolation at low frequency with a Drude model (solid line in Fig. 5). Our procedure is explained in more detail in the main part of this paper. The corresponding Drude parameters, a plasma frequency $\omega_{\rm P} = 9.0$ eV and a relaxation parameter $\gamma = 30$ meV are in reasonable agreement with existing knowledge from solid state physics.

The second plot has been designed by ourselves as an attempt to reproduce the computations of [8]. The triangles are optical data taken from [32]. These data are not exactly identical but they are in reasonable agreement with those taken from [30,31]. However only three data points are given in [32] for the frequency range $10^{14}-2\times10^{15}$ rad/s whereas a much larger number of data points may be found in [30,31]. In contrast to our treatment, a specific interpolation procedure had therefore to be used in [8] to fill the gaps between the data points. Although this procedure is not described explicitly in [8] we have been able to reproduce a curve having the same appearance (compare with Fig. 1a in [8]). This curve results from a linear interpolation between the data points on a lin-lin scale. It appears clearly in Figure 5 that this interpolation procedure produces bumps on the dielectric response functions (dashed line) which are largely outside the data known from [30,31]. Optical data are in fact consistent with a linear interpolation on a log-log scale rather than on a lin-lin scale. This is the first important difference between the two treatments. The second important difference is associated with the extrapolation of data at low frequencies. In [8] the data points were extrapolated by a power law proportional to $1/\omega$ starting from the lowest frequency data available in [32]. The whole curve of [8] is not at all consistent with a Drude model at frequencies below 10^{15} rad/s. To summarize this presentation of the dielectric function used in [8] we may say that it corresponds to values too large in the range $10^{14}-2\times10^{15}$ rad/s by a factor which can be more than 10 and too small below 10^{14} rad/s by a factor up to 6.

The case of low frequency extrapolation requires more cautious discussions. As explained in the main part of this paper, the optical data available for Cu do not permit an unambiguous estimation of the two parameters $\omega_{\rm P}$ and γ separately. Other couples of value can be chosen which would also be consistent with optical data. To make this point explicit, we have drawn a third plot in Figure 5 (dashed-dotted line) which corresponds to a Drude model fitting the optical data of [32] and the low frequency behavior of [8]. Obviously it does not reproduce the extra bumps of [8]. The associated Drude parameters

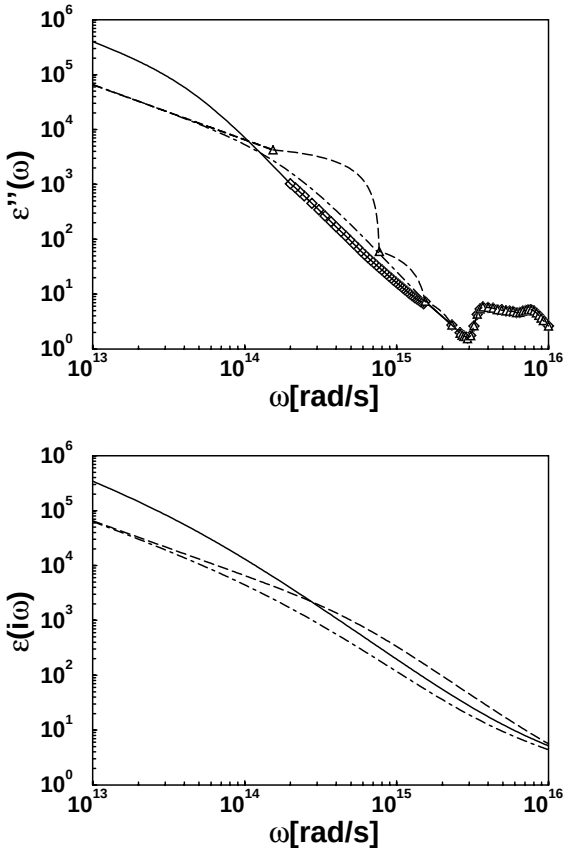

Fig. 5. Imaginary part of the dielectric constant as a function of frequency (upper graph) and dielectric constant as function of imaginary frequency (lower graph) for copper. The diamonds are data points from reference [30,31] and the solid line is our extrapolation at low frequencies of these data. The triangles correspond to data points from [32]. The dashed line represents the extrapolation at low frequencies and the interpolation between the last three data points as in [8]. The dotted-dashed line corresponds to another extrapolation of the same data. More detailed explanations are given in the text.

$\omega_{\rm P} = 7.5$ eV and $\gamma = 130$ meV correspond to an effective mass $m^*/m \simeq 2.1$ and to a ratio $\gamma/\omega_{\rm P} \simeq 1.7\times10^{-2}$ which are quite different from those used in our treatment. In order to have an indication of the effect of the uncertainties associated with optical data, we will however proceed to the computations with this curve, too.

We now perform the calculations as explained in the main part of the text. The lower graph in Figure 5 shows the different results for the dielectric constant $\varepsilon(\mathrm{i}\omega)$ as a function of imaginary frequency for the three different dielectric functions. As expected from the previous discussion, the values $\varepsilon(\mathrm{i}\omega)$ found in [8] are too small at frequencies lower than 10^{14} rad/s but too large around 10^{15} rad/s when compared to those deduced from our calculation. This has a significant consequence for the evaluation of the reduction factors $\eta_{\rm F}$ and $\eta_{\rm E}$ drawn in Figure 6 for a plate separation ranging from 0.1 μm to 10 μm.

Our reconstruction of the computations of [8] reproduce pretty well the published results at the distance

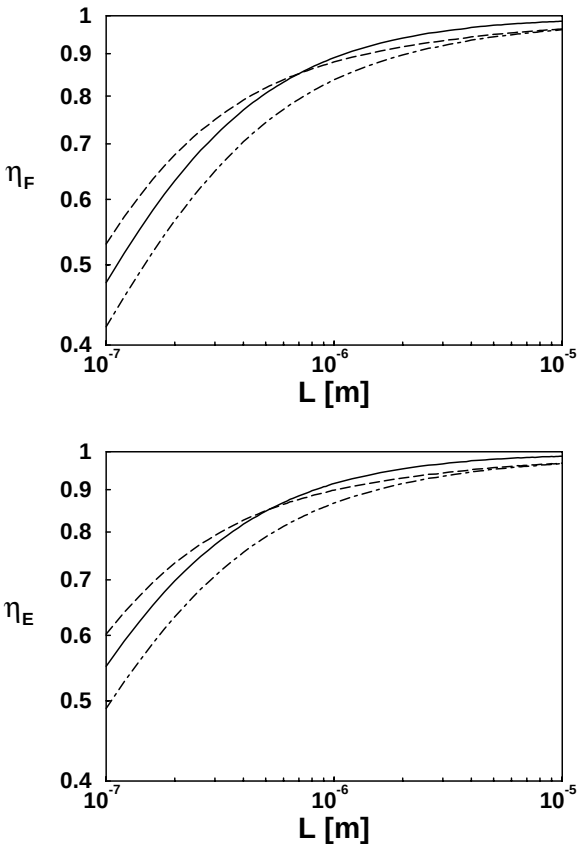

Fig. 6. Reduction factors η_F for the Casimir force (upper graph) and η_E for the Casimir energy (lower graph) as a function of the plate separation L. The solid line corresponds to the calculation of the present paper, the dashed line to the calculation in [8]. The dotted-dashed line corresponds to a calculation with a Drude model fitting the optical data of [32] and the low frequency behavior of [8].

of 0.5 μm for which numerical values are given. However, the general behaviors of the curves are quite different. The Casimir force and Casimir energy obtained from the optical data used in [8] are too large at small distances and too small at large distances. These features, which are made explicit with values of η_E given in the following table, are consistent with the discussions of the preceding paragraphs. The three columns 1, 2, 3 correspond respectively to the solid lines, dashed lines and dotted-dashed lines of Figures 5 and 6.

	1	2	3
η_E [0.1 μm]	0.55	0.60	0.49
η_E [0.5 μm]	0.85	0.85	0.79
η_E [3.0 μm]	0.97	0.94	0.93

(B.1)

The crossing of the results in columns 1 and 2 at the distance of 0.5 μm appears as an accidental compensation of these two flaws. The relative difference between the two results may be as large as 10%.

A claim of agreement between experiment and theory could be based on a comparison of values of η_E obtained at different distances with values in the column 1 or, perhaps, in the column 3. As explained above, both columns correspond to reasonable extrapolations of the optical data. The advantage of column 1 over column 3 lies in values of the Drude parameters in better accordance with the knowledge in solid state physics. The difference between columns 1 and 3 may be considered as giving an idea of the uncertainties associated with the incompleteness of optical data. In any case the two corresponding curves, drawn as solid and dotted-dashed lines in Figure 6, have similar dependences on the plate separation although the absolute values are shifted from one curve to the other. In contrast the dashed curve in Figure 6 which corresponds to the calculations of [8] and crosses the two former curves cannot be considered as consistent with the known optical data.

References

1. H.B.G. Casimir, Proc. Kon. Nederl. Akad. Wet. **51**, 793 (1948).
2. B.V. Deriagin, I.I. Abrikosova, Sov. Phys. JETP **3**, 819 (1957).
3. M.J. Sparnaay, Physica **XXIV**, 751 (1958); W. Black, J.G.V. De Jongh, J.Th.G. Overbeek, M.J. Sparnaay, Trans. Faraday Soc. **56**, 1597 (1960).
4. D. Tabor, R.H.S. Winterton, Nature **219**, 1120 (1968).
5. E.S. Sabisky, C.H. Anderson, Phys. Rev. A **7**, 790 (1973).
6. S.K. Lamoreaux, Phys. Rev. Lett. **78**, 5 (1997); erratum in Phys. Rev. Lett. **81**, 5475 (1998).
7. U. Mohideen, A. Roy, Phys. Rev. Lett. **81**, 4549 (1998); A. Roy, C. Lin, U. Mohideen, Phys. Rev. D **60**, 111101 (1999).
8. S.K. Lamoreaux, Phys. Rev. A **59**, R3149 (1999).
9. E.M. Lifshitz, Sov. Phys. JETP **2**, 73 (1956); E.M. Lifshitz, L.P. Pitaevskii, *Landau and Lifshitz Course of Theoretical Physics: Statistical Physics* (Butterworth-Heinemann, 1980), Part 2, Chap. VIII.
10. N.E. Dzyaloshinshii, E.M. Lifshitz, L.P. Pitaevskii, Sov. Phys. Uspekhi **4**, 153 (1961).
11. C.M. Hargreaves, Proc. Kon. Nederl. Akad. Wet. B **68**, 231 (1965).
12. J. Schwinger, L.L. de Raad Jr, K.A. Milton, Ann. Phys. (NY) **115**, 1 (1978).
13. J. Mehra, Physica **57**, 147 (1967).
14. L.S. Brown, G.J. Maclay, Phys. Rev. **184**, 1272 (1969).
15. G.L. Klimchitskaya, A. Roy, U. Mohideen, V.M. Mostepanenko, Phys. Rev. A **60**, 3487 (1999).
16. B.V. Deriagin, I.I. Abrikosova, E.M. Lifshitz, Quart. Rev. **10**, 295 (1968).
17. J. Blocki, J. Randrup, W.J. Swiatecki, C.F. Tsang, Ann. Phys. (NY) **105**, 427 (1977).
18. V.M. Mostepanenko, N.N. Trunov, Sov. J. Nucl. Phys. **42**, 812 (1985).
19. V.B. Bezerra, G.L. Klimchitskaya, C. Romero, Mod. Phys. Lett. **12**, 2613 (1997).
20. C.R. Hagen, preprint `hep-th/9902057`.
21. A. Roy, U. Mohideen, Phys. Rev. Lett. **82**, 4380 (1999).
22. M.T. Jaekel, S. Reynaud, J. Phys. I France **1**, 1395 (1991).
23. D. Kupiszewska, Phys. Rev. A **46**, 2286 (1992).

24. S.M. Barnett, C.R. Gilson, B. Huttner, N. Imoto, Phys. Rev. Lett. **77**, 1739 (1996).
25. L. Landau, E.M. Lifshitz, *Landau and Lifshitz Course of Theoretical Physics: Electrodynamics in Continuous Media* (Butterworth-Heinemann, 1980), Chap. X.
26. A. Lambrecht, M.T. Jaekel, S. Reynaud, Phys. Lett. A **225**, 188 (1997).
27. H.B.G. Casimir, D. Polder, Phys. Rev. **73**, 360 (1948).
28. N.W. Ashcroft, N.D. Mermin, *Solid State Physics* (HRW International, 1976).
29. L. Landau, E.M. Lifshitz, Chap. IX in [25].
30. In *Handbook of Optical Constants of Solids*, edited by E.D. Palik (Academic Press, New York, 1995).
31. In *Handbook of Optics II* (McGraw-Hill, New York, 1995).
32. In *CRC Handbook of Chemistry and Physics*, 79th edn. (CRC Press, Boca Raton, FL, 1998).
33. L.G. Schulz, Philos. Mag. Suppl. **6**, 102 (1957).
34. H. Ehrenreich, H.R. Philipp, Phys. Rev. **128**, 1622 (1962).
35. R. Onofrio, G. Carugno, Phys. Lett. A **198**, 365 (1995).
36. A. Grado, E. Calonni, L. Di Fiori, Phys. Rev. D **59**, 42002 (1999).
37. E. Fischbach, C. Talmadge, *The Search for Non Newtonian Gravity* (AIP Press/Springer Verlag, 1998) and references therein; E. Fischbach, D.E. Krause, Phys. Rev. Lett. **82**, 4753 (1999).
38. G. Carugno, Z. Fontana, R. Onofrio, C. Rizzo, Phys. Rev. D **55**, 6591 (1997).
39. J.C. Long, H.W. Chan, J.C. Price, Nucl. Phys. B **539**, 23 (1999).
40. M. Bordag, B. Geyer, G.L. Klimchitskaya, V.M. Mostepanenko, Phys. Rev. D **60**, 55004 (1999).

Reproduction de l'article "Temperature dependence of the Casimir effect between metallic mirrors", C. Genet, A. Lambrecht, and S. Reynaud, *Phys. Rev.* **A 62**, 012110 (2000)

Temperature dependence of the Casimir effect between metallic mirrors

Cyriaque Genet, Astrid Lambrecht, and Serge Reynaud
Laboratoire Kastler Brossel, Unité de l'Ecole Normale Supérieure, de l'Université Pierre et Marie Curie, et du Centre National de la Recherche Scientifique, Campus Jussieu, case 74, 75252 Paris Cedex 05, France
(Received 22 February 2000; published 15 June 2000)

We calculate the Casimir force and free energy for plane metallic mirrors at nonzero temperature. Numerical evaluations are given with temperature and conductivity effects treated simultaneously. The results are compared with the approximation where both effects are treated independently and the corrections simply multiplied. The deviation between the exact and approximated results takes the form of a temperature dependent function for which an analytical expression is given. The knowledge of this function allows simple estimations that are accurate below the 1% level.

PACS number(s): 12.20.Ds, 03.70.+k, 42.50.Lc

I. INTRODUCTION

The Casimir force [1] has been observed in a number of ''historic'' experiments [2–5]. It has been measured recently with an improved experimental precision [6–8]. This should allow for an accurate comparison with the predictions of quantum field theory, provided that these predictions account for the differences between real experiments and the idealized Casimir situation. In particular, experiments are performed at room temperature between metallic mirrors and not at zero temperature between perfect reflectors. The theoretical expectations should be computed with a high accuracy if the aim is to test agreement between theory and experiment at, say, the 1% level. The efforts for accuracy are also worth for making it possible to control the effect of Casimir force when studying small short range forces [9–11].

The influence of thermal field fluctuations on the Casimir force are known to become important for distances of the order of a typical length [12–15]

$$\lambda_T=\frac{2\pi c}{\omega_T}=\frac{\hbar c}{k_B T}. \tag{1}$$

When evaluated at room temperature, this length λ_T is approximately 7 μm. In contrast, the finite conductivity of metals has an appreciable effect for distances smaller than or of the order of the plasma wavelength λ_P determined by the plasma frequency ω_P of the metal (see Ref. [16], and references therein)

$$\lambda_P=\frac{2\pi c}{\omega_P}. \tag{2}$$

For metals used in the recent experiments, this wavelength lies in the range 0.1–0.2 μm. This means that conductivity and thermal corrections to the Casimir force are important in quite different distance ranges. Thermal corrections are usually ignored in the sub-μm range where the effect of imperfect reflection is significant whereas the conductivity correction is unimportant above a few μm where the effect of temperature becomes appreciable. This explains why the two corrections are usually treated independently from each other. When an accurate comparison between experimental and theoretical values of the Casimir force is aimed at, the error induced by this approximation has, however, to be precisely evaluated. Furthermore, the region of overlap of the two corrections is precisely in the μm range, which is a crucial distance range for the comparison between experiment and theory.

The purpose of this paper is to give an accurate evaluation of the Casimir force F taking into account finite conductivity and temperature corrections at the same time. To characterize the whole correction, we will compute the factor η_F describing the combined effect of conductivity and temperature

$$\eta_F=\frac{F}{F_{\rm Cas}},\qquad F_{\rm Cas}=\frac{\hbar c A\pi^2}{240L^4}. \tag{3}$$

$F_{\rm Cas}$ is the ideal Casimir force corresponding to perfect mirrors in vacuum. L is the distance between the mirrors, A their surface, and $\hbar$ and c, respectively, the Planck constant and the speed of light. We will also evaluate the factors associated with each effect taken separately from each other

$$\eta_F^P=\frac{F^P}{F_{\rm Cas}},\qquad \eta_F^T=\frac{F^T}{F_{\rm Cas}}. \tag{4}$$

F^P is the Casimir force evaluated by accounting for finite conductivity of the metals but assuming zero temperature and F^T is the Casimir force evaluated at temperature T for perfect reflectors. Of course η_F^P depends on the ratio L/λ_P and η_F^T on the ratio L/λ_T.

Now the question raised in the previous paragraphs may be stated precisely: to which level of accuracy can the complete correction factor η_F be approximated as the product of the factors η_F^P and η_F^T? To answer this question we will evaluate the quantity

$$\delta_F=\frac{\eta_F}{\eta_F^P\eta_F^T}-1 \tag{5}$$

which measures the degree of validity of the approximation where both effects are evaluated independently from each other. We will give an analytical estimation of this deviation which may thus be taken into account without any difficulty.

We will also give the same results for the Casimir energy by defining a factor η_E measuring the whole correction of Casimir energy due to conductivity and temperature and then discussing the factors η_E^P and η_E^T and the deviation δ_E in the same manner as for the force.

Some additional remarks have to be made at this point. First, recent experiments are not performed in the plane-plane but in the plane-sphere configuration. The Casimir force in this geometry is usually estimated from the proximity theorem [17–21]. Basically this amounts to evaluating the force by adding the contributions of various distances as if they were independent. In the plane-sphere geometry the force evaluated in this manner turns out to be given by the Casimir energy evaluated in the plane-plane configuration for the distance L being defined as the distance of closest approach in the plane-sphere geometry. Hence, the factor η_E evaluated in this paper for energy can be used to infer the factor for the force measured in the plane-sphere geometry. Then, surface roughness corrections will not be considered in the present paper. Finally the dielectric response of the metallic mirrors will be described by a plasma model. This model is known to describe correctly the Casimir force in the long distance range which is relevant for the study of temperature effects. Keeping these remarks in mind, our results will provide one with an accurate evaluation of the Casimir force in the whole range of experimentally explored distances.

II. CASIMIR FORCE AND FREE ENERGY

When real mirrors are characterized by frequency-dependent reflection coefficients, the Casimir force is obtained as an integral over frequencies and wavevectors associated with vacuum and thermal fluctuations [22]. The Casimir force is a sum of two parts corresponding to the two field polarizations with the two parts having the same form in terms of the corresponding reflection coefficients

$$F=\sum_{k=-\infty}^{\infty}\frac{\omega_T}{2}\mathbb{F}[k\omega_T],$$

$$\mathbb{F}[\omega\geqslant 0]=\frac{\hbar A}{2\pi^2}\int_{\frac{\omega}{c}}^{+\infty}d\kappa\kappa^2 f,$$

$$f=\frac{r_\perp^2(i\omega,i\kappa)}{e^{2\kappa L}-r_\perp^2(i\omega,i\kappa)}+\frac{r_{||}^2(i\omega,i\kappa)}{e^{2\kappa L}-r_{||}^2(i\omega,i\kappa)}, \tag{6}$$

$$\mathbb{F}[-\omega]=\mathbb{F}[\omega].$$

$r_\perp(r_{||})$ denotes the amplitude reflection coefficient for the orthogonal (parallel) polarization of one of the two mirrors. The mirrors are here supposed to be identical, otherwise $r_\perp^2$ should be replaced by the product of the two coefficients. ω is the frequency and κ the wave vector along the longitudinal direction of the cavity formed by the two mirrors. $\mathbb{F}[\omega]$ is defined for positive frequencies and extended to negative ones by parity.

The Casimir force (6) may also be rewritten after a Fourier transformation, as a consequence of Poisson formula [15]

$$F=\sum_{m=-\infty}^{\infty}\tilde{\mathbb{F}}(m\lambda_T),$$

$$\tilde{\mathbb{F}}(x)=\int_0^\infty d\omega\cos\left(\frac{\omega x}{c}\right)\mathbb{F}[\omega]. \tag{7}$$

The contribution of vacuum fluctuations, that is also the limit of a null temperature ($\omega_T\rightarrow 0$) in Eq. (6), corresponds to the contribution $m=0$ in Eq. (7)

$$F^P=\tilde{\mathbb{F}}(0)=\int_0^\infty d\omega\mathbb{F}[\omega]. \tag{8}$$

Hence, the whole force (7) is the sum of this vacuum contribution $m=0$ and of thermal contributions $m\neq 0$.

We will consider metallic mirrors with the dielectric function $\varepsilon(i\omega)$ for imaginary frequencies given by the plasma model

$$\varepsilon(i\omega)=1+\frac{\omega_P^2}{\omega^2}. \tag{9}$$

ω_P is the plasma frequency related to the plasma wavelength λ_P by Eq. (2). For the metals used in recent experiments, the values chosen for the plasma wavelength λ_P will be 107 nm for Al and 136 nm for Cu and Au. These values are in agreement with knowledge from solid state physics [23,24] as well as with the integration of optical data described in detail in Ref. [16]. As already known, the results obtained from the plasma model departs from the more accurate integration of optical data for small distances. In this limit, however, the thermal corrections do not play a significant role. In the present paper we will restrict our attention to the plasma model and discuss the validity of the results obtained in this manner at the end of the next section.

We will also focus the attention on mirrors with a large optical thickness for which the reflection coefficients $r_\perp(i\omega,i\kappa)$ and $r_{||}(i\omega,i\kappa)$ correspond to a simple vacuum-metal interface. With the plasma model, these coefficients are read as

$$r_\perp=-\frac{\sqrt{\omega_P^2+c^2\kappa^2}-c\kappa}{\sqrt{\omega_P^2+c^2\kappa^2}+c\kappa},$$

$$r_{||}=\frac{\sqrt{\omega_P^2+c^2\kappa^2}-c\kappa(1+\omega_P^2/\omega^2)}{\sqrt{\omega_P^2+c^2\kappa^2}+c\kappa(1+\omega_P^2/\omega^2)}. \tag{10}$$

For wave vectors $c\kappa$ smaller than ω_P, mirrors may be considered to be perfectly reflecting. When converted to the distance domain, this entails that the force approaches the ideal Casimir expression when evaluated at large distances $L\gg\lambda_P$.

The Casimir energy will be obtained from the force by integration over the mirrors relative distance

$$E=\int_L^\infty F(x)dx. \tag{11}$$

As this procedure is performed at constant temperature, the energy thus obtained corresponds to the thermodynamical definition of a free energy. For simplicity we will often use the denomination of an energy. We will define a factor η_E measuring the whole correction of energy due to conductivity and temperature effects with respect to the ideal Casimir energy

$$\eta_E=\frac{E}{E_{\mathrm{Cas}}},\qquad E_{\mathrm{Cas}}=\frac{\hbar cA\pi^2}{720L^3}. \tag{12}$$

The positive value of the energy here means that the Casimir energy is a binding energy while the positive value of the force is associated with an attractive character. We will then define two factors η_E^P and η_E^T associated with each effect taken separately from each other, as in Eq. (4). As already done for the force correction factors in Eq. (5), we will finally evaluate the quantity δ_E which characterizes the degree of validity of the approximation where both effects are evaluated independently from each other. As mentioned in the Introduction, the results obtained for energy allows one to deal with the Casimir force in the plane-sphere geometry when trusting the proximity force theorem.

III. NUMERICAL EVALUATIONS

In the following we present the numerical evaluation of the correction factors of the Casimir force and energy using equations written in the former section. The force correction factor was evaluated for the experimentally relevant distance range of 0.1–10 μm with the help of Eq. (7), supposing explicitly a plasma model for the dielectric function, and the result was normalized by the ideal Casimir force. A double integration over frequencies and wavevectors had to be performed. Due to the cosine dependence in Eq. (7), the integrand turned out to be a highly oscillating function. Hence, the integration required care although it was performed with standard numerical routines. The energy correction factor was then calculated by numerically integrating the force and normalizing by the ideal Casimir energy [see Eq. (12)]. Integration was restricted to a finite interval, the upper limit exceeding at least by a factor of 10^4 the distance at which the energy value was calculated. Extending the integration range by a factor of 100 changed the numerical result by less than 10^{-7}.

The results of the numerical evaluation of η_F are shown as the solid lines in Fig. 1 for Al and for Cu-Au assuming a temperature of $T=300$ K. They are compared with the force reduction factor η_F^P due to finite conductivity (dashed lines) and the force enhancement factor η_F^T calculated for perfect mirrors at 300 K (dashed-dotted lines).

Figure 2 shows similar results for the factor η_E obtained through numerical evaluation of the Casimir free energy. The

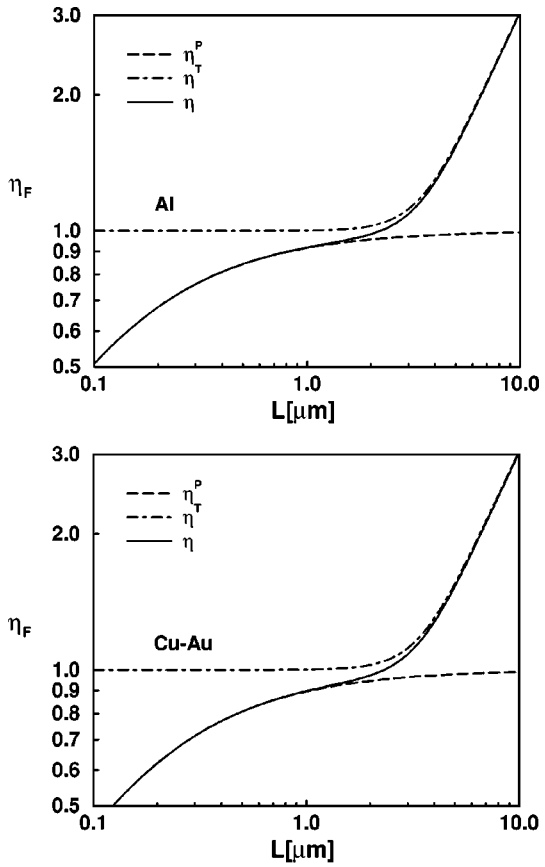

FIG. 1. Force correction factor for Al (upper figure) and Cu and Au (lower graph) as function of the mirrors distance at $T=300$ K.

shape of the graphs is similar to the ones of the force. However, while finite conductivity corrections are more important for the force, thermal effects have a larger influence on energy.

For the force as well as for the energy, temperature corrections are negligible in the short distance limit while conductivity corrections may be ignored at large distances. The whole correction factor η behaves roughly as the product $\eta^P\eta^T$ of the two correction factors evaluated separately. However, both correction factors are appreciable in the distance range $1-4$ μm in between the two limiting cases. Since this range is important for the comparison between experiments and theory, it is necessary to discuss in a more precise manner how good is the often used approximation which identifies η to the product $\eta^P\eta^T$. In order to assess the quality of this approximation, we have plotted in Fig. 3 the quantities δ_F and δ_E as a function of the distance for Al, Cu-Au, and two additional plasma wavelengths. A value of $\delta=0$ would signify that the approximation gives an exact estimation of the whole correction. An important outcome of our calculation is that the errors δ_F and δ_E are of the order of 1% for Al and Cu-Au at a temperature of 300 K.

For estimations at the 5% level, the separate calculation of η^P and η^T and the evaluation of η as the product $\eta^P\eta^T$ can therefore be used. However, if a 1% level or a better accuracy is aimed at, this approximation is not sufficient. It should be noticed furthermore that the error increases when

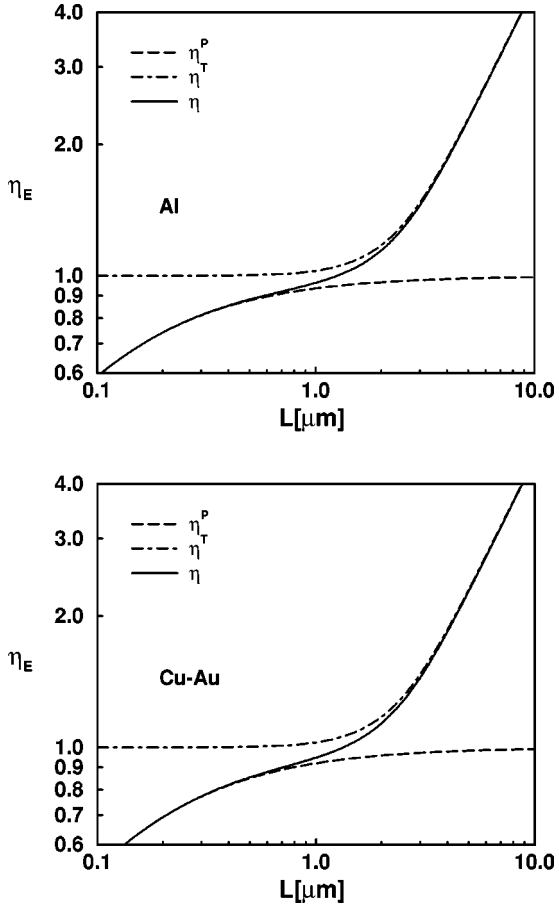

FIG. 2. Energy correction factor for Al (upper figure) and Cu and Au (lower graph) as function of the mirrors distance at $T = 300$ K.

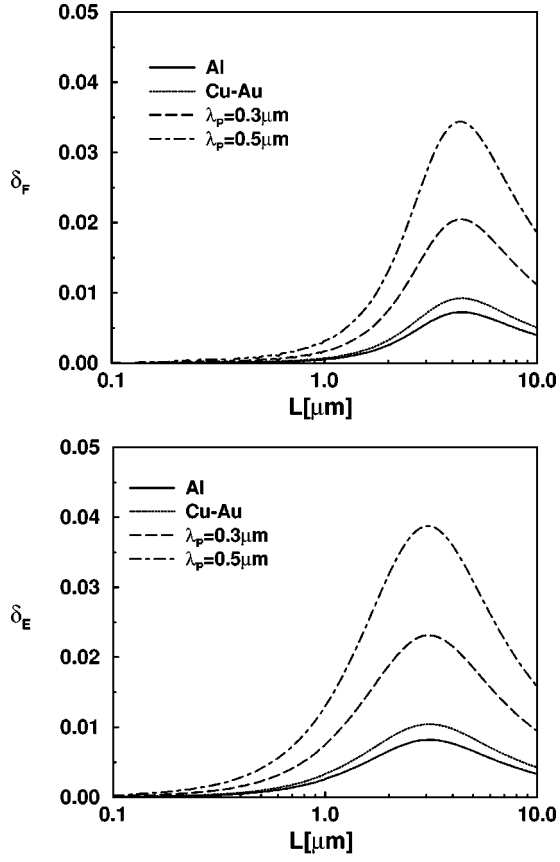

FIG. 3. δ_F (upper graph) and δ_E (lower graph) as a function of the mirrors distance. The results are given for the three metals Al, Cu-Au, and two larger plasma wavelengths.

the temperature or the plasma wavelength are increased. It becomes of the order of 4% for a plasma wavelength of 0.5 μm at 300 K. The sign obtained for δ means that the approximation gives too small values of force and energy.

We want now to emphasize a few points. In order to make the discussion precise, we give numerical values of the correction factors for two experimentally relevant distances, namely, 0.5 and 3 μm. The first distance corresponds to the smallest distance for which the plasma model gives results in correct agreement with the integration of optical data [16]. For this distance, $L = 0.5$ μm, the thermal corrections do not play a significant role ($\eta_F^T = 1.000$; $\eta_E^T = 1.004$).

	Al	Cu−Au	
η_F^P	0.843	0.808	
η_F	0.843	0.808	
η_E^P	0.879	0.851	(13)
η_E	0.883	0.855	

At shorter distances the results obtained with the plasma model depart from the values calculated from the integration of optical data by more than 1%. Hence, the values of η_F^P and η_E^P used for distances smaller than 0.5 μm have to take into account the more accurate dielectric function obtained through an integration of optical data [16]. In this short distance range however, the whole correction factors η_F and η_E may be obtained as the products $\eta_F^P \eta_F^T$ and $\eta_E^P \eta_E^T$.

In the long distance range in contrast, the temperature correction becomes predominant. The conductivity correction has still to be accounted for but it may be calculated by using the plasma model. This is illustrated by the correction factors obtained for a distance of $L = 3$ μm ($\eta_F^T = 1.117$; $\eta_E^T = 1.470$):

	Al	Cu−Au	
η_F^P	0.971	0.963	
$\eta_F^P \eta_F^T$	1.084	1.076	
η_F	1.090	1.083	(14)
η_E^P	0.978	0.972	
$\eta_E^P \eta_E^T$	1.437	1.429	
η_E	1.449	1.444	

For this distance, all corrections have to be taken into account. The metals cannot be considered as perfect reflectors yet, the temperature corrections are significant and the deviation between the exact correction and the mere product has to be included if a high accuracy is aimed at. This is especially true in the case of Casimir energy.

IV. SCALING LAWS FOR THE DEVIATIONS

An inspection of Fig. 3 shows that the curves corresponding to different plasma wavelengths λ_P have similar shapes

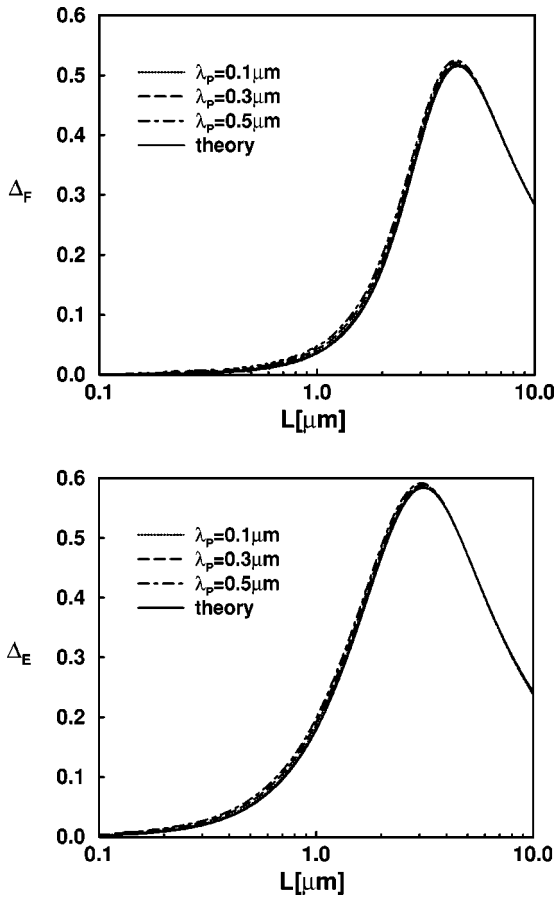

FIG. 4. The deviations are represented for the force (upper graph) and the free energy (lower graph) after the rescaling described by Eq. (15). Different plasma wavelengths lead to nearly identical functions, drawn as dotted, dashed, and dotted-dashed lines. These functions are hardly distinguishable from the solid lines which represent the analytical expressions derived in the next section.

with a maximum which is practically attained for the same distance between the mirrors. The amplitude of the deviations, which is larger for the energy than for the force, is found to vary linearly as a function of the plasma wavelength λ_P.

This scaling property is confirmed by Fig. 4 where we have drawn the deviations after an appropriate rescaling

$$\Delta = \frac{\lambda_T}{\lambda_P}\delta. \tag{15}$$

The curves obtained for Δ_F and Δ_E for different plasma wavelengths at temperature $T=300$ K are nearly perfectly identical to each other. These curves correspond to values of the plasma wavelength small compared to the thermal wavelength and the scaling law would not be obeyed so well otherwise.

In other words, the deviations δ_F and δ_E are proportional to the factor λ_P/λ_T on one hand, and to the functions Δ_F and Δ_E on the other hand. The latter functions, which no longer depend on λ_P, provide a simple method for reaching a good accuracy in the theoretical estimation of the whole correction factor

$$\eta = \eta^P \eta^T \left(1 + \frac{\lambda_P}{\lambda_T}\Delta\right). \tag{16}$$

This method is less direct than the complete numerical integration of the forces which has been performed for obtaining the curves presented in the previous section. But it requires easier computations while nevertheless giving accurate estimations of the correction factors. Typically, the deviation δ with a magnitude of the order of the % may be estimated with a much better precision through the mere inspection of Fig. 4. Alternatively, one may use the analytical expression of the functions Δ presented in the next section and drawn as the solid lines on Fig. 4.

V. ANALYTICAL EXPRESSIONS OF THE DEVIATIONS

The results of numerical integrations presented in the foregoing section have shown that the deviations δ_F and δ_E are proportional to the plasma wavelength λ_P, for plasma wavelengths small compared to the thermal wavelength. In this final section, we explain this scaling law by using a partial analytical integration of the whole correction factors.

To this aim, we write the force correction factor by dividing Eq. (7) by the value of the ideal Casimir force

$$\eta_F = \eta_F^P + (\eta_F^T - 1) + \Delta\eta_F. \tag{17}$$

The first term in Eq. (17) corresponds to the vacuum contribution (8)

$$\eta_F^P = \frac{120L^4}{\pi^4}\int_0^\infty d\kappa\,\kappa^3 \int_0^1 dy\, f \tag{18}$$

with f still given by Eq. (6). A dimensionless frequency $y=\omega/c\kappa$ measured with respect to the wave vector has been introduced. Note also that the wavevector κ is involved through the dimensionless quantity κL, except in the expressions of reflection coefficients. In Eq. (18), the integration over y may be performed analytically (see Appendix). At long distances, η_F^P tends to the limit of perfect reflection with a known correction [15]

$$L \gg \lambda_P \rightarrow \eta_F^P = 1 - \frac{8}{3\pi}\frac{\lambda_P}{L} + \cdots. \tag{19}$$

This expansion has been the subject of a number of papers and it has been used to propose interpolation formulas [20,21]. However such a series expansion can hardly reproduce the behavior at small distances where η_F^P varies as L/λ_P, which just means that the conductivity effect is not a small perturbation at short distances (see the Appendix).

Coming back to the whole expression (17) of the force correction factor, it remains to discuss the thermal contributions, that is, the second and third terms. These two terms come from the contributions $m\neq 0$ to Eq. (7). The opposite values of m give equal contributions and they have been

gathered. The thermal contributions have been split in to two parts, the second and third terms in Eq. (17), which correspond respectively to the limit of perfect mirrors on one hand,

$$\eta_F^T-1=\frac{240L^4}{\pi^4}\sum_{m=1}^{\infty}\int_0^{\infty}d\kappa\,\kappa^3\int_0^1 dy\,\cos(my\kappa\lambda_T)f_1,$$
$$f_1=\frac{2}{e^{2\kappa L}-1} \tag{20}$$

and the remainder, on the other hand,

$$\Delta\eta_F=\frac{240L^4}{\pi^4}\sum_{m=1}^{\infty}\int_{\omega/c}^{\infty}d\kappa\,\kappa^3\int_0^1 dy\,\cos(my\kappa\lambda_T)\Delta f,$$
$$\Delta f=f-f_1 \tag{21}$$
$$=-\frac{e^{2\kappa L}}{e^{2\kappa L}-1}\left(\frac{1-r_\perp^2}{e^{2\kappa L}-r_\perp^2}+\frac{1-r_{||}^2}{e^{2\kappa L}-r_{||}^2}\right).$$

The contribution (20) has been denoted (η_F^T-1) with η_F^T the correction factor obtained for perfect mirrors at a nonzero temperature. For this term the integration over y is trivial and the integration over κ may be performed analytically, leading to the known expression [13–15]

$$\eta_F^T-1=\frac{480L^4}{\pi^4}\sum_{m=1}^{\infty}\int_0^{\infty}d\kappa\frac{\kappa^2}{e^{2\kappa L}-1}\frac{\sin(m\kappa\lambda_T)}{m\lambda_T}$$
$$=30\sum_{m=1}^{\infty}\left(\frac{1}{(\alpha m)^4}-\frac{\cosh(\alpha m)}{\alpha m\sinh^3(\alpha m)}\right), \tag{22}$$
$$\alpha=\frac{\pi\lambda_T}{2L}.$$

To obtain the overall correction factor (17) it now remains to evaluate the last expression (21). This can be done numerically, thus leading to the same results as in the previous section since no approximation has been performed up to now. But the results of the previous section suggest that we may obtain an accurate estimation of this term through an expansion in powers of λ_P. The plasma wavelength λ_P is indeed much smaller than the thermal wavelength λ_T in all experimental situations studied up to now. Also, the deviation studied in the foregoing section is appreciable only for distances L much larger than λ_P. Hence an accurate description of the deviation factor should be obtained by evaluating $\Delta\eta_F$ at the first order in λ_P.

This first order term is easily deduced from Eqs. (10), (21)

$$\Delta f\simeq-\frac{e^{2\kappa L}}{(e^{2\kappa L}-1)^2}(1-r_\perp^2+1-r_{||}^2),$$
$$\simeq-\frac{e^{2\kappa L}}{(e^{2\kappa L}-1)^2}\frac{2\kappa\lambda_P}{\pi}(1+y^2). \tag{23}$$

It is proportional to λ_P and to a function ϕ_F which does no longer depend on λ_P

$$\Delta\eta_F\simeq\frac{\lambda_P}{L}\phi_F,$$
$$\phi_F=\frac{15}{\pi}\sum_{m=1}^{\infty}\left(\frac{\cosh(\alpha m)}{(\alpha m)^3\sinh(\alpha m)}+\frac{1}{(\alpha m)^2\sinh^2(\alpha m)}\right.$$
$$\left.+\frac{4\cosh(\alpha m)}{\alpha m\sinh^3(\alpha m)}-\frac{2+4\cosh^2(\alpha m)}{\sinh^4(\alpha m)}\right). \tag{24}$$

Collecting the results obtained up to now, we get an estimation of the force correction factor η_F valid in the long distance range $L\gg\lambda_P$

$$\eta_F=\eta_F^P\eta_F^T+(1-\eta_F^P)(\eta_F^T-1)+\Delta\eta_F,$$
$$\simeq\eta_F^P\eta_F^T+\frac{8}{3\pi}\frac{\lambda_P}{L}(\eta_F^T-1)+\frac{\lambda_P}{L}\phi_F. \tag{25}$$

Coming back to the notations of the previous section, this result is equivalent to the following expression for the function Δ_F:

$$\Delta_F=\frac{8}{3\pi}\frac{\lambda_T}{L}\frac{\eta_F^T-1}{\eta_F^T}+\frac{\lambda_T}{L}\frac{\phi_F}{\eta_F^T}. \tag{26}$$

This function is plotted as the solid line on Fig. 4 and it is found to fit well the results of the complete numerical integration presented in the previous section.

Similar manipulations can be done for evaluating correction factors for the Casimir free energy. We give below the main results, that is the thermal correction factor evaluated for perfect mirrors

$$\eta_E^T-1=45\sum_{m=1}^{\infty}\left(-\frac{2}{(\alpha m)^4}+\frac{1}{(\alpha m)^3\tanh(\alpha m)}\right.$$
$$\left.+\frac{1}{(\alpha m)^2\sinh^2(\alpha m)}\right) \tag{27}$$

and the first order correction

$$\Delta\eta_E\simeq\frac{\lambda_P}{L}\phi_E,$$
$$\phi_E=\frac{45}{\pi}\sum_{m=1}^{\infty}\left(-\frac{4}{(\alpha m)^4}+\frac{1}{(\alpha m)^3\tanh(\alpha m)}\right.$$
$$\left.+\frac{1}{(\alpha m)^2\sinh^2(\alpha m)}+\frac{2\cosh(\alpha m)}{\alpha m\sinh^3(\alpha m)}\right). \tag{28}$$

Since the long distance expansion of η_E^P up to first order in the plasma wavelength is given by

$$L\gg\lambda_P\rightarrow\eta_E^P=1-\frac{2}{\pi}\frac{\lambda_P}{L}+\cdots \tag{29}$$

we deduce the function Δ_E

$$\Delta_E=\frac{2}{\pi}\frac{\lambda_T}{L}\frac{\eta_E^T-1}{\eta_E^T}+\frac{\lambda_T}{L}\frac{\phi_E}{\eta_E^T}. \tag{30}$$

This function is plotted as the solid line on the second graph of Fig. 4 and also found to fit well the results of the numerical integration.

VI. SUMMARY

In the present paper, we have given an accurate evaluation of the Casimir force and Casimir free energy between two plane metallic mirrors, taking into account conductivity and temperature corrections at the same time. The whole corrections with respect to the ideal Casimir formulas, corresponding to perfect mirrors in vacuum, have been characterized by factors η_F for the force and η_E for the energy. These factors have been computed through a numerical evaluation of the integral formulas. They have also been given a simplified form as a product of three terms, namely, the reduction factor associated with conductivity at null temperature, the increase factor associated with temperature for perfect mirrors, and a further deviation factor measuring a kind of interplay between the two effects. This last factor turns out to lie in the 1% range for metals used in the recent experiments performed at ambient temperature. Hence the conductivity and temperature corrections may be treated independently from each other and simply multiplied for theoretical estimations above this accuracy level.

However, when accurate comparisons between experimental and theoretical values of the Casimir force are aimed at, the deviation factor has to be taken into account in theoretical estimations. The deviation factor is appreciable for distances greater than the plasma wavelength λ_P but smaller or of the order of the thermal wavelength λ_T. We have used this property to derive a scaling law of the deviation factor. This law allows one to obtain a simple but accurate estimation of the Casimir force and free energy through a mere inspection of Fig. 4. Alternatively one can use analytical expressions which have been obtained through a first order expansion in λ_P of the thermal contributions to Casimir forces and fit well the results of complete numerical integration.

We have represented the optical properties of metals by the plasma model. This model does not lead to reliable estimations of the forces at small distances but this deficiency may be corrected by using the real dielectric function of the metals. This does not affect the discussion of the present paper, except for the fact that the pure conductivity effect has to be computed through an integration of optical data for distances smaller than 0.5 μm. Finally surface roughness corrections, which have not been considered in the present paper, are expected to play a significant role in theory-experiment comparisons in the short distance range.

ACKNOWLEDGMENTS

We wish to thank Ephraim Fischbach, Marc-Thierry Jaekel, David Koltick, Paulo Americo Maïa Neto, and Roberto Onofrio for stimulating discussions.

APPENDIX: THE VACUUM CONTRIBUTION

In the present appendix, we give further analytical expressions for the correction factor η_F^P due to conductivity, calculated with the plasma model for a null temperature. Introducing the notations

$$\rho=\frac{\sqrt{\omega_P^2+c^2\kappa^2}-c\kappa}{\sqrt{\omega_P^2+c^2\kappa^2}+c\kappa}, \qquad y=\frac{\omega}{c\kappa}$$

we rewrite the reflection coefficients (10)

$$r_\perp=-\rho, \qquad r_{||}=\rho\frac{y^2(1-\rho)-2}{y^2(1-\rho)+2\rho}.$$

In this case one integration may be performed analytically in Eq. (18)

$$\eta_F^P=\frac{120L^4}{\pi^4}\int_0^\infty d\,\kappa\kappa^3\frac{2\rho^2+\rho e^{\kappa L}g}{e^{2\kappa L}-\rho^2},$$

$$g=\frac{1+a_-^2}{a_-}\arctan\frac{1}{a_-}-\frac{1+a_+^2}{a_+}\arctan\frac{1}{a_+},$$

$$a_\pm=\sqrt{\frac{e^{\kappa L}\pm\rho}{e^{\kappa L}\mp\rho}\frac{1+\rho}{1-\rho}-1}.$$

At the large distance limit, η_F^P tends to unity, that is the value obtained for perfect reflectors. At the small distance limit, η_F^P is found to vary as [16]

$$\eta_F^P\simeq\alpha\frac{L}{\lambda_P}, \quad L\ll\lambda_P$$

$$\alpha=\frac{30}{\pi^2}\int_0^\infty dK e^{-3K/4}\left(\frac{K^2}{\sqrt{\sinh(K/2)}}-\frac{K^2}{\sqrt{\cosh(K/2)}}\right)$$

$$\simeq 1.193.$$

[1] H.B.G. Casimir, Proc. K. Ned. Akad. Wet. **51**, 793 (1948).
[2] B.V. Deriagin and I.I. Abrikosova, Sov. Phys. JETP **3**, 819 (1957).
[3] M.J. Sparnaay, Physica (Amsterdam) **XXIV**, 751 (1958); W. Black, J.G.V. De Jongh, J.Th.G. Overbeek, and M.J. Sparnaay, Trans. Faraday Soc. **56**, 1597 (1960).
[4] D. Tabor and R.H.S. Winterton, Nature (London) **219**, 1120 (1968).

[5] E.S. Sabisky and C.H. Anderson, Phys. Rev. A **7**, 790 (1973).
[6] S.K. Lamoreaux, Phys. Rev. Lett. **78**, 5 (1997); **81**, 5475 (E) (1998).
[7] U. Mohideen and A. Roy, Phys. Rev. Lett. **81**, 4549 (1998).
[8] A. Roy, C.Y. Lin, and U. Mohideen, Phys. Rev. D **60**, 111101 (1999).
[9] E. Fischbach and C. Talmadge, *The Search for Non-Newtonian Gravity* (AIP, New York, 1998), and references therein; E. Fischbach and D.E. Krause, Phys. Rev. Lett. **82**, 4753 (1999).
[10] G. Carugno, Z. Fontana, R. Onofrio, and C. Rizzo, Phys. Rev. D **55**, 6591 (1997).
[11] M. Bordag, B. Geyer, G.L. Klimchitskaya, and V.M. Mostepanenko, Phys. Rev. D **60**, 055004 (1999).
[12] E.M. Lifshitz, Sov. Phys. JETP **2**, 73 (1956); E.M. Lifshitz and L.P. Pitaevskii, *Landau and Lifshitz Course of Theoretical Physics: Statistical Physics* (Butterworth-Heinemann, Oxford, 1980), Pt. 2, Chap. VIII.
[13] J. Mehra, Physica (Amsterdam) **57**, 147 (1967).
[14] L.S. Brown and G.J. Maclay, Phys. Rev. **184**, 1272 (1969).
[15] J. Schwinger, L.L. de RaadJr., and K.A. Milton, Ann. Phys. (N.Y.) **115**, 1 (1978).
[16] A. Lambrecht and S. Reynaud, Eur. Phys. J. **D8**, 309 (2000).
[17] B.V. Deriagin, I.I. Abrikosova, and E.M. Lifshitz, Q. Rev. Chem. Soc. **10**, 295 (1968).
[18] J. Blocki, J. Randrup, W.J. Swiatecki, and C.F. Tsang, Ann. Phys. (N.Y.) **105**, 427 (1977).
[19] V.M. Mostepanenko and N.N. Trunov, Sov. J. Nucl. Phys. **42**, 812 (1985).
[20] V.B. Bezerra, G.L. Klimchitskaya, and C. Romero, Mod. Phys. Lett. A **12**, 2613 (1997).
[21] G.L. Klimchitskaya, A. Roy, U. Mohideen and V.M. Mostepanenko, Phys. Rev. A **60**, 3487 (1999).
[22] M.T. Jaekel and S. Reynaud, J. Phys. I **1**, 1395 (1991).
[23] L.G. Schulz, Philos. Mag. Suppl. **6**, 102 (1957).
[24] H. Ehrenreich and H.R. Philipp, Phys. Rev. **128**, 1622 (1962).

La décohérence due aux ondes gravitationnelles

6.1 Description du phénomène

En collaboration avec P.A. Maia Neto de l'Université de Rio de Janeiro, et avec Brahim Lamine qui a effectué un stage de DEA sous ma co-responsabilité en printemps 2001, j'ai commencé récemment à m'intéresser à un autre phénomène, à savoir la diffusion des ondes gravitationnelles et la décohérence induite par celles-ci. Nous avons en particulier étudié l'influence des ondes gravitationnelles sur le mouvement planétaire, par exemple celui de la Lune autour de la Terre. Bien que l'effet des ondes gravitationnelles soit négligeable en ce qui concerne la dissipation du mouvement, leur influence devient très importante en ce qui concerne la décohérence du mouvement. En effet, de la même façon qu'on peut attribuer aux photons du fond micro-ondes cosmique une température moyenne, on peut aussi associer aux gravitons du fond galactique une température équivalente. Cette température est extrêment grande et, par conséquent, la diffusion des ondes gravitationnelles galactiques par les planètes est le mécanisme dominant responsable de la décoherence dans leur mouvement [1, 2].

6.2 Publication jointe

Reproduction de l'article "Gravitational decoherence of planetary motions", S. Reynaud, P. Maia Neto, A. Lambrecht, and M.T. Jaekel, *Europhys. Lett.* **54**, 135 (2001)

1. S. Reynaud, P. Maia Neto, A. Lambrecht, and M.T. Jaekel, *Europhys. Lett.* **54**, 135 (2001)
2. S. Reynaud, B. Lamine, A. Lambrecht, P. Maia Neto, and M.-T. Jaekel, *Int. J. Mod. Phys.* **A 17**, 1003 (2002)

EUROPHYSICS LETTERS 15 April 2001

Europhys. Lett., **54** (2), pp. 135–140 (2001)

Gravitational decoherence of planetary motions

S. Reynaud[1](*), P. A. Maia Neto[2], A. Lambrecht[1] and M.-T. Jaekel[3]

[1] *Laboratoire Kastler Brossel*(**) *- Campus Jussieu case 74, F75252 Paris, France*
[2] *Instituto de Física, UFRJ - Caixa Postal 68528, 21945-970 Rio de Janeiro, Brazil*
[3] *Laboratoire de Physique Théorique*(***) *- 24 rue Lhomond, F75231 Paris, France*

(received 13 November 2000; accepted 9 February 2001)

PACS. 04.30.-w – Gravitational waves: theory.
PACS. 03.65.Yz – Decoherence; open systems; quantum statistical methods.
PACS. 95.10.Ce – Celestial mechanics (including n-body problems).

Abstract. – We study the effect of the scattering of gravitational waves on planetary motions, say the motion of the Moon around the Earth. Though this effect has a negligible influence on dissipation, it dominates fluctuations and the associated decoherence mechanism, due to the very high effective temperature of the background of gravitational waves in our galactic environment.

Decoherence plays an important role in the transition between microscopic and macroscopic physics since it kills quantum coherences on a time scale which becomes extremely short for systems with a large degree of classicality [1–4]. The details of this transition depend on the coupling mechanisms between the system under consideration and its environment. A lot of different models have been considered theoretically and decoherence has been experimentally observed in mesoscopic systems, such as a few microwave photons in a high-Q cavity [5], for which the decoherence time is neither too short nor too long.

For large macroscopic masses, say the Moon orbiting around the Earth, decoherence is so efficient that it precludes the observation of quantum coherences. It remains however important from a conceptual point of view to study the dominant decoherence mechanisms and to obtain a reliable estimation of the decoherence time scale. For motions in the solar system, decoherence is often attributed to the scattering of the electromagnetic fluctuations associated with solar radiation or cosmic microwave background. In this letter we show that the decoherence of planetary motions is not dominated by electromagnetic processes but rather by the scattering of stochastic gravitational waves present in our galactic environment.

Gravitational fluctuations have already been proposed as a universal mechanism able to explain the transition from quantum to classical physics. If these fluctuations are characterized by length scales of the order of the Planck length [6, 7], microscopic and macroscopic regions may be delineated by comparing the Planck length $l_{\rm P} = \sqrt{\frac{\hbar G}{c^3}}$ and the Compton length

(*) E-mail: reynaud@spectro.jussieu.fr
(**) Laboratoire ENS, Université Pierre et Marie Curie, CNRS.
(***) Laboratoire CNRS, ENS, Université Paris-Sud.

$l_{\rm C} = \frac{\hbar}{mc}$ associated with typical quantum phenomena for a mass m [8–10]. Remarkably, this leads to a frontier determined by the Planck mass $m_{\rm P} = \sqrt{\frac{\hbar c}{G}}$, *i.e.* the mass scale built on the Planck constant $\hbar$, the velocity of light c and the Newton constant G with a value 22 μg lying on the borderland between microscopic and macroscopic masses. However, this simple scaling argument is not by itself sufficient to reach any precise conclusion.

In order to compare gravitational and electrodynamical contributions to decoherence, one has to discuss the corresponding fluctuation levels as well as their effects on the system, at the frequencies of interest for the latter. In this letter, we present a quantitative study of decoherence of planetary motions in the stochastic background of gravitational waves in our environment [11, 12]. We give a precise estimate of the associated gravitational decoherence rate and show that it largely dominates the electromagnetic contribution.

The interaction of macroscopic motions with gravitational fluctuations is well known from the theory of gravitational wave emission and gravitational wave detection [13–15]. At the limit of non-relativistic velocities, the gravitational perturbation on a planetary system may be represented as a tidal acceleration acting on each mass

$$x_i''(t) = -R_{i0j0}(t)\, x_j(t)\ , \qquad R_{i0j0}(t) = -\frac{1}{2} h_{ij}''(t)\ . \tag{1}$$

The prime denotes a time derivative. The tidal tensor R_{i0j0} is built up from components of the Riemann curvature tensor with the index 0 representing time components and indices i, j representing spatial components. R_{i0j0} has been written as the second-order derivative of the metric perturbation h_{ij} evaluated at the center of mass of the planetary system in the transverse traceless (TT) gauge. The interaction is equivalently described by a Lagrangian perturbation coupling the quadrupole momentum of the system to the tidal tensor

$$S'(t) = \frac{1}{4} h_{ij}''(t)\, Q_{ij}(t)\ , \qquad Q_{ij}(t) = m\left(x_i(t)\, x_j(t) - \frac{\delta_{ij}}{3} x_k(t)\, x_k(t)\right)\ . \tag{2}$$

The quadrupole Q_{ij} is reduced to its traceless part with δ_{ij} a spatial Kronecker symbol. S' is the time derivative of the action integral as it is perturbed along a given trajectory, for example a circular orbit in the plane $x_1 x_2$

$$x_1(t) = \rho\cos(\Omega t + \theta)\ , \qquad x_2(t) = \rho\sin(\Omega t + \theta)\ , \qquad \rho^3\Omega^2 = GM\,. \tag{3}$$

For a system of two masses m_a and m_b, m denotes the reduced mass $\frac{m_a m_b}{m_a + m_b}$, x_i the relative position and ρ the distance between the two masses. The last relation in (3) is the Kepler law which connects the radius ρ, the orbital frequency Ω and the total mass $M = m_a + m_b$.

Our aim is to evaluate decoherence between two neighbouring motions on the same circular orbit. These motions correspond to slightly different values of θ with the difference denoted by $\Delta\theta$. The differential perturbation between the two motions is thus described by a quantity $\Delta S'$ written as in (2) with Q_{ij} replaced by the difference ΔQ_{ij} of the quadrupoles on the two motions. We write it as the product of a distance Δx and a force F

$$\Delta S'(t) = F(t)\,\Delta x\,, \qquad \Delta x = \rho\Delta\theta\,, \qquad F(t) = \frac{1}{2} h_{ij}''(t)\, m x_i(t)\, \frac{x_j'(t)}{\rho\Omega}\,. \tag{4}$$

Δx is the distance between the 2 motions, constant on a circular orbit, and F the component of the relative force projected along the mean motion. F may be expressed in terms of the circularly polarized metric perturbation h which fits the circular motion of the planetary system

$$F(t) = \frac{m\rho}{2\sqrt{2}}\left(h'' e^{2i\Omega t} + h^{*\prime\prime} e^{-2i\Omega t}\right)\ , \qquad h(t) = \frac{1}{\sqrt{2}}\left(h_{12} + \frac{h_{22} - h_{11}}{2i}\right)\ . \tag{5}$$

The circular polarization h is normalized so that it corresponds to the same noise level as the two linear polarizations h_{12} and $\frac{h_{22}-h_{11}}{2}$ in the case of an unpolarized background. Polarizations are defined with respect to the plane of the orbit and the two motions chosen in the vicinity of $\theta = 0$.

We now come to a Fourier representation of the force F and metric h. Accordingly, force and metric fluctuations are described by noise spectra C_{FF} and C_{hh}:

$$F[\omega] = \int \mathrm{d}t\ F(t)\ e^{i\omega t}\,, \qquad C_{FF}[\omega] = \int \mathrm{d}t\ \langle F(t) \cdot F(0) \rangle\ e^{i\omega t}\,. \tag{6}$$

The dot specifies a symmetrical ordering when quantum fluctuations are considered [16, 17]. The force (5) is driven by gravitational waves through a frequency transposition due to the evolution of the quadrupole momentum at frequencies $\pm 2\Omega$

$$F[\omega] = -m\rho \frac{(\omega+2\Omega)^2\, h[\omega+2\Omega] + (\omega-2\Omega)^2\, h^*[\omega-2\Omega]}{2\sqrt{2}}\,. \tag{7}$$

We are mainly interested in the long-term cumulative effect of fluctuations, that is in the momentum perturbation p_t integrated over an interaction time t longer than the correlation time. The variance of p_t is determined by the noise spectrum $C_{FF}[0]$ evaluated at zero frequency and expressed in terms of a momentum diffusion coefficient D:

$$p_t = \int_0^t \mathrm{d}s\ F(s)\,, \qquad \left\langle p_t^2 \right\rangle = C_{FF}[0]\ t = 2Dt\,. \tag{8}$$

The diffusion coefficient D_{gr} due to gravitational waves is finally obtained as

$$2D_{\mathrm{gr}} = C_{FF}[0] = 4m^2a^2C_{hh}[2\Omega]\,, \qquad a = \rho\Omega^2\,; \tag{9}$$

a is the acceleration on the circular orbit and $C_{hh}[2\Omega]$ is the gravitational wave spectrum at frequency 2Ω of the circular polarization h coupled to the system. Note that a gravitational background of galactic origin is certainly not isotropic, whereas an extragalactic background may probably be considered as isotropic. For simplicity, forthcoming discussions are phrased in terms of an unpolarized and isotropic background but the general case is recovered by coming back to eq. (9).

The frequency of interest for the planetary motion of the Moon is $\frac{2\Omega}{2\pi} \simeq 0.8 \times 10^{-6}\,\mathrm{Hz}$. Information on stochastic gravitational waves around this frequency may be deduced from studies devoted to the detectability of gravitational background by interferometers [18, 19]. We express the spectrum C_{hh} as a gravitational wave energy $k_{\mathrm{B}}T_{\mathrm{gr}}$ or, equivalently, as a number n_{gr} of gravitons per mode

$$C_{hh}[\omega] = \frac{16G}{5c^5} k_{\mathrm{B}} T_{\mathrm{gr}}[\omega] = \frac{16G}{5c^5}\left(\frac{1}{2} + n_{\mathrm{gr}}[\omega]\right)\hbar\omega\,; \tag{10}$$

k_{B} is the Boltzmann constant and T_{gr} is an effective temperature of the gravitational background. Figure 1 of [18] and eq. (3.1) of [19] lead, respectively, to $C_{hh}[2\Omega] \simeq 10^{-34.5}\,\mathrm{Hz}^{-1}$ and $C_{hh}[2\Omega] \simeq 10^{-33}\,\mathrm{Hz}^{-1}$ for $\frac{2\Omega}{2\pi} \simeq 10^{-6}\,\mathrm{Hz}$. Taking as a conservative estimate $C_{hh} \simeq 10^{-34}\,\mathrm{Hz}^{-1}$, we obtain an effective temperature $T_{\mathrm{gr}} \approx 10^{41}\,\mathrm{K}$ or, equivalently, a graviton number per mode $n_{\mathrm{gr}} \approx 2 \times 10^{57}$. These numbers correspond to the high temperature limit $k_{\mathrm{B}}T_{\mathrm{gr}} \gg \hbar\omega$. Hence the gravitational noise is much larger than vacuum fluctuations which correspond to the term $\frac{1}{2}$ in (10) and lead to ultimate fluctuations of geodesic distances of the order of Planck length [17].

The estimations of C_{hh} used here correspond to the confusion background of gravitational waves emitted by binary systems in our Galaxy. They rely on the laws of physics and astrophysics as they are known in our local celestial environment. There also exist more speculative predictions for gravitational backgrounds emitted by cosmic processes [18–21]. Depending on the parameters used in the models, these cosmic backgrounds may surpass the binary confusion background in the μHz frequency range. Hence the latter can be considered as a minimum noise level in our gravitational environment.

The diffusion coefficient may be written under the form of an Einstein fluctuation-dissipation relation, *i.e.* as the product of the effective temperature by a damping factor

$$D_{\rm gr} = m\Gamma_{\rm gr} k_{\rm B} T_{\rm gr}\,, \qquad \Gamma_{\rm gr} = \frac{32Gma^2}{5c^5}\,. \tag{11}$$

The damping rate $\Gamma_{\rm gr}$ is the inverse of the damping time associated with the emission of gravitational waves by the planetary system [13–15]. It does not depend on temperature and is so small, $\Gamma_{\rm gr} \approx 10^{-34}\,{\rm s}^{-1}$ for Moon, that it does not affect the classical motion on the orbit. Gravitational damping, however, has a noticeable effect in strongly bound binary systems such as millisecond pulsars [22].

At this point it is worth comparing the effects of gravitational and electromagnetic scattering. Modelling the moving mass as a sphere which perfectly scatters thermal photons at temperature $T_{\rm em}$, the damping rate $\Gamma_{\rm em}$ associated with radiation pressure of these electromagnetic fluctuations is evaluated as [23]

$$\Gamma_{\rm em} = \frac{4\pi^3\hbar r^2}{45m}\left(\frac{k_{\rm B}T_{\rm em}}{\hbar c}\right)^4. \tag{12}$$

The radius r has been supposed to be large compared to the wavelength of the photons. For the Moon, the temperature $T_{\rm em} = 2.7\,{\rm K}$ of the cosmic microwave background is already sufficient to produce a damping rate $\Gamma_{\rm em} \approx 2 \times 10^{-32}\,{\rm s}^{-1}$ which is 200 times larger than $\Gamma_{\rm gr}$. Since $\Gamma_{\rm em}$ varies as $T_{\rm em}^4$ in agreement with Stefan-Boltzmann law, the damping due to solar radiation is more than 10^{10} times larger than $\Gamma_{\rm gr}$. In fact, the damping of the Moon, as is revealed by the secular variation of lunar rotation [24], is mainly due to the interaction between Earth and Moon tides and it corresponds to a damping rate more than 10^{16} times larger than $\Gamma_{\rm gr}$. The role of gravitational scattering on damping of the Moon may thus be ignored but this is no longer the case for decoherence, as is shown in the next paragraphs.

In order to evaluate decoherence rates, we consider the effect of gravitational perturbation on the action difference ΔS_t after an interaction time t,

$$\Delta S_t = \int_0^t {\rm d}s F(s)\,\Delta x = p_t \Delta x\,, \qquad \left\langle \Delta S_t^2 \right\rangle = \left\langle p_t^2 \right\rangle \Delta x^2\,. \tag{13}$$

The decoherence between the two neighbouring trajectories is measured by the mean value $\left\langle \exp\left[\frac{i\Delta S_t}{\hbar}\right]\right\rangle$ of the exponentiated dephasing. Since ΔS_t is linearly driven by gravitational waves, it can be treated as a Gaussian classical stochastic variable which leads to

$$\left\langle \exp\left[\frac{i\Delta S_t}{\hbar}\right]\right\rangle = \exp\left[-\frac{\left\langle \Delta S_t^2\right\rangle}{2\hbar^2}\right] = \exp\left[-\Lambda_{\rm gr}\Delta x^2 t\right]\,,$$
$$\Lambda_{\rm gr} = \frac{D_{\rm gr}}{\hbar^2} = \frac{32Gm^2a^2}{5c^5\hbar^2} k_{\rm B} T_{\rm gr}\,. \tag{14}$$

Decoherence has been evaluated in the long-term limit, where the force fluctuations may be approximated as a white noise characterized by a momentum diffusion coefficient $D_{\rm gr}$. This expression can also be derived by evaluating the Feynman-Vernon influence functionals [25], often used in the study of decoherence [26], at the limit of high temperature. Note that the decoherence rate $\Lambda_{\rm gr}$ is proportional to the square of the acceleration and, hence, would vanish if evaluated for an inertial motion. This has a simple interpretation through the Einstein formula (11). The damping rate $\Gamma_{\rm gr}$ associated with the emission of gravitational waves indeed vanishes for inertial motion, while the other factors entering the expression of $D_{\rm gr}$ do not depend on the specific motion.

Using the Einstein fluctuation-dissipation relation (11) and the expression (14) of decoherence rates, the ratio between gravitational and electromagnetic contributions to decoherence can be rewritten as

$$\frac{\Lambda_{\rm gr}}{\Lambda_{\rm em}} = \frac{D_{\rm gr}}{D_{\rm em}} = \frac{\Gamma_{\rm gr}}{\Gamma_{\rm em}} \frac{T_{\rm gr}}{T_{\rm em}} \,. \tag{15}$$

For the motion of the Moon, the gravitational decoherence rate $\Lambda_{\rm gr}$ is found to be 10^{38} larger than the rate $\Lambda_{\rm em}$ corresponding to scattering of the cosmic photon background. It is still enormously larger than the effect corresponding to the scattering of solar photons. The same conclusion is reached for the comparison with the effect of tides. The latter effect determines the damping of the main motion of the Moon but its contribution to decoherence is overshadowed by gravitational scattering owing to the very high value of the effective gravitational temperature. As a consequence of this high temperature, the decoherence time is exceedingly short even for ultrasmall distances Δx. To fix ideas, the gravitational decoherence rate $\Lambda_{\rm gr} \approx 10^{75}\,{\rm s}^{-1}{\rm m}^{-2}$ obtained for the motion of the Moon corresponds to a decoherence time in the $10\,\mu$s range for a distance Δx between two trajectories as small as Planck length.

The large value of gravitational temperature implies that decoherence should still be dominated by gravitational scattering for smaller size planetary systems. This can be discussed by writing the ratio between gravitational and electromagnetic decoherence rates as a product of dimensionless factors

$$\frac{\Lambda_{\rm gr}}{\Lambda_{\rm em}} = \frac{72}{\pi^3} \frac{m^2}{m_{\rm P}^2} \frac{\rho^2}{r^2} \left(\frac{\hbar\Omega}{k_{\rm B} T_{\rm em}} \right)^4 \frac{T_{\rm gr}}{T_{\rm em}} \,. \tag{16}$$

The factor $\frac{m^2}{m_{\rm P}^2}$ is clearly reminiscent of the simple scaling arguments presented in the introduction, illustrating the role of Planck mass as a reference on the borderland between microscopic and macroscopic masses. However the whole formula shows that these scaling arguments are not sufficient for obtaining reliable quantitative predictions. The factor $\frac{\rho^2}{r^2}$ is a geometrical factor depending on the radius ρ of the orbit and the radius r of the orbiter. Then the ratio (16) also depends on the inverse fourth power of the photon number $\frac{k_{\rm B} T_{\rm em}}{\hbar\Omega}$ per mode at the orbital frequency Ω and on the already discussed ratio between temperatures of graviton background and photon background. Clearly the last three dimensionless factors appearing in (16) have no relation with the scaling arguments of the introduction but have to be known for a quantitative comparison of gravitational and electromagnetic contributions. If we consider as an example a man-made gravitationally bound planetary system consisting of two spheres having an ordinary metallic density, we obtain comparable decoherence rates for gravitational scattering and electromagnetic scattering of cosmic microwave background in the case of a compact geometry with masses of the order of 10^3 kg.

We have shown in this letter that the scattering of gravitational waves in our celestial environment is a dominant cause of decoherence for planetary motions such as the motion of the Moon around the Earth. Due to the very large effective temperature of the gravitational wave background, this mechanism leads to a decoherence by far more efficient than the

other fluctuation mechanisms, though its contribution to damping of the mean motion can be neglected. As far as the theory of measurement is concerned, this implies that the ultimate fluctuations of the motion of the Moon are determined by the same classical gravitation theory which also explains its mean motion. Precisely these fluctuations are determined by the classical gravitational waves present in our local celestial environment.

* * *

PAMN wishes to thank CAPES, CNPq, FAPERJ, PRONEX, COFECUB, ENS and MENRT for their financial support which made possible his stays in Paris during which this work was performed.

REFERENCES

[1] Zeh H. D., *Found. Phys.*, **1** (1970) 69.
[2] Dekker H., *Phys. Rev. A*, **16** (1977) 2126.
[3] Zurek A. J., *Phys. Rev. D*, **24** (1981) 1516; **26** (1982) 1862.
[4] Joos E. and Zeh H. D., *Z. Phys. B*, **59** (1985) 223.
[5] Brune M., Hagley E., Dreyer J. *et al.*, *Phys. Rev. Lett.*, **77** (1996) 4887; Davidovich L., Brune M., Raimond J. M. and Haroche S., *Phys. Rev. A*, **53** (1996) 1295.
[6] Wheeler J. A., *Ann. Phys.*, **2** (1957) 604.
[7] DeWitt B. S., *Gravitation, An Introduction to Current Research*, edited by L. Witten (Wiley) 1962, p. 266.
[8] Karolyhazy F., *Nuovo Cimento A*, **42** (1966) 390.
[9] Diosi L., *Phys. Rev. A*, **40** (1989) 1165.
[10] Penrose R., *Gen. Relativ. Gravit.*, **28** (1996) 581.
[11] Hils D., Bender P. L. and Webbink R. F., *Astrophys. J.*, **360** (1990) 75.
[12] Giazotto A., Bonazzola S. and Gourgoulhon E., *Phys. Rev. D*, **55** (1997) 2014.
[13] Landau L. D. and Lifshitz E. M., *The Classical Theory of Fields* (Butterworth-Heinemann) 1998, p. 110.
[14] Misner C. W., Thorne K. S. and Wheeler J. A., *Gravitation* (Freeman) 1973, p. 37.
[15] Blanchet L., Kopeikin S. and Schäfer G., *arXiv* (2000) gr-qc/0008074.
[16] Grishchuk L. P., *Usp. Fiz. Nauk*, **121** (1977) 629 (*Sov. Phys. Usp.*, **20** (1977) 319); *Usp. Fiz. Nauk*, **156** (1988) 297 (*Sov. Phys. Usp.*, **31** (1988) 940).
[17] Jaekel M. T. and Reynaud S., *Phys. Lett. A*, **185** (1994) 143; *Quantum. Semiclass. Opt.*, **7** (1995) 639; *Ann. Phys. (Leipzig)*, **4** (1995) 68.
[18] Schutz B., *Class. Quantum. Grav.*, **16** (1999) A131.
[19] Ungarelli C. and Vecchio A., *arXiv* (2000) gr-qc/0003021.
[20] Grishchuk L. P., Lipunov V. M., Postnov K. A. *et al.*, *arXiv* (2000) astro-ph/0008481.
[21] Maggiore M., *Phys. Rep.*, **331** (2000) 283.
[22] Taylor J. H., Wolszczan A., Damour T. and Weisberg J. M., *Nature*, **355** (1992) 132.
[23] Dalvit D. and Maia Neto P. A., *Phys. Rev. Lett.*, **84** (2000) 798; Maia Neto P. A. and Dalvit D., *Phys. Rev. A*, **62** (2000) 042103.
[24] Bois E., Boudin F. and Journet A., *Astron. Astrophys.*, **314** (1996) 989.
[25] Feynman R. P. and Vernon F. L., *Ann. Phys.*, **24** (1969) 118.
[26] Caldeira A. O. and Leggett A. J., *Physica A*, **121** (1983) 587; *Phys. Rev. A*, **31** (1985) 1059.

Troisième partie

Conclusion et perspectives

Mes thèmes de recherche actuels sont centrés autour des effets mécaniques des fluctuations du vide. Ces fluctuations constituent une prédiction importante de la théorie quantique. Elles ont de nombreuses conséquences observables comme l'effet Casimir, qui est maintenant mesuré avec une bonne précision.

Mais la densité d'énergie du vide, calculée par addition sur tous les modes du champ, est beaucoup plus grande que celle qui est observée autour de nous par l'intermédiaire des phénomènes gravitationnels. Cette "catastrophe du vide" est un problème crucial non résolu à l'interface entre théorie quantique d'une part, phénomènes gravitationnels et inertiels d'autre part. Il existe cependant des questions bien posées au voisinage de ce paradoxe. Ces questions sont directement liées à des conséquences observables portant sur le principe de relativité du mouvement dans le vide quantique.

L'énergie du vide est aussi un problème important pour les chercheurs en cosmologie et astrophysique. Des observations récentes en astrophysique semblent démontrer que la constante cosmologique n'est pas nulle[1]. Une des interprétations les plus naturelles de cet effet est lié à l'énergie du vide quantique. Les mesures de la force de Casimir présentent l'avantage d'être des expériences de laboratoire, dont tous les paramètres sont bien connus et contrôlés, ce qui n'est évidemment pas possible pour une expérience en astrophysique. Les résultats des mesures récentes de la force de Casimir sont très intéressants car ils permettent pour la première fois une comparaison détaillée avec les prédictions théoriques. Cependant, il reste beaucoup de travail à faire.

Au niveau expérimental, d'autres mesures vont venir confirmer et améliorer la précision de la mesure. J'ai moi-même décidé de m'investir dans des projets d'expérience. Dans ce but, j'ai récemment mis en place deux collaborations internationales avec des équipes expérimentales. La première collaboration est avec le groupe de Clive Speake à l'Université de Birmingham (Grande Bretagne), qui a une longue expérience dans les tests de précision de la loi gravitationnelle[2,3,4,5]. Notre idée est d'utiliser un pendule de torsion pour mesurer avec haute précision la force de Casimir à des distances au dessus du micromètre. A ces distances, l'influence des fluctuations thermiques sur la force devient prédominante, tandis que l'effet d'une réflectivité imparfaite des miroirs est négligeable. Le but est d'étudier précisément la dépendance en température de la force de Casimir. Dans la seule expérience à ce jour où des distances au-dessus du micromètre ont été ex-

1. Voir par exemple le numéro spécial de *Class. Quantum Grav.* du 19/06/2002.
2. C.C. Speake, T.M. Niebauer, M.P. McHugh, P.T. Keyser, J.E. Faller, J.Y. Cruz, J.C. Harrison, J. Mäkinen, and R.B. Beruff, *Phys. Rev. Lett.* **65**, 1967 (1990)
3. R.C. Ritter, C.E. Goldblum, W. Ni, G.T. Gillies, and C.C. Speake, *Phys. Rev.* **D 42**, 977 (1990)
4. C.C. Speake, *Class. Quantum Grav.* **13**, A291 (1996)
5. C. Trenkel and C.C. Speake, *Phys. Rev.* **D 60**, 107501 (1999)

plorées[6], l'effet de la température n'a pas été observé. Ceci est probablement dû à un problème de précision de cette expérience. Rappelons que la force de Casimir décroît rapidement quand la distance entre les miroirs augmente. Il faut alors une précision bien meilleure pour des mesures à grande distance qu'à courte distance. L'expérience que nous comptons mettre en place vise une précision de 1% ou mieux pour des distances jusqu'à 2 μm, où la force de Casimir est déjà notablement changée par l'effet d'une température ambiante.

J'ai entamé une deuxième collaboration avec le groupe d'Ephraim Fischbach à l'Université de Purdue (Etats-Unis). Nous envisageons une expérience dans le domaine des nouvelles forces hypothétiques à des distances bien inférieures au micromètre. A ces distances, la force de Casimir est la force prédominante entre deux objets neutres. Afin de s'en affranchir, l'idée consiste à utiliser deux matériaux qui ont des propriétés optiques voisines, mais des propriétés très différentes vis à vis des nouvelles forces qui sont determinées par une combinaison du nombre baryonique, du nombre leptonique et de l'isospin. Des matériaux possibles seraient par exemple l'or et le cuivre pour lesquels j'ai déjà effectué des calculs détaillés. Dans une mesure différentielle, la force de Casimir serait moins visible, ce qui permettrait d'améliorer la précision expérimentale pour l'étude des nouvelles forces.

Au niveau théorique, j'ai déjà traité les corrections dues à la conductivité des miroirs et à la température non nulle. Mais l'influence d'autres effets n'est pas encore bien connue. La plupart des expériences récentes ne mesure pas la force entre deux plaques, mais entre une surface sphérique et une plaque. Au niveau théorique, ces deux situations sont a priori très différentes. Jusqu'à ce jour, la force dans la géométrie plan-sphère est calculée en utilisant une méthode approximative, dite approximation de proximité. Elle donne des bons résultats si le rayon de la sphère est beaucoup plus grand que la distance entre les deux objets, situation rencontrée dans toutes les expériences à ce jour. Cependant, la précision de cette approximation n'est pas connue et, avec une précision expérimentale accrue, il deviendra indispensable de la caractériser.

De plus, l'état d'une surface n'est jamais parfait. Tout miroir a une certaine rugosité qui influence la force de Casimir. Dans la comparaison entre théorie et expériences, cet effet a également été traité en utilisant l'approximation de proximité. Des calculs récents ont evalué plus précisément l'influence de la rugosité sur la force de Casimir dans le cas particulier de miroirs parfaitement réfléchissants[7]. Il est également nécessaire de calculer les corrections de rugosité en même temps que les corrections de conductivité. Autrement

6. S.K. Lamoreaux, *Phys. Rev. Lett.* **78**, 5 (1997)
7. T. Emig, A. Hanke, R. Golestanian, and M. Kadar, *Phys. Rev. Lett.* **87**, 260 (2001)

dit, la sensibilité spectrale de l'effet de rugosité doit être corrélée à l'effet de conductivité[8], de la même façon que les corrections de conductivité et de température sont corrélées. En fait, il faut en principe calculer toutes les corrections en même temps, et ceci constitue un défi théorique considérable.

Comme je l'ai expliqué plus haut, les fluctuations du vide n'ont pas seulement des effets statiques comme la force de Casimir, mais également des effets dynamiques directement liés au principe de relativité du mouvement. La mise en évidence de ces effets reste un de mes principaux objectifs, même si j'ai pu montrer par mes calculs que c'était un objectif difficile. Jusqu'à présent, les calculs ont été effectués dans des modèles simplifiés où le champ se propage dans un espace à une seule dimension. Comme on le sait d'après les calculs de l'oscillateur paramétrique optique, cette approche décrit correctement un mode de la cavité si la taille de celui-ci est plus petite que la taille des miroirs. En ce qui concerne le rayonnement motionnel, nos calculs actuels correspondent donc à la contribution au rayonnement d'un seul mode de la cavité. Dans une expérience réelle, tous les modes de la cavité vont contribuer au rayonnement. Il faut alors un traitement théorique des fluctuations quantiques qui permette de considérer des cavités électromagnétiques dans l'espace réel à trois dimensions et qui traite simultanément les effets de transmission partielle et de dimension transverse finie des miroirs ainsi que ceux de la diffraction du champ. En collaboration avec P.A. Maia-Neto, j'ai étudié ce problème pendant mon séjour de longue durée au Brésil (novembre/décembre 1998) et pendant ses deux séjours à Paris (décembre 1999/janvier 2000 et juillet 2000). Le problème s'est avéré très difficile à traiter en toute généralité. En particulier, dans le domaine des ondes micrométriques, la finesse de la cavité n'est pas limitée par la transmission des miroirs mais par les pertes par diffraction aux bords. La diffraction est donc un phénomène prédominant qui ne peut pas être négligé. Par rapport aux calculs dans le domaine optique, le calcul de la diffraction dans le domaine des micro-ondes présente la difficulté qu'aucune approximation (approximation paraxiale, nombre de Fresnel grand) ne peut être effectuée.

Le problème de l'excitation mécanique du mouvement est inévitable pour toute réalisation expérimentale dans ce domaine. Il faudrait donc analyser de manière précise le bruit associé à cette excitation qui dépend de manière cruciale de la qualité mécanique du système de suspension des miroirs, ainsi que des moyens utilisés pour faire bouger les miroirs avec une amplitude et une fréquence suffisantes.

Vu la difficulté intrinsèque d'une telle expérience, il parait également intéressant d'étudier d'autres voies expérimentales dans lesquelles la force de Casimir statique et le rayon-

8. A.A. Maradudin and P. Mazur, *Phys. Rev.* **B 22**, 1677 (1980)

nement motionnel se rejoignent. Récemment une expérience a mis en évidence la force de Casimir latérale entre un miroir plan et une sphère[9] dont la surface présentait des corrugations sinusoïdales. Un mouvement transverse relatif entre les deux objets mettait en évidence une force de Casimir s'exerçant parallèlement aux surfaces. On peut penser utiliser ce schéma dans une mise en évidence du rayonnement motionnel entre deux miroirs plans de très haute qualité, corrugués et en mouvement relatif. Cette idée semble d'autant plus prometteuse qu'un calcul récent du rayonnement motionnel à trois dimensions pour des miroirs parfaits a montré qu'un mouvement oscillatoire entre les deux miroirs plans devrait donner lieu à un rayonnement émis parallèlement aux plaques[10]. Elle est également liée à une proposition récente où une molécule en mouvement oscillatoire au dessus d'une surface corruguée devrait émettre un rayonnement cohérent observable[11]. Une autre idée consiste à réaliser le mouvement non pas par une oscillation mais par une rotation entre deux miroirs circulaires autour d'un même axe, l'un par rapport à l'autre. Une corrugation symétrique par rapport à l'axe de rotation devrait permettre d'obtenir une fréquence équivalente d'oscillation assez grande tout en gardant une fréquence de rotation raisonnable.

L'observation du rayonnement motionnel parait ainsi réalisable avec de nouveaux systèmes nanométriques ou microélectromécaniques. Dans la même lignée le rayonnement motionnel et la force de Casimir pourraient devenir des enjeux pour le contrôle et le fonctionnement de ces systèmes. Ceci ouvre de vastes perspectives trés intéressantes à la frontière entre la physique microscopique et macroscopique.

Tous ces aspects permettent d'étudier des questions ouvertes en physique fondamentale avec des systèmes simples et bien définis. Cela constitue une approche complémentaire aux stratégies développées en astrophysique et cosmologie, tout en se servant de nouvelles technologies très performantes. Dans la même veine, on peut aussi se demander quel est l'effet des fonds gravitationnels sur ces systèmes simples. Les fonds gravitationnels seront très bien étudiés par les interféromètres d'ondes gravitationnelles sur Terre comme VIRGO, LIGO, TAMA, GEO, et par l'interféromètre spatial LISA. Dans ces expériences, le but est d'observer pour la première fois des ondes gravitationnelles au travers du déphasage qu'elles doivent produire dans des interféromètres très sensibles.

Pour ma part, je compte étudier un autre effet observable des fonds gravitationnels, à savoir la décohérence qu'elles pourraient induire. Nous avons récemment étudié la propo-

9. F. Chen, U. Mohideen, GL. Klimchitskaya, and V.M. Mostepanenko, *Phys.Rev. Lett.* **88**, 101801 (2002)
10. J.P.F. Mendonça, P.A. Maia Neto, and F.I. Takakura, *Optics Comm.* **160**, 335-343 (1999)
11. A. Belyanin, Va. Kocharovsky, Vl. Kocharovsky, and F. Capasso, *Phys. Rev. Lett* **88**, 053602 (2002)

sition de mission spatiale HYPER[12]. Il s'agit d'une proposition d'expérience pour mesurer la décohérence due aux ondes gravitationnelles dans un interféromètre atomique. Notre calcul a montré que l'expérience telle qu'elle était conçue ne pourrait pas voir cet effet. Il serait néanmoins très intéressant de trouver des systèmes sensibles à cet effet afin de pouvoir l'étudier expérimentalement. Il faut souligner que les perturbations gravitationnelles ont la particularité de ne pas pouvoir être éliminées.

On peut aussi se demander si la gravitation ne joue pas un rôle universel pour la transition entre le monde microscopique et le monde macroscopique. L'échelle de masse "naturelle", c'est à dire la seule que l'on peut construire avec des constantes fondamentales, est la masse de Planck qui vaut 22 μg. Elle se trouve à la limite entre les masses microscopiques, dont la dynamique est determinée par la mécanique quantique, et les masses macroscopiques, dont la dynamique est gouvernée par les lois classiques. Un système qui mettrait en évidence la décohérence gravitationnelle, pourrait permettre d'étudier ces questions précisément. Là encore, une telle expérience permettrait de proposer une nouvelle approche observationnelle de l'interface crucial entre fluctuations quantiques d'une part et phénomènes gravitationnels d'autre part.

12. ESA-SCI(2001)10, ESA Assessment Study Report (2001)